Editors Sascha Kosleck & Karsten Breddermann

Contributions on the Theory of Fishing Gears and Related Marine Systems

Vol. 12

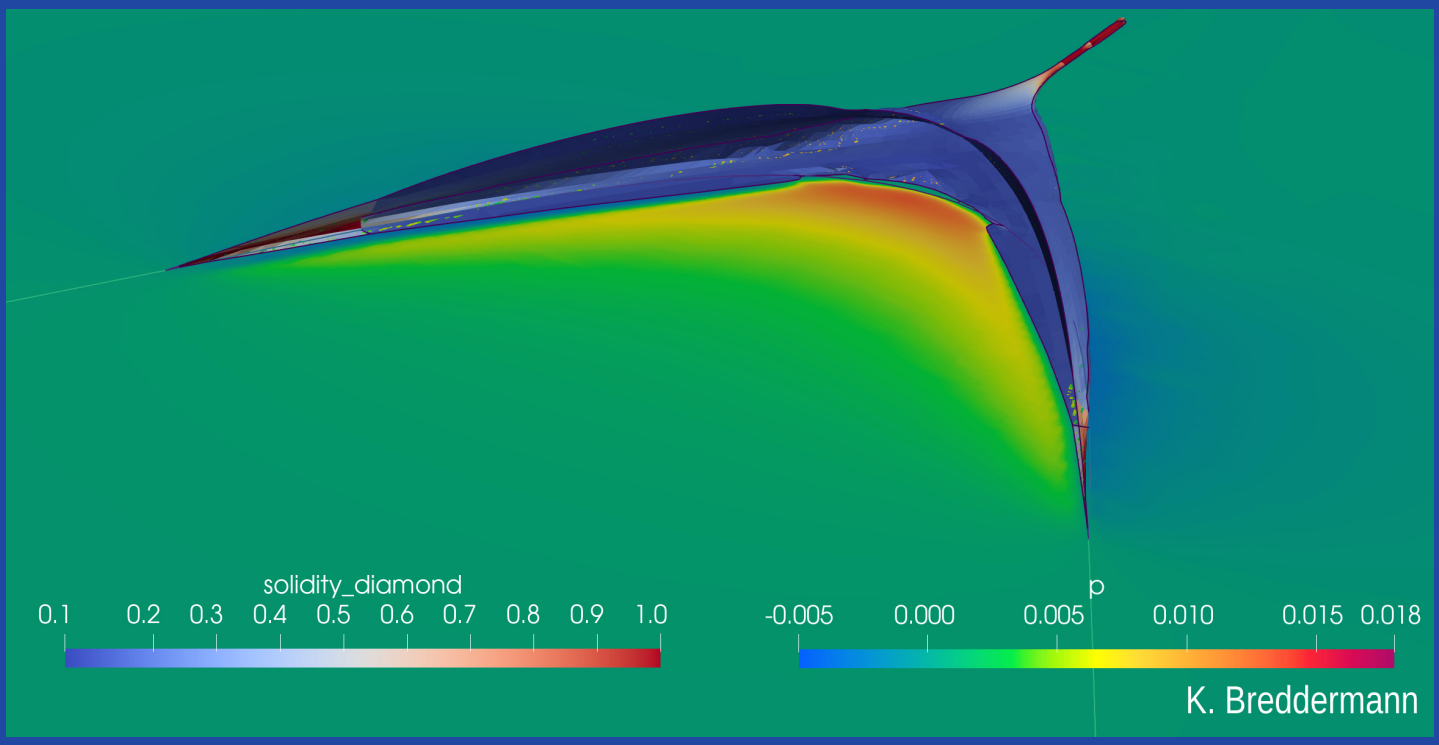

MENZEL-Verlag

PROCEEDINGS OF THE FIFTEENTH INTERNATIONAL WORKSHOP ON METHODS FOR THE DEVELOPMENT AND EVALUATION OF MARITIME TECHNOLOGIES
ROSTOCK, SEPTEMBER 13th - 15th, 2022

Contributions on the Theory of Fishing Gears and Related Marine Systems Vol. 12

edited by
Sascha Kosleck[1] & Karsten Breddermann[1]

Universität Rostock Traditio et Innovatio

[1]University of Rostock, Department of Mechanical Engineering and Marine Technology

Bibliographic information of the Deutschen Nationalbibliothek.
The Deutschen Nationalbibliothek lists this publication in the Deutschen Nationalbibliothek; detailed bibliographic data are available on the website via „http://dnb.d-nb.de“.

Editors Sascha Kosleck & Karsten Breddermann
PROCEEDINGS OF THE FIFTEENTH INTERNATIONAL WORKSHOP ON METHODS FOR THE DEVELOPMENT AND EVALUATION OF MARITIME TECHNOLOGIES ROSTOCK, SEPTEMBER 13th - 15th, 2022

1st edition January 2023

ISBN 978-3-946694-06-9

The texts of the various papers in this volume were set individually by typists under the supervision of each of the authors concerned.

Contents

Preface

The international Workshop Methods for the Development and Evaluation of Maritime Technologies – DEMaT has a 29 year long history since it was first held in Rostock in 1993. The founding idea was to initiate an international working group that gravitates around topics such as fishing technology and marine aquaculture. Over the years, DEMaT's focus has been widened, welcoming participants that work in areas such as oceanographic research, general ocean engineering and naval architecture. The 15th edition of the workshop was somewhat special as we were forced to interrupt the usual bi-annual rhythm and postpone the meeting for one year. Furthermore, after many successful years, the longstanding head of the steering committee Prof. Dr.-Ing. habil. Mathias Paschen handed his responsibilities over to his successor Prof. Dr.-Ing. Sascha Kosleck.

To address the actual global developments with regard to climate change and sustainable living including the associated changes needed in handling precious resources, the 2022 DEMaT centred around "Technologies to ensure a sustainable marine food production".

Many researchers, from academia, research institutions and industry alike accepted the challenge. Over three days, their attendance and participation sparked a diverse and interesting discussion from large health monitoring networks over general aspects of marine food production to detailed solutions for specific day to day problems. In this context we would like to express our special gratitude to this year's keynote speakers,

- Prof. Tsutomu TAKAGI, Hokkaido University, Faculty of Fisheries Science, Japan
- Antonello SALA, National Research Council, Institute of Marine Biological Resources and Biotechnologies, Italy
- Prof. Nils GOSEBERG, Technical University Braunschweig, Leichtweiß-Institute for Hydraulic Engineering and Water Resources, Germany
- Hans POLET, Science Director, ILVO - Flanders Research Institute for Agriculture, Fisheries and Food, Belgium
- Prof. Ana IVANOVIC, University of Aberdeen, School of Engineering, United Kingdom

The following summary of this year's contributions intend to round up the 2022 workshop and provide a basis for further discussions and new research ideas. Special thanks go out to my team at the Chair of Ocean Engineering for their hard work which started long before the first talk and only ends with the delivery of these proceedings. It wouldn't have been possible without all of you.

Rostock, January 2023
Sascha Kosleck

USING HYDRODYNAMICS TO OPTIMIZE THE DESIGN OF SEA STAR TRAWLS

Karen B. BURGAARD[1], Stefan CARSTENSEN[2], David R. FUHRMAN[2], Finbarr G. O'NEILL[1]
[1] Technical University of Denmark, National Institute of Aquatic Resources, 2, Willemoesvej, Hirtshals, 9850, Denmark
[2] Technical University of Denmark, Department of Civil and Mechanical Engineering, 403, Koppels Allé, Kgs. Lyngby, 2800, Denmark

Abstract

Towed fishing gear can be used to catch sea stars where the hydrodynamics around the gear is used to lift the sea stars from the seabed. An experimental investigation has been carried out in a current flume, measuring flow velocities with laser Doppler velocimetry around a simplified model of the groundgear of a realistic fishing gear. The experimental data is used to validate a computational fluid dynamics (CFD) model in OpenFOAM. The results from the CFD model are then used in a particle path model to provide an initial estimate of how the hydrodynamics around the groundgear affect the sea star dynamics. The trajectory of the sea star is found to depend on when in the vortex shedding cycle the groundgear approaches the sea star.

Keywords

Sea star, trawl, Computational Fluid Dynamics, particle path

Nomenclature

D – diameter of cylinder
U_0 – free stream velocity

e – gap between cylinder and bed
u – velocity component in x-direction
v – velocity component in y-direction
v_s – settling velocity
x_p – position in x-direction
y_p – position in y-direction

Δt – time step

Introduction

Globally sea stars are major predators of molluscs and other benthic invertebrates, and can have considerable impact on cultivated beds and natural populations of shellfish species such as mussels, oysters, scallops and clams. Consequently, methods must be developed to protect shellfish beds from sea stars. Towed fishing gear can be used to catch sea stars where the hydrodynamics around the gear are used to lift the sea stars from the seabed.

The traditional sea star trawl fishing gear used in Europe can have a large detrimental impact on the seabed. The frontal part of the gear can come into contact with the seabed, which can both damage the shellfish that the sea stars are predating and have broader environmental consequences for the local ecosystem. Hence, efforts have been made to develop trawl fishing gears which minimise these impacts.

One of the methods being considered is to use hydrodynamics to lift sea stars from the seabed rather than to lift them mechanically with seabed-contacting gear components. Part of the design process involves computational fluid dynamics (CFD) and experimental trials in a flume channel.

The hydrodynamics have been studied around parts of the fishing gear e.g. the trawl doors, where optimization techniques have been developed to reduce drag, and thereby fuel consumption (Parente et al. (2008) and Leifsson et al. (2015)). Further, the fluid-net interaction has been studied by Tang et al. (2017) and the effect of mesh size and trawl gear accessories on the bottom trawl hydrodynamic performance by Thierry et al. (2019). However, the hydrodynamics around the groundgear, and how it can be used to optimize the efficiency of the gear, have not been studied to date.

This paper presents some preliminary studies involving both experimental measurements and CFD results performed on sea star fishing gear, and how they can be used to optimize the design. For simplicity, the frame of reference is reversed in the study such that the model of the groundgear is stationary and subject to a steady, uniform current just upstream, mimicking a towed groundgear in a stationary water column.

Experimental methodology

Direct velocity measurements were carried out in a current flume within the Hydraulics Laboratory at Technical University of Denmark Department of Civil and Mechanical Engineering. The flow velocities were measured with laser Doppler velocimetry upstream, around and downstream of a simplified model of a realistic groundgear for a sea star trawl. The model of the groundgear was a

circular cylinder with a diameter of D=10 cm which is mounted at a fixed gap distance to the bed, e=10 cm.

A schematic diagram of the experimental configuration is shown in Figure 1. A coordinate system with origin at the centre of the cylinder is chosen. The flume provides a steady, uniform current, U_0=0.54 m/s and a free stream turbulence intensity less than 2% upstream of the cylinder. The measurements will serve to validate the CFD model, described below, whose output is used to model sea star trajectories.

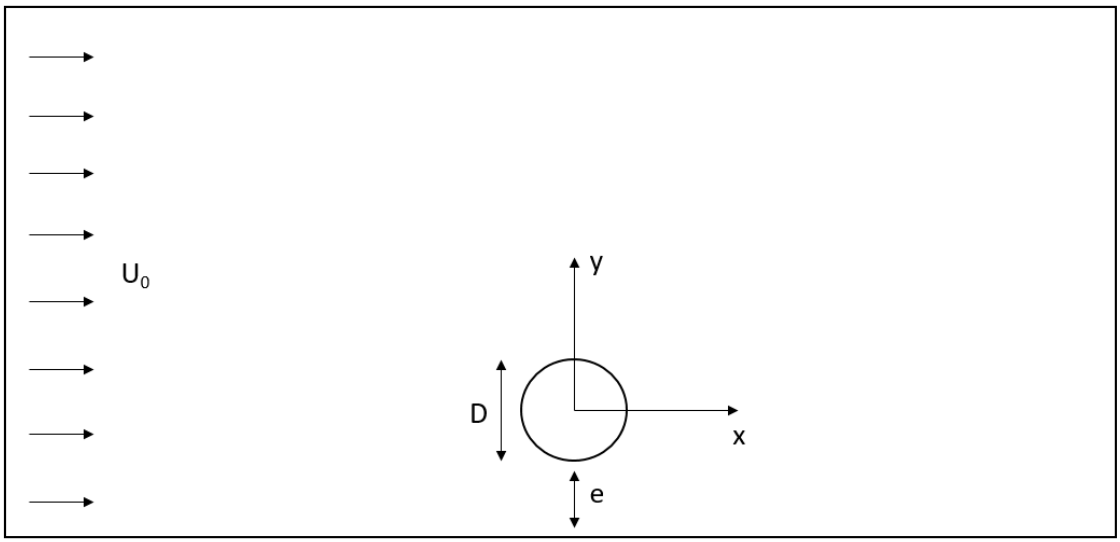

Figure 1
Schematic diagram of the experimental setup and coordinate system.

Computational method

The numerical simulations are performed using the open-source software OpenFOAM v2006. The CFD model is based on Reynolds-Averaged Navier-Stokes equations coupled with a k-ω turbulence model of Wilcox (2006) and implemented in OpenFOAM as in Li et al. (2022).

The dimensions of the cylinder in the computational model are the same as the model in the flume, such that the experimental data can be used to directly validate the CFD model. The mesh used in the CFD model is shown in Figure 2. A smaller cell size is used closer to the cylinder and the bed, where higher resolution is required to capture the flow correctly.

A no-slip boundary condition is used at the bed and the cylinder, and the inlet conditions are set to match the background velocity and turbulence field in

the experiments. After validation of the CFD model, additional models with different *e/D* values were additionally simulated. In these subsequent simulations, the fixed value of the velocity at the seabed was now changed to have the same value as the free stream velocity. This set up the model now represents towing conditions as in the field.

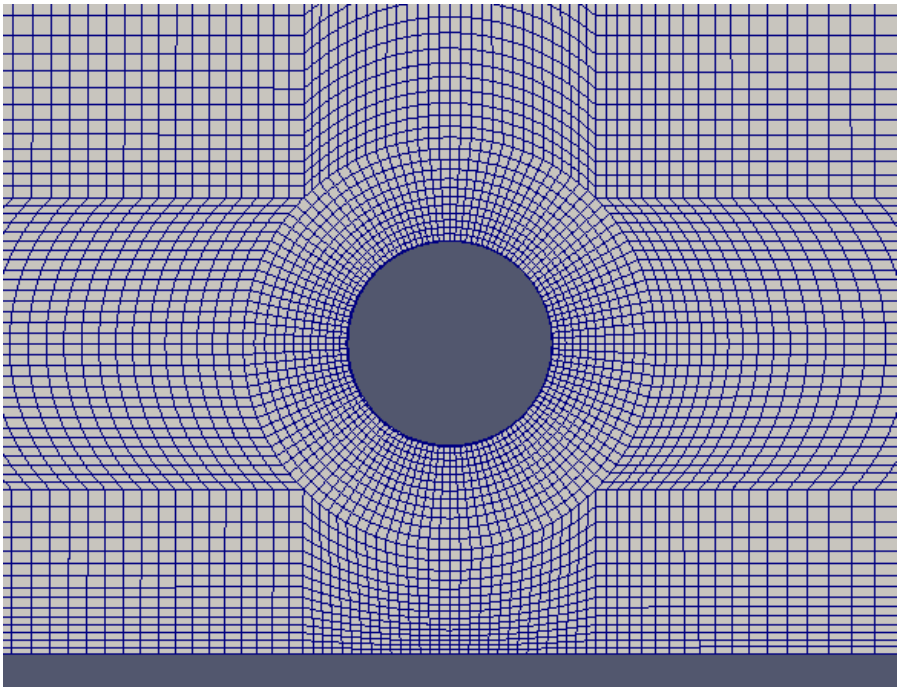

Figure 2
Close up of computational grid used in computational fluid dynamics model.

Particle path model

The velocity field obtained from the CFD model is used together with a particle path model to estimate the movement of the sea stars. The position of the sea stars at each new time step (time level n+1) is determined from the position at the previous time level (n) and the velocity in the following way

$$x_p^{(n+1)} = x_p^{(n)} + u^{(n)}\Delta t \tag{1}$$

$$y_p^{(n+1)} = y_p^{(n)} + (v^{(n)} - v_s)\Delta t \tag{2}$$

corresponding to a explicit forward Euler method. The particle paths are calculated by post-processing the output of the CFD simulation. In addition to the flow velocities (u and v), the settling velocity, v_s, is also needed when calculat-

ing the sea star trajectory. Preliminary measurements conducted at the Danish Shellfish Centre suggest the fall velocity of sea stars is in the range 0.08 m/s to 0.2 m/s. A value of the settling velocity in the lower end of this range was chosen for the below presented particle trajectories, namely a settling velocity of v_s=0.08 m/s. The sea stars are inserted in the model as particles. A restriction is applied for the lower position of the sea star, such that it cannot obtain a position lower than *y/D*=0.1, corresponding to the approximate thickness of a sea star. Further, the sea stars are not allowed to move in the *x*-direction when they are at the bed (*y/D*=0.1).

Results

Comparison of CFD model and experiments

The measured mean velocity profile for the streamwise and vertical velocity are shown in Figure 3 together with the corresponding profiles obtained in the CFD model. The profiles are found at seven *x*-positions, *x/D*= -2.5, -1.5, 0, 1.5, 3.5, 5.5, 7.5. The CFD model predicts the velocity field very well and captures how the water is flowing around the cylinder. The streamwise velocity is increasing on either side of the cylinder at *x/D*=0, while a downward and upward flow is seen from the vertical velocity in the gap and above the cylinder, respectively. Downstream of the cylinder it can be seen from both the data and the CFD model that the streamwise velocity is decreasing in the wake region at the centre of the cylinder *y/D*=0.

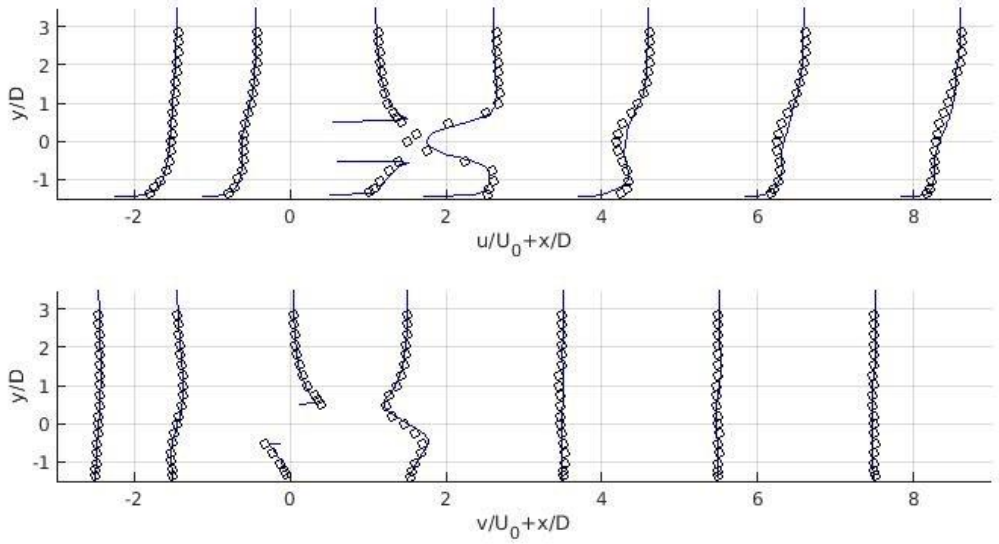

Figure 3

Mean streamwise (*u*) and vertical (*v*) velocity profiles at *x/D*= -2.5, -1.5, 0, 1.5, 3.5, 5.5, 7.5 for LDV measurements (o) and CFD model (-) .

Particle path model

The particle paths of the sea stars are found from the velocity fields obtained with the CFD simulation and eqns. (1) and (2). The mobilization of the sea stars is highly related to the vortex shedding. A vortex shed from the bottom part of the cylinder will cause an upwards flow, ejecting the sea star from the seabed, while a vortex shed from the upper part will cause a downwards flow, hence the sea star will remain at the seabed. The upwards flow must exceed the settling velocity for the sea stars to be ejected. The particle paths are found during several vortex shedding cycles, such that all aspects of the cycle are captured. All the paths are combined to obtain the probability of the sea star location downstream of the groundgear.

Figure 4 shows the probability of the sea star location downstream of the cylinder for the gap ratios e/D=0.5, 0.625, 0.75, 0.875, 1. From the figure it is seen that the gap ratio has a large impact on the ejection and paths of the sea stars. The sea stars are ejected at x/D=1.5 at the earliest for the smallest gap ratio, which increases to x/D=3 for the largest gap ratio. The number of sea stars ejected is also smaller when the gap ratio is increased, however, the paths are more regular than for small e/D, where the sea stars are affected by the rotating flow of the vortices, causing them to move up and down in the water column. There is no configuration where all of the sea stars are ejected, due to the downwards flow from the shedding from the upper vortex.

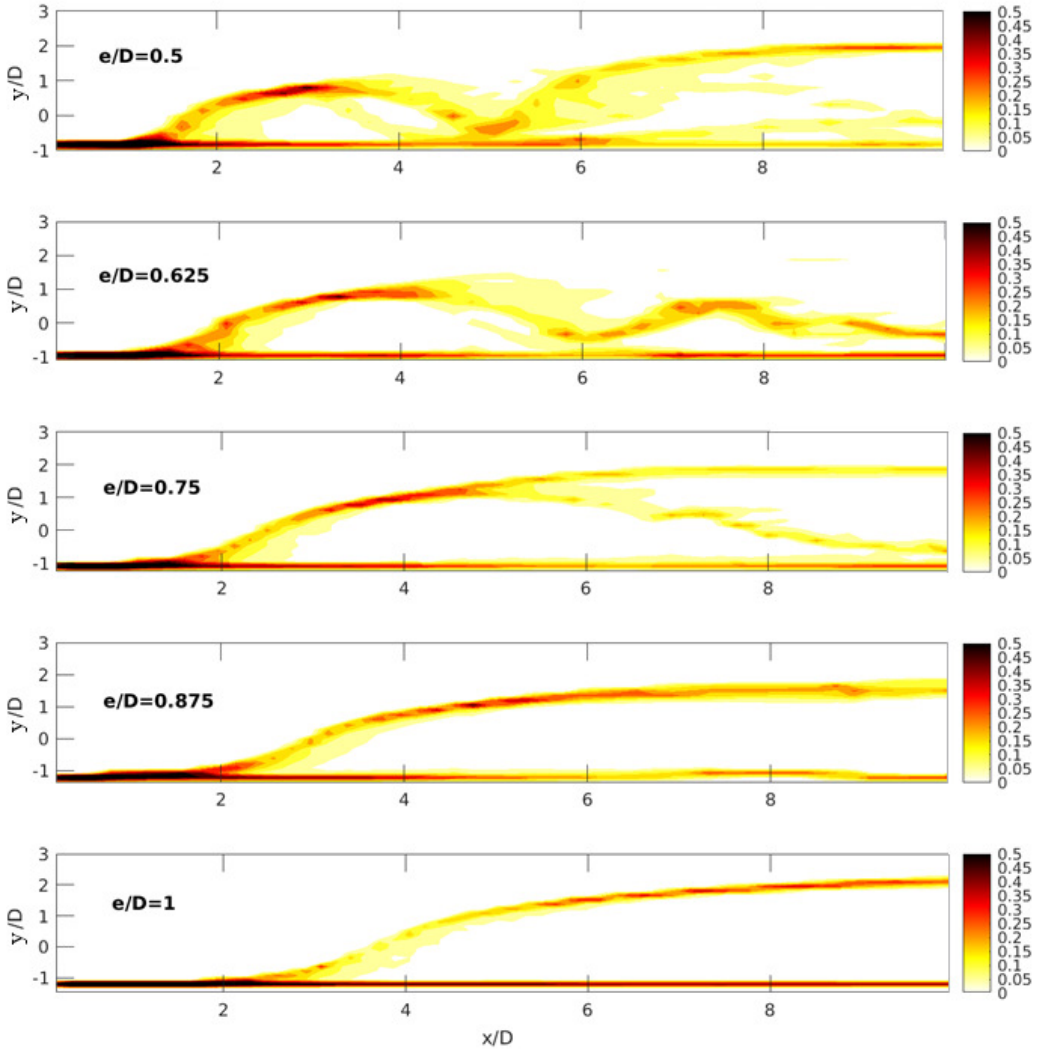

Figure 4
Computed probability of sea star location based on the particle paths downstream of groundgear.

Discussion

The probability of the sea star position can be used to design the sea star trawl, thus increasing the efficiency of the gear. For example, the gap ratio effects the ejection and path of the sea star, meaning that the position of the net has to be positioned according to the gap ratio, where the gap ratio depends on the fishing grounds.

The gap ratio is not the only parameter that has an impact on the path of the sea stars. Other parameters such as the velocity of the flow, diameter of the cylinder and the settling velocity of the sea stars, which may depend on the season, will also affect the paths but has yet to be covered in this study. Further, it

should be noted that the sea stars are modelled as passive particles in the model, whereas their size and mutual interaction could have an impact on their paths.

Conclusions

The velocities around a groundgear of a sea star trawl have been measured with LDV and compared with a CFD model. The CFD model provides promising results and was able to capture flow velocities around the cylinder. The velocity field from the CFD model was used together with a particle path model to find the probability of sea star location downstream of the groundgear. The sea star location was dependent on the gap between the cylinder and the seabed. The ejection of the sea stars occurred later for a large gap ratio. Further, a larger percentage of the sea stars were ejected into the water column when the gap was small.

Acknowledgements

The research leading to these results has received funding from the European Fisheries Fund and is part of the project Using hydrodynamics to develop more selective fishing gears (HydroSel), grant number 33113-I-19-130.

References

1. Leifsson, L., Hermannsson, E., Koziel, S. – Optimal shape design of multi-element trawl-doors using loval surrogate models – Journal of Computational Science, 20, 2015, 55-62.
2. Li, Y., Larsen, B. E., and Fuhrman, D. R. – Reynolds stress turbulence modelling of surf zone breaking waves – Journal of Fluid Mechanics, 937, 2022, 937, A7.
3. Parente, J., Fonseca, P., Henriques, V., Campos, A. – Strategies for improving fuel efficiency in the Portuguese trawl fishery – Fisheries Research, 93, 1, 2008, 117-124
4. Tang, M.F., Dong. G.H., Xu. T.J., Zhao, Y.P., Bi, C.W. – Numerical simulation of the drag force on the trawl net –Turkish Journal of Fisheries & Aquatic Sciences. 17, 6, 2017, 1219-1230.
5. Thierry, N., N., B., Tang, H., Liuxiong, X., You, X., Hu, F., Achile, N. P., Kindong, R. – Hydrodynamic performance of bottom trawls with different materials, mesh sizes, and twine thicknesses – Fisheries Research, 221, 2020, 105403.
6. Wilcox, D. C. – Turbulence Modeling for CFD – DCW Industries, 3rd Edition, 2006.

HYDRODYNAMIC DRAG AND CATCH EFFICIENCY OF LOW POROSITY CALANUS NETS

Enis N. KOSTAK[1], Eduardo GRIMALDO[1,2], Jesse BRINKHOF[1,2], Bent HERRMANN[1,2,3], Roger B. LARSEN[1]
1[1]UiT the Arctic University of Norway, Norwegian College of Fishery and Aquatic Science, Breivika, 9037, Tromsø, Norway
[2]SINTEF Ocean, Department of Fisheries Technology, Trondheim, Norway
[3]Technical University of Denmark, Section for Fisheries Technology, Institute for Aquatic Resources, Willemoesvej 2, 9850, Hirtshals, Denmark

Abstract
A major challenge for the aquaculture sector is access to sustainable and cost-effective raw materials for feed. New materials should preferably be from marine sources outside the human food chain. The ocean hosts many species, especially in lower trophic levels that are either not harvested or only marginally utilized. One of this species, *Calanus finmarchicus*, has potential to contribute with new and large volumes of marine raw materials enabling sustainable growth of the Norwegian aquaculture production. Lack of an efficient fishing method has been the most important limitation in the development of fishing for Calanus. Fine-meshed trawls, as those currently used in Calanus trawling, have high drag forces, causing high levels of greenhouse gas emissions (GHGE). Therefore, it is important to increase catch efficiency and reduce drag and thus GHGE. This study aims at developing more energy effective and catch-efficient Calanus harvesting technology. We studied the hydrodynamic performance of Calanus nets with different mesh sizes at various flow velocities in a flume tank. The catch efficiency of the same set of nets used in the flume tank was assessed during experimental fishing in the Norwegian Sea. While the net with 750 μm mesh size had the lowest drag force in all flow speeds, the 500 μm mesh size net provided the highest catch efficiency with a small margin to 250 μm mesh size. Results demonstrated the challenge of obtaining a reduction in drag and simultaneously increase catch efficiency when trawling for Calanus.

Keywords
Plankton nets, mesh sizes, catch efficiency, drag force, Calanus

Nomenclature

F_D	–	Drag Force	[N]
t	–	Twine diameter	[µm]
a	–	Inside measured vertical mesh size	[µm]
d	–	Inside measured diagonal mesh size	[µm]
b	–	Inside measured horizontal mesh size	[µm]
S_n	–	Solidity ratio	
n	–	Number of meshes in the imaged frame	
x	–	Vertical measure of the projected area	[µm]
y	–	Horizontal measure of the projected area	[µm]

Introduction

Due to the increasing demand for global marine products as feed in aquaculture and human consumption, there is a growing need for suitable alternatives that can provide omega-3-rich oil, protein, and other bioactive compounds. (Lenihan-Geels et al., 2013; Hua et al., 2019). The ocean hosts many species, especially in lower trophic levels that are either not harvested or only marginally utilized (FAO 2020). One of these species, *Calanus finmarchicus*, has the potential to provide new and significant quantities of marine raw materials that would enable the production of aquaculture in Norway to increase sustainably. Only recently a commercial quota on Calanus has been set, opening possibilities to harvest and utilize this nearly unexploited resource, with an estimated biomass of 290 million tons. (Aksnes and Blindheim, 1996; Skjoldal et al., 2004; Prellezo, 2019).

Currently, in Calanus fisheries, fine-meshed trawls (~500 µm bar length) are being used with mouth openings up to 100 m^2. The catch rates with these trawls are up to 2 tons per hour with a 100 m^2 trawl and a tow resistance of approx. 20 tons at 1 knot towing speed (Grimaldo and Gjøsund, 2012). This results in a high greenhouse gas emission if Calanus is to be used as a significant ingredient in salmon feed in the future.

Therefore, to reduce greenhouse gas emissions it is important to develop harvesting technology that provides a significantly lower energy consumption per unit of catch than current technology (Jafarzadeh et al., 2016). To achieve this, we need to understand the interaction between the hydrodynamic properties of low-porosity nets with different mesh sizes and their respective harvesting efficiencies.

Gjøsund and Enerhaug (2010) obtained basic relations for the flow through and forces on tapered net sections, based on pressure drop and streamline deflection through porous screens, and present parametric examples for the filtration efficiency and drag on conical nets. The model allows easy assessment of the effect of varying mesh opening, twine thickness, porosity, taper angle and flow velocity. For a tapered net, it is the pressure drop through the net panels that defines the degree to which the flow is blocked, and the pressure drop will primarily be a function of the ratio between the total open mesh area of the section and the inlet area of the section (Gjøsund and Enerhaug 2010). The filtration efficiency is defined as the ratio between the average velocity across the net mouth and the velocity of the net through the water (e.g., the towing velocity through quiescent water) (Grimaldo and Gjøsund, 2012). A net panel or a trawl section will always cause some blocking of the flow. However, the blocking will only become noticeable if the panel has both sufficiently low porosity (small mesh opening, high solidity) and steep tapering angle (Valdemarsen et al., 2011). Clogging of mesh panels is a common problem in Calanus trawls, and a problem that this theoretical model cannot account for. It is expected that clogging of net panels will be positively correlated increasing drag, but its effect on fishing efficiency is unknown. Once again, there is a need of conducting controlled hydrodynamic tests combined with fishing trials to have a better understanding of the processes affecting catch efficiency.

Generally, towing resistance increases in relationship with towing velocity. This is rarely a problem for small sampling nets like those used in this study, but it can be extremely important for the fuel efficiency of full-scale commercial plankton trawls. Also, one of the main concerns for commercial plankton trawls is catch efficiency along with fuel consumption (Grimaldo and Gjøsund, 2012).

Therefore, if we want to optimize fuel efficiency considering catch efficiency, more improved hydrodynamic designs are needed for Calanus trawlers.
Thus, to enable development of the optimal design of Calanus trawls we need to investigate; i) which mesh size and solidity has the lowest drag under given flow speeds, and ii) what is the catch efficiency for those mesh sizes?

Materials and methods

Experimental nets

In this study, four different mesh sizes (250, 500, 750, and 1000 μm) in experimental plankton nets were used with a 5º tapering angle (Fig. 1, left). All nets were attached to a plastic ring (hoop) of 1 m diameter. The total length of the nets was 5 m (4.9 m from opening to the codline). The nets were built from polyamide monofilament material (Nylon PA 6.6 – KC Denmark).

The mesh size and twine diameter were measured using a scaled microscope with a "Leica" camera microscope and imaging software. Images (Fig. 1, left) were analyzed in the FISHSELECT software tool (Herrmann et al., 2009). The twine diameter (*t*) and inner mesh size were measured vertically (*a*) and horizontally (*b*) from the middle of the bars (Fig. 1, right).

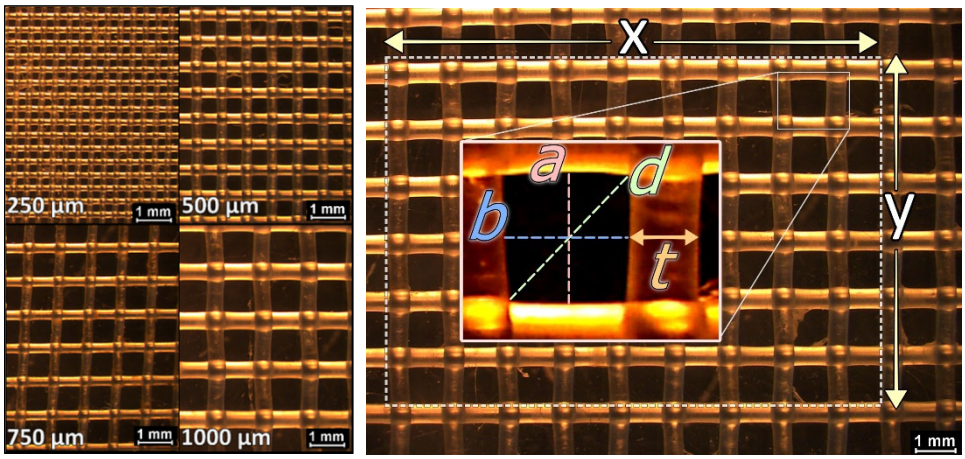

Figure 1
Scaled images of the net samples (left). Measured parameters and their positions in the image (right).

The solidity depends on twine thickness and mesh size (Tang et al., 2017). Solidity ratio (S_n) is often used to describe the geometrical characteristic of netting, and it can be formulated as the projected area's ratio to the total area covered by the outline of the netting panel by using number of meshes (n) in a frame with area $x \times y$ (Fig. 1).

$$S_n = 1 - \frac{nab}{xy} \quad (1)$$

Flume tank experiments

The plankton nets were tested at the SINTEF flume tank in Hirtshals, Denmark (2-3 June 2022). The rings were tied to the main towing wire with 4 bridles from the hoop. To prevent swaying, the towing wire passed through a small ring which was fixed to the tank walls from the side (Fig. 2). Also 2 floaters with each 80 g lifting capacity, were attached to 3 of the nets to maintain the neutral buoyancy and prevent it from rotating. Except for the 1000 µm net which required 4 floaters with the same lifting capacity due to its higher weight. The drag measurements were performed with 0.31, 0.51, 0.72, 0.98 m/s flow speeds for each net. All nets were tested individually, by increasing the speed, respectively, and only horizontal towing direction flow velocity was considered for this study.

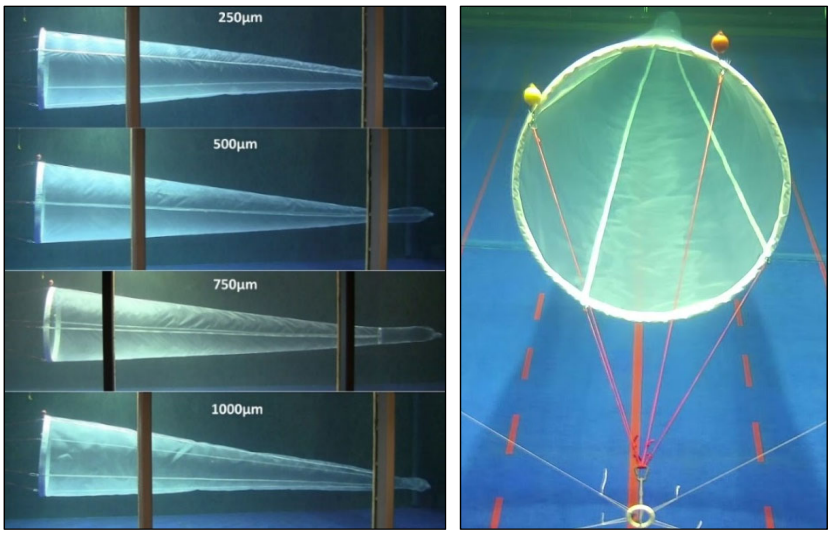

Figure 2
Flume tank photo of all nets that were used in the study (left). Front view of the 500 µm net and experimental setup (right).

Field experiments

Experimental trials were carried out onboard the R/V “Helmer Hanssen" (63.8 m LOA, 4080 HP) during 15-16 June 2022 in the Norwegian Sea, between 69º06′-69º24′N and 14º00′-15º08′E along continental shelf across Langøya Island. All hauls were carried out with an average towing speed of 1.97 (1.1-2.6) knots (0.57-1.34m/s) with a towing time of 60 min. and an average towing depth of 7.3 (13.8-2.5) m.

Figure 3
Experimental setup that was used in sea trials.

The same nets were used in sea trials as flume tank tests, however this time four nets were fitted in 2.1x2.1 m steel frame (Fig. 3). Four plastic floats were tied at the top side of the frame, and chain weight attached to the bottom of the frame to maintain a perpendicular towing position. A Scanmar SS4 depth sensor was attached in the middle of the upper bar of the frame. The four nets were towed simultaneously in the frame, lined up in clockwise directions 250, 500, 750 and 1000 μm, respectively.

Statistical methods

The data set was analysed by using the statistical software tool SELNET (Herrmann et al., 2012). Uncertainties in estimated values for drag forces and catch values were obtained by none-parametric bootstrapping (Efron, 1982) with 1000 repetitions. Specifically, we used Efron 95% percentile confidence bands (Efron, 1982).

Results

Netting properties

10 different and random mesh size and twine diameter measurements were conducted for each net using microscope images. Mean measurements for the mesh sizes and twine diameters are given in Table 1.

Table 1

Mean measurement values for twine diameter (t) and mesh sizes for each vertical (a), horizontal (b) and diagonal (d) directions for all nets along with solidity ratio (Sn) and measured mesh sizes. Measured mesh size values represent mean values for a and b.

Mesh size (μm)	Nominal	250	500	750	1000
	Measured	194	446	655.5	898.5
t (μm)		198	345	318	514
a (μm)		187	431	676	929
b (μm)		201	461	635	868
d (μm)		274.53	631.09	927.47	1271.40
S_n		0.7398	0.6528	0.5517	0.5895

Flume tank experiments

In this study, the 750 μm mesh sized net was used as the baseline for analysis. In Fig. 4, changes in drag can be seen for each mesh size with increased flow velocity. All the nets showed a decrease in drag force for all flow speeds when increasing the mesh. Contrary to expectation the net with 750 μm mesh size has

the lowest drag force compared to the other mesh sizes. Solidity ratio values were calculated for each mesh size and fitted into a plot corresponding to the relevant nominal mesh size (Fig. 4). The coefficient of determination gave us high R^2 values for the solidity ratio for the regression model. Due to the low margin of error around the estimated values in Fig. 4, the 95% confidence limits are presented in Table 2.

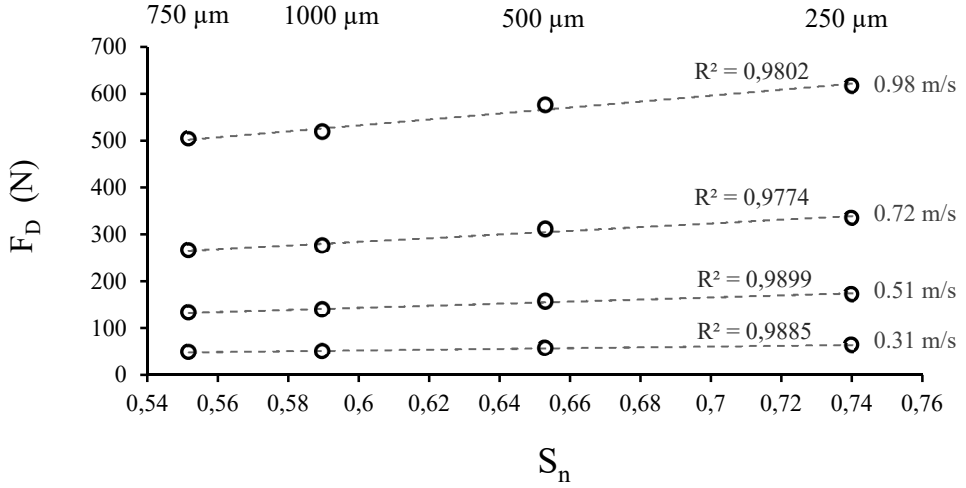

Figure 4
Solidity ratio (S_n) for each mesh size versus drag force (F_D).

Table 2
Mean drag force F_D (N) values for the tested nominal mesh sizes at each flow speed (m/s). Values in '()' represent 95% confidence limits.

	250 µm	500 µm	750 µm	1000 µm
0.31 m/s	64.33(64.2-64.5)	57.84(57.7-57.9)	49.35(48.8-49.7)	50.99(50.8-51.3)
0.51 m/s	172.37(171.4-172.9)	157.49(156.6-157.9)	133.85(133.7-134.0)	140.24(139.1-141.2)
0.72 m/s	335.20(332.6-337.8)	311.52(307.8-314.3)	266.6 (262.8-270.1)	276.89(272.7-280.1)
0.98 m/s	617.41(611.7-623.2)	577.40(573.8-581.0)	505.08(496.5-510.3)	521.64(517.1-526.5)

Sea Trials

A total of 10 valid hauls were carried out during the sea trials. After each tow, the catch from the four nets was put into separate containers, and the catch weight was recorded for each codend. Total weight of about 23.9 kg was caught for all hauls. Onboard microscope examination of the catch revealed that the catches consisted predominantly of *Calanus spp.*, along bycatch species, like jellyfish, algae, fish eggs, and larvae etc.

According to the total catch data, the mesh size with 500 µm showed a slightly higher catch efficiency than 250 µm, but not statistically significant, as opposed to net with 1000 µm mesh size (Fig. 5).

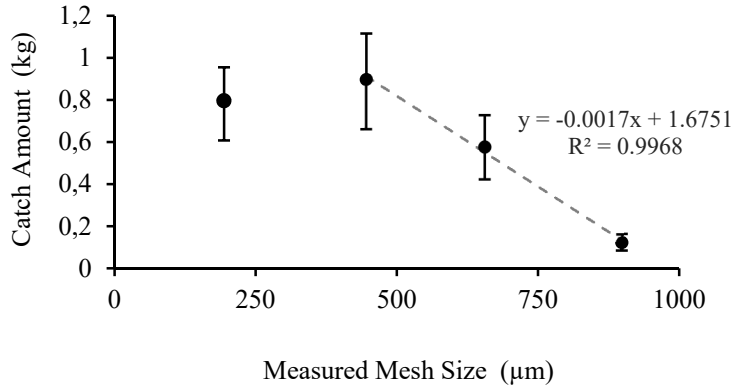

Figure 5
Catch amounts for all measured mesh sizes. Error bars represent 95 % confidence limits.

On the other hand, for the estimated catch ratio, the difference between 500 µm and 750 µm is significant with a 55.6% estimated increase in the catch (Fig. 6). In addition, we have a 78.8% estimated catch loss with 1000 µm net.

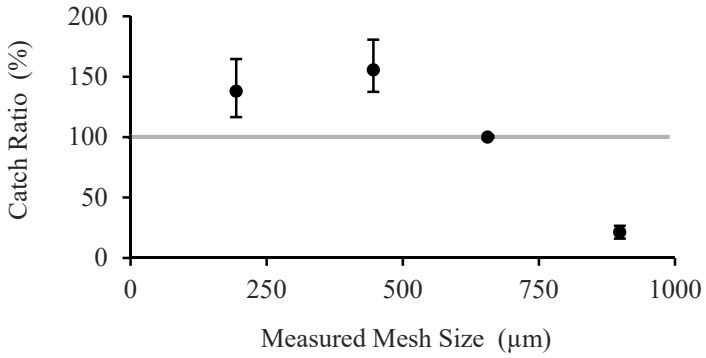

Figure 6
Estimated catch ratio for measured mesh sizes with the net with 750 µm mesh size as baseline. Error bars represent 95 % confidence limits.

The 750 µm mesh sized net, which was selected as the baseline for the experiments, demonstrated the lowest drag force values. However, the 250 µm and 500 µm mesh nets, which demonstrated higher catch efficiency than the net with 750 µm mesh size, performed also higher drag force. The 1000 µm mesh net showed the poorest results both in terms of catch efficiency, and a high drag force value compared to 750 µm.

Discussions and conclusions

This study showed that solidity highly affects the drag force of the fine meshed Calanus nets. A similar correlation is found between the amount of catch and mesh size (Fig. 5), except for the smallest mesh size.

The amount of catch between the net with 250 µm and 500 µm mesh size was not significantly different. One possible explanation could be that the nets retained the same size distribution of Calanus, meaning that the net with 500 µm mesh size already retained the entire size distribution encountered in the fishing area. Another possible explanation could be that the small mesh size in the net with 250 µm mesh size caused a “bucket-effect" pushing the water and target species in front of the net opening. Both possible explanations need further investigation.

Nevertheless, the 750 µm mesh size can be an alternative to the 500 µm mesh size which is used in commercial Calanus trawls. The net with the 750 µm mesh size had both a lower catch efficiency and drag force compared to the net with the 500 µm mesh size. In this case the optimal mesh size becomes a cost-benefit trade-off between catch efficiency (income) and drag force which leads to increased fuel consumption and GHGE (cost).

Acknowledgements

We would like to thank Kristine Cerbule, Ilmar Brinkhof, Waranya Wataniyakun, Amanda Schadeberg, and the crew members of the R/V “Helmer Hanssen” for their help during the sea trials. This study was funded by SFI Harvest research project (project no: 309661, Research Council of Norway 2020-2028) and UiT the Arctic University of Norway.

References

1. Agriculture Organization of the United Nations. Fisheries Department. – The State of World Fisheries and Aquaculture, 2020 – Food & Agriculture Org, 3, 2020
2. Aksnes, D.L., and Blindheim, J. – Circulation patterns in the North Atlantic and possible impact on population dynamics of Calanus finmarchicus. – Ophelia, 44, 1996, 7–28
3. Efron, B. – The jackknife, the bootstrap and other resampling plans – SIAM Monograph No. 38, CBSM-NSF, 1982
4. Gjøsund, S.H., and Enerhaug, B. – Flow through nets and trawls of low porosity - Ocean engineering, 37(4), 2010, 345-354
5. Grimaldo, E., and Gjøsund, S.H. – Commercial exploitation of zooplankton in the Norwegian Sea – The Functioning of Ecosystems/InTech, 2012, 213-228

6. Herrmann, B., Krag, L.A., Frandsen, R.P., Madsen, N., Lundgren, B., and Stæhr, K.J. – Prediction of selectivity from morphological conditions: methodology and a case study on cod (Gadus morhua) – Fisheries Research, 97(1-2), 2009, 59-71
7. Herrmann, B., Sistiaga, M., Nielsen, K.N., and Larsen, R.B. – Understanding the size selectivity of redfish (*Sebastes spp.)* in North Atlantic trawl codends – J. Northw. Atl. Fish. Sci., 2012, 44: 1-13.
8. Hua, K., Cobcroft, J.M., Cole, A., Condon, K., Jerry, D.R., Mangott, A., Praeger, C., Vucko, M.J., Zeng, C., Zenger, K., and Strugnell, J.M. – The future of aquatic protein: implications for protein sources in aquaculture diets – One Earth, 1(3), 2019, 316 329
9. Jafarzadeh, S., Ellingsen, H., and Aanondsen, S. A. – Energy efficiency of Norwegian fisheries from 2003 to 2012 – Journal of Cleaner Production, 112, 2016, 3616-3630
10. Lenihan-Geels, G., Bishop, K. S., and Ferguson, L. R. – Alternative sources of omega-3 fats: can we find a sustainable substitute for fish? – Nutrients, 5(4), 2013, 1301-1315
11. Prellezo, R. – Exploring the economic viability of a mesopelagic fishery in the Bay of Biscay - ICES Journal of Marine Science, 76(3), 2019, 771-779
12. Skjoldal, H.R., Dalpadado, P., and Dommasnes, A. – Food webs and trophic interactions - The Norwegian Sea ecosystem/Tapir Academic Press, 2004, 447-506
13. Valdemarsen J.W., Øvredal, J.T., Åasen, A., Gjøsund, S.H., Hansen, K. - Trålfangst: Årsaken til redusert effektivitet for enkelte tråltyper når fangsten øker. Sluttrapport til Fiskeri- og havbruksnæringens forskningsfond. Prosjekt 900285. Rapport fra Havforskningen Nr. 2-2011, 2011, 22 pp
14. Tang, M.F., Dong, G.H., Xu, T.J., Zhao, Y.P., and Bi, C.W. – Numerical simulation of the drag force on the trawl net – Turkish Journal of Fisheries and Aquatic Sciences, 17(6), 2017, 1219-1230

ENGINEERING PERFORMANCE OF SELF-ADJUSTING OTTERBOARDS IN COMPARISON WITH A CONVENTIONAL TRAWL OTTERBOARD

Morteza EIGHANI, Tiago VEIGA-MALTA, Finbarr G O'NEILL

National Institute of Aquatic Resources (DTU AQUA), Technical University of Denmark, North Sea Science Park, 9850 Hirtshals, Denmark

Abstract

For the purpose of improving hydrodynamic performance and reducing contact with the seabed, a new self-adjusting otter board (SAO) has been developed by MLD (https://mld.one/) for operating in demersal trawl fishery. The SAO has two flaps (upper and lower) that can be opened and closed in order to control the lift on the otter boards and thus control the horizontal and vertical position in the water. These dynamic otter boards can be controlled remotely by the skipper or by a positive feedback control system using acoustic signals. A full-scale experiment was conducted to compare the engineering performances of SAO against a conventional seabed-contacting design. There was no seabed contact when SAO was set to a target height of 5 meter above the seabed. Lift and drag coefficients at a towing speed of 1.54 m/s were calculated to be 2.25 and 0.48 for SAO and 1.48 and 1.18 for conventional door respectively. Thus, the efficiency (lift/drag ratio) of the SAO was 4.68 whereas that of the conventional otter board was 1.25. The results provide the information for fishermen to make an informed decision about the viability, engineering performance and fuel efficiency of self-adjusting otter boards.

Keywords

Self-adjusting otterboard; Hydrodynamic drag; Lift/drag ratio; Seabed contact; Trawl.

Nomenclature

C_L – lift force coefficient	[-]
C_D – drag force coefficient	[-]
ρ – sea water density	[kg/m^3]
V – towing speed	[m/s]
A – projected area of otter board	[m^2]
F_{spread} – lift force of otter board	[kgf]
F_{drag} – drag force of otter board	[kgf]
α – otter board attack angle	[◦]
φ – pitch angle of the otter board	[◦]

Introduction

The otter boards produce a hydrodynamic lift (spreading) force acting perpendicular to the direction of tow that is related to the horizontal expansion of the trawl at the cost of generating a drag force acting against the towing direction that must be overcome by trawler. While drag causes energy/fuel consumption, lift directly relates to the effectiveness, and lift-to-drag ratio characterizes the efficiency of the otter board (Balash et al. 2020). Otter boards can account for approximately 30% of the total trawl-system drag force trawling operations (Sterling and Eayrs, 2010; You et al., 2020). In general, the improvement of hydrodynamic performance, reducing the resistance, and mitigating seabed contact are the main challenges in the design of the otter board. In recent years, various studies have been conducted to improve the design and hydrodynamic characteristics of trawl otter boards. Developed designs include a door with a rectangular curved surface and a high aspect ratio, a comprehensive door with a slotted elliptical surface, cambered otter boards, multi-wing otter boards, airfoil-shaped otter board, a door with a vertical curved V-shaped surface, and a rectangular otter board with a slotted curved V-shaped surface (SEAFISH et al. 1993; Reite and Sørensen, 2004, 2006; Prat et al. 2008; Sala et al. 2009; Liu et al., 2014; Takahashi, et al. 2015; Wang et al. 2017; Su et al. 2018; Xu et al. 2017; Balash et al. 2020; Chu et al. 2020; Wan et al. 2021).

A new self-adjusting otter board (SAO) has been developed by the door manufacture MLD, Esbjerg, Denmark. The SAO is made up of three thin static foils of sheet material placed above a thicker flapfoil that contains the mechanical parts. Each otter board has two flaps that can be rotated about a shaft from 0◦ to 45◦ in order to control the otter board in both horizontal and vertical directions as follows: the upper flap controls movement in downward direction, the lower flap controls movement is upward direction, and the two flaps in combination controls movement in horizontal direction (Fig 1). Sonars positioned at the bottom of the SAO measure height above the seabed and a dynamic feedback system

controls the flap angles to ensure that the door spread and the height above the seabed are kept constant. Lift coefficient and lift to drag ration could be changed by changing upper and lower flaps angle consequently, it is possible to control the spreading force and altitude of the doors. Here we measure the lift and drag coefficients and the efficiency of the MLD doors and compare them with those of a conventional seabed-contacting door.

Material and methods

The trials were carried out in the Kattegat/Skagerrak Sea onboard of RV "Havfisken" (17 m L.O.A., 373 kW engine power). All hauls took place in same area with similar depth and substrata where water depth varied from 35 to 42 m and the substrata was sandy and muddy. Warp lengths were paid out 200 m for conventional and 136 m for SAO. A typical otter board Thyborøn type 2 with area of 1.78 m^2 was selected as the reference door. When the otter boards were changed through the trials, the rigging, the net, groundgear, floats etc. were kept identical. For the SAO, the door height was targeted as 5 m above the seabed. Each set comprised different speed settings along with two reciprocal course legs, one directly with the tide and one directly opposite to account for the effects of prevailing wind and water current conditions. 15 minutes of readings were then recorded from the instrumentations. During every haul the following technical data was recorded: warp and sweep tension (recorded at 1 second intervals from the load shackle), speed of the vessel (recorded by GPS) and speed of the net through the water (recorded by flowmeter), water depth, wind speed, and warp and sweep angles (reading from DST tilts).

The total length of SAO defined as the distance from the leading edge of the door to back edge of flapfoil. The door area calculated as 1.74 m^2.

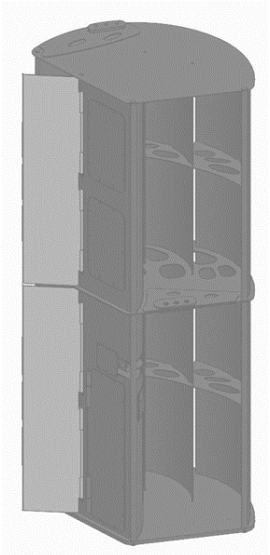

Figure 1
Schematic view of the self-adjusting otter board used during the sea trials; both flaps in 40 degrees adjustment expected to increase ~40% lift/spread.

The main parameters describing the hydrodynamic performance of otter board are lift coefficient (C_L), drag coefficient (C_D) and efficiency (C_L/C_D), whose calculation formulas can be described as follows:

$$C_L = \frac{Fspread}{0.5\frac{\rho}{g}V2A} \quad (1)$$

$$C_D = \frac{Fdrag}{0.5\frac{\rho}{g}V2A} \quad (2)$$

$$\text{Efficiency} = \frac{CL}{CD} \quad (3)$$

where the door spread and drag forces are calculated from the resolved components of the sweep tension behind the door and the warp tension ahead of the door, ρ is the fluid density (ρ = 1026 kg/m^3), g is gravity acceleration (m/s^2), V is the velocity of the otter board relative to fluid (m/s), A is the projected area of otter board (m^2), F_{spread} is the lift or spreading (kgf) force and F_{drag} is the drag (kgf) force. The efficiency (lift-drag ratio) is a main parameter for the performance of the otter board which enable to direct comparison of two otter boards. The higher the value of C_L/C_D the more efficient the otter board is.

The data was modelled using a generalized linear mixed effects model (GLMM) with a Gaussian distribution (Zuur et al. 2013). The mixed effect model's structure was:

$$Y = X\,ɞ + H + \varepsilon \quad (4)$$

Where Y is the outcome variable; X is a predictor variable; ɞ is the fixed-effects regression coefficients; H is the random effects and ε is the residuals. There are a random source where H denotes a vector of haul random effect of each door type, and is assumed to follow a normal (Gaussian) distribution: $H_i \sim N(0, Var(H_i))$ where H_i is hauls random effect in observation *i*. Therefore, Var(Y) = Var(H) + Var(ε). The variance components are estimated by the method of restricted maximum-likelihood (REML) (Patterson and Thompson, 1971), which set unbiased estimates for the variance components. The mixed effect model was implemented using the 'lme4′ package in R (Bates et al., 2012; R Core Team, 2020).

Results and discussion

The results of the trials are summarized in Table 1. Door drag force, coefficients of lift, drag, and efficiency for each door type are shown in Fig. 2, Fig. 3, Fig. 4, and Fig. 5 respectively, as a function of net speed.

The mean gear drag force at intermediate speed showed 19% reduction by SAO. The results showed that door type and speed significantly affect door drag. The door drag for SAO was consistently estimated to be significantly lower than for conventional door by about 69% at intermediate speed and this difference increases as speed increase. The resistance of the SAO accounts for up to 14% of the total-system drag while this value is estimated to be 28% for conventional doors.

Results for the SAO show lower values of drag coefficient and higher values of lift coefficient than the conventional door (Table 4). The drag coefficient of the conventional door is constant with speed while that of the SAO goes slightly down. The lift coefficient of both doors reduces with speed but the decline is steeper for the SAO. There is more variability in the measurements of the SAO values because of movement of the flaps. The efficiency (lift/drag ratio) of the SAO was 4.48 whereas that of the conventional otter board was much lower and in the range 1.16 to 1.36. Drag coefficient and efficiency of conventional doors were reported as 1.0 and 1.49 in a flume tank study (SEAFISH, 1993). The higher C_D value in our study in comparison with flume tank study might be due to seabed friction and ground shear effect. On the other hand, the drag coefficient and efficiency of the SAO were estimated to be 0.73 and 3.74 respectively in a flume tank experiment done by MLD (SINTEF, 2015). Generally, it is difficult to achieve a dynamic similarity between the prototype and the full-scale gear in particular when flap angle of prototype door was set at constant angle. Further, as seen in Fig. 6, there was no seabed contact in target height of 5 m above the seabed.

Conclusion

Engineering performance of SAO has been validated comprehensively through CFD simulations, flume experiments, and sea trials. First two phases have been completed by MLD and the final phase validated through the current study. In this study, full-scale trials is conducted to investigate the hydrodynamic performance and seabed contact of self-adjusting otter boards. Through an analysis of the results, the following conclusions are drawn:

(1) Overall, compared to the conventional otter boards, the SAO had up to ~69% less drag significantly. The resistance of the SAO accounts for up

to 14% of the total-system drag while this value is estimated to be 28% for conventional doors.

(2) Results for the SAO show lower values of C_D and higher values of C_L than the conventional door. The lift-to-drag ratio of SAO was exceeded 4.4, which is 3.5 times greater than for conventional otter boards, implying a 19% drag reduction for trawling systems.

(3) There was no seabed contact at all when the SAO height set as 5 m.

(4) Further study needs to investigate the catching performance of SAO in a demersal trawl fishery.

Table 1
Estimated values of angles and hydrodynamic coefficients respect to different speeds. Conventional (Con) and self-adjusting otter board (SAO), angle of attack of otter board (α), gear drag (GD), door drag (DD), drag force coefficient (C_D), spreading force coefficient (C_L), efficiency of otter board (Eff), and pitch angle of the otter board (ϕ).

Door type	Speed (m/s)	α	GD (kgf)	DD (kgf)	C_D	C_L	Eff	φ
Con	1.28	35	1456	366.5	1.23	1.68	1.36	10.1
	1.54	35	2028	555.5	1.24	1.55	1.25	12.3
	1.81	35	2483	754.5	1.24	1.44	1.16	15.2
SAO	1.28	16	1205	155	0.52	2.39	4.5	7.7
	1.54	16	1632	209	0.48	2.22	4.6	9.1
	1.81	16	2011	245	0.43	1.98	4.6	11.3

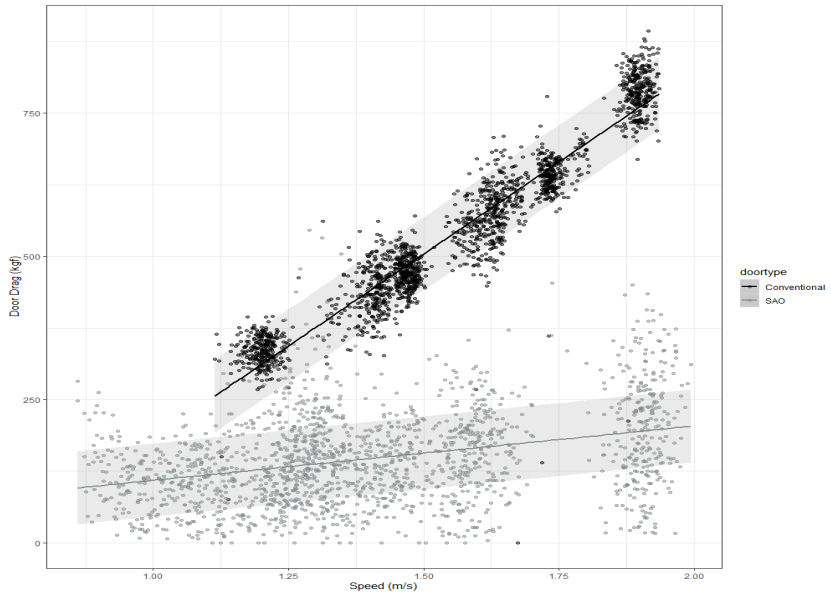

Figure 2
Estimated curve for comparing door drag between door types. Points represented experimental observations and shaded area represented 95% confidence interval.

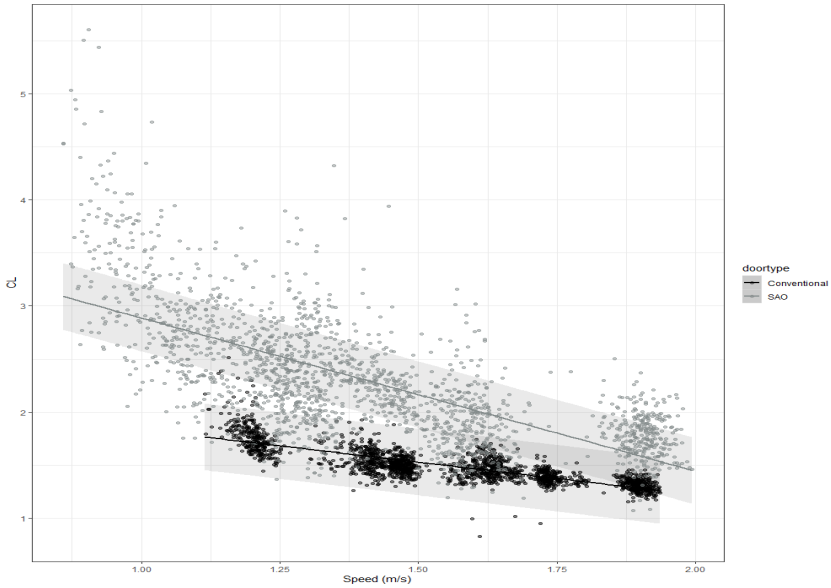

Figure 3
Comparison of lift coefficient between SAO and conventional doors. Shaded area represented 95% confidence interval.

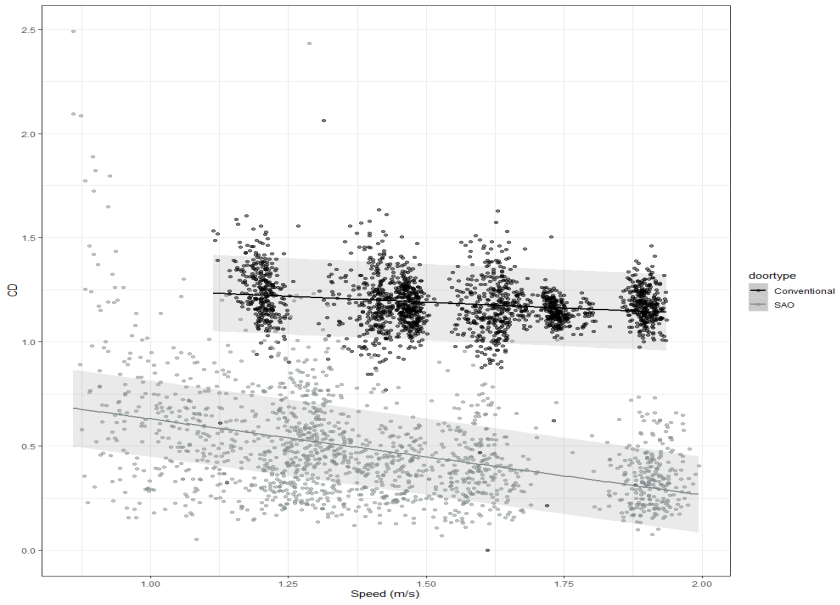

Figure 4
Comparison of drag coefficient between SAO and conventional doors. Shaded area represented 95% confidence interval.

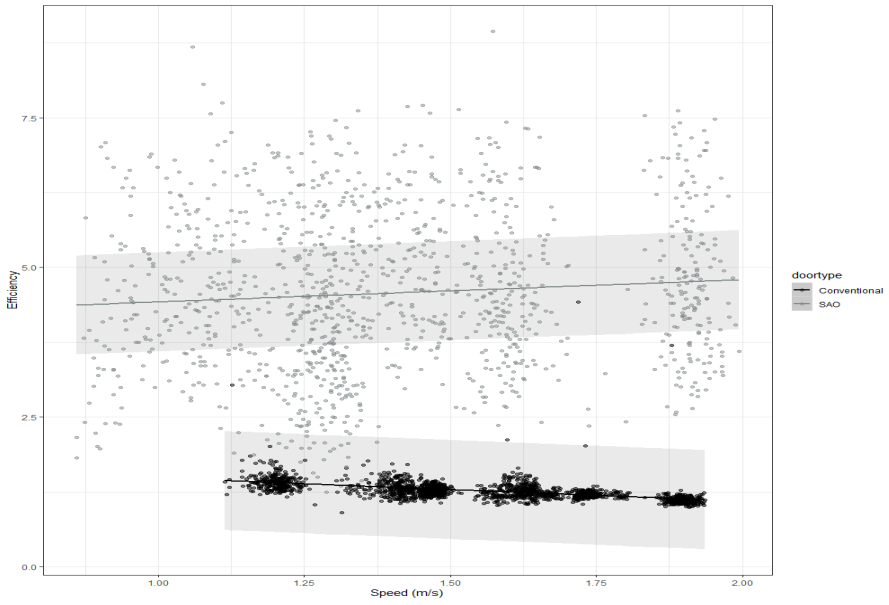

Figure 5
Predicted efficiency of SAO in comparison with conventional door. Shaded area represented 95% confidence interval.

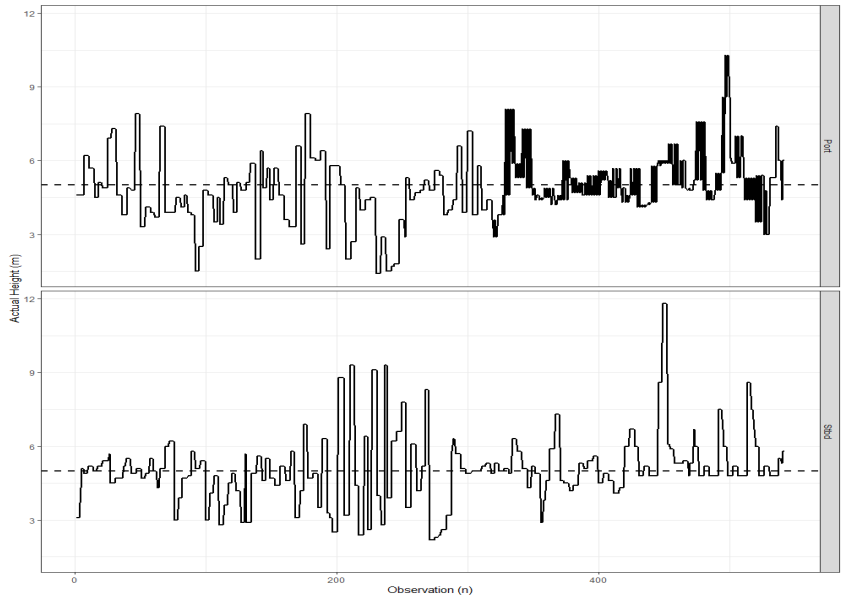

Figure 6
Actual height of SAO during the hauls respect to the port and starboard sides. Black dashed line shows target height.

Acknowledgements

This study received funding from the Ministry of Environment and Food of Denmark through the Green Development and Demonstration Program (GUDP), project STEER 34009-20-1649.

References

1. Balash, C., Blake, W., and Sterling, D. - Seeking maximum effectiveness and efficiency for large multi-sail penaeid otter boards - Ocean Engineering, 200, 2020, 107093.
2. Bates, D., Maechler, M., and Bolker, B. - lme4: Linear mixed-effects models using Eigen and S4. R package version 1.0-5 - Available at http://CRAN.R-project.org (July 2022).
3. Chu, W., Chen, G., Ye, X., and Cui, X. - Hydrodynamic performance and structural response characteristics of the double-slotted vertical cambered V-Type otter board - Aquaculture and Fisheries, 5, 2020, 201-209.
4. Liu, J., Huang, H., and Wu, Y. - Model test of hydrodynamic characteristics of two types of vertical cambered slotted otter boards - South China Fisheries Science, 1, 2014, 68–74.
5. Patterson, H.D., and Thompson, R. - Recovery of Inter-Block Information When Block Size Are Unequal - Biometrika, 58, 1971, 545-554.

6. Prat, J., Antonijuan, J., Folch, A., Sala, A., Lucchetti, A., Sardà, F., and Manuel, A. - A simplified model of the interaction of the trawl warps, the otterboards and netting drag - Fisheries Research, 94, 2008, 109–117.
7. R Development Core Team. 2020. R: A language and environment for statistical computing. Vienna, Austria: R Foundation for Statistical Computing. Retrieved from http://www.R-project. org. Accessed on 14 Jun 2021.
8. Reite, K.J., Sørensen, A. - Mathematical modelling of the hydrodynamic forces on a trawl door. Journal of Ocean Engineering, 31, 2006, 432–453.
9. Reite, K.J., Sørensen, A.J. - Hydrodynamic properties important for control of trawl doors. In: Katebi, R., Longhi, S. (Eds.), Control Applications in Marine Systems. International Federation of Automatic Control, 2004, Ancona, Italy, pp. 143–148.
10. SEAFISH, IFREMER, DIFTA, 1993 - Otterboard Performance and Behaviour - Commission of the European Communities FAR, 159 pp.
11. SINTEF, 2015 - Flume tank tests with controllable trawl door - Project memo, 15 pp.
12. Sterling, S., Eayrs, S. - Trawl-gear innovations to improve the energy efficiency of Australian prawn trawling - First International Symposium on Fishing Vessel Energy Efficiency, E-Fishing, Vigo, Spain, May 2010.
13. Su, X., Lu, H., and Feng, B. - Hydrodynamic characteristics of the double-winged otter board in the deep waters of the Mauritanian Sea – Journal of Oceanology and Limnology, 36, 2018, 1417–1424.
14. Takahashi, Y., Fujimori, Y., Hu, F., and Kimura, N. - Design of trawl otter boards using computational fluid dynamics - Fisheries Research, 161, 2015, 400-407.
15. Wan, R., Guan, Q., Huang, L., Li, Z., Zhou, C., Wang, L., and Jia, M. - Effects of otter board and cable length on hydrodynamic performance of Antarctic krill trawl system - Ocean Engineering, 236, 2021, 109408.
16. Wang, L., Wang, L., Feng, C., Zhou, A., Yu, W., Zhang, Y., and Zhang, X - Influence of main-panel angle on the hydrodynamic performance of a single-slotted cambered otter-board - Aquaculture and Fisheries, 5, 2017, 234-240.
17. Xu, Q., Huang, L., Zhao, F., and Liu, C. - Study on the hydrodynamic characteristics of the rectangular V-type otter board using computational fluid dynamics - Fisheries Science, 83, 2017, 181–190.
18. You, X., Hu, F., Kumazawa, T., Dong, S., and Shiode, D. - Hydrodynamic performance of a newly designed biplane-type hyper-lift trawl door for otter trawling - Applied Ocean Research, 104 (2020), Article 102354.
19. Zuur, A.F., Hilbe, J,F., and Ieno, E,N. - A Beginner's Guide to GLM and GLMM with R - Highland Statistics Ltd. 2013, 256 P.

EXPERIMENTS ON THIN-TWINE NET PANELS

Uwe LICHTENSTEIN[a], Karsten BREDDERMANN[b], Sascha KOSLECK[b]

[a] Thünen Institut of Baltic Sea Fisheries, Alter Hafen Süd, Rostock, 18069, Germany
[b] University of Rostock, Ocean Engineering, Department of Mechanical Engineering and Marine Technology, Justus-von-Liebig-Weg 2, Rostock, 18059, Germany

Abstract

New high-strength materials used for production of netting structures allow for a reduction of the twine diameter. This results in a reduced drag of the netting when exposed to a fluid flow. Consequently, a trawl built with such materials has less drag, so less fuel would be consumed during trawling.
Also, aquaculture cages would benefit from using smaller twine diameter netting. A good water quality inside the cage is of utmost importance for the health of the fish stock. The use of netting with a smaller twine diameter would reduce the blockage of the netting and thus would result in an enhanced fluid exchange in the cage, keeping the water quality at a high level.

However, precise information of drag and lift of these high strength materials is missing, which is necessary as input for simulation tools to predict the shape of netting structures as well as the fluid field inside and around these. Therefore, wind tunnel experiments have been conducted to record drag and lift coefficients of a high strength PE material with a twine diameter of 1.8 mm and a half mesh size of 60 mm. Four net panels have been measured with a hanging ratio of 0.2, 0.3, 0.4 and 0.5 respectively. The angle of attack varied from 0° to 90° and the measurements were done at wind speeds of 16, 20, 24 and 28 m/s.
The unique details and the results of the experiments will be presented here.

Keywords

net panel, drag and lift coefficients, wind tunnel tests, net hydrodynamics

Nomenclature

A – area
C – hydrodynamic Coefficient
F – force
L – length
Re – Reynolds Number
a – mesh size (half mesh)

m – number of meshes in length of net panel
n – number of meshes in width of net panel
u – hanging ratio (u1 – lateral, u2 – longitudinal mesh-direction)
v – velocity
α – mesh opening angle ($\alpha = \sin^{-1}(u1)$)
β – angle of attack
η – dynamic Viscosity
ρ – density

Introduction

With the increased use of high strength materials for netting, the overall twine area and therefore the drag of the trawl decreases. However, little is known about the hydrodynamic behaviour of such materials.

The aim of this work was therefore to provide detailed information about the behaviour of thin twine netting material in a flow field. To do so, the forces acting on the net panel in the flow were recorded at known air speeds and angles of attack in the wind tunnel.
Four net panels of 8 x 8 meshes of the same 1.8 mm twine material but at different hanging ratios have been investigated. The mesh size of the net panels was 60 mm. With the forces recorded, the geometrical parameters of the net panels and the flow information from the wind tunnel, the force coefficients in longitudinal and transverse direction with respect to the flow direction have been calculated for each setup.

Previous Work

Many experiments like this have been conducted either substituting the actual net with a grid made from metal bars (Bortlik and Hoffmann [1] and Kruse [2]) or placing the net panel in a rigid frame (Madsen et al [3]). Both methods have their drawbacks. With rigid bars, usually the knots of the net are neglected and the surface of the bars is smoother than that of the actual netting material. Using actual nets on the other hand requires said frame to place the net panel rigidly in the flow field. However, the frame tends to influence the flow field significantly. Subtracting that influence from the results is sometimes hard to realize.
Another simplification is the limited size of the net panel compared to the net structures in real life applications. The flow often reaches the net panel undisturbed which is not the case for a section of netting within a trawl. Here most parts of the netting structure would be in a flow field effected by other parts of the trawl. One way to overcome this modelling problem is to place an object, preferably netting or a grid, in the flow in front of the net panel. Bortlik and Hoffmann as well as Kruse used for their experiments a metal grid with

hinges at the knot positions. That way, the hanging ratio could be adjusted as desired. The hinges at the knot position were an additional deviation from the real life netting. Bortlik and Hoffmann also investigated the effect of placing an extra row of the grid in front of the actual grid panel.

Materials and Methods

The experiments have been conducted at the wind tunnel facility of the Chair of Ocean Engineering at the University of Rostock in February 2022.
The net panels investigated were made from high strength polyethylene with a twine diameter of 1.8 Millimetre and a mesh size of 60 Millimetre half mesh. There have been four net panels of 8 x 8 meshes with hanging ratios of 0.2, 0.3, 0.4 and 0.5 respectively. As the number of meshes kept constant, the hanging ratio is also a reference for the solidity of the panels.
When it comes to testing of net panels, usually, the influence of the model holder has to be considered very carefully. Even more so with decreasing twine diameter as the ratio between twine area and covered area decreases as well which in turn increases the effect of the model holder in relation to the effect of the actual model. In order to reduce the model holding bracket to a minimum size, the netting material has been cut to four pieces which were soaked in epoxide resin and put in frames under tension with the desired hanging ratio to let the resin set.

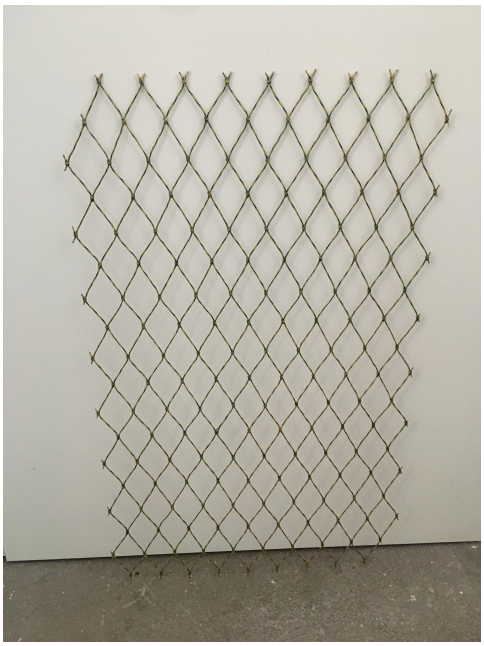

Figure 1
Netting material after treatment with epoxide resin

This process resulted in stiff net panels with fixed mesh openings as shown in Figure 1. However, due to the small twine diameter, the net panels were still too flexible to be fixed with a single bracket to the 6-axis load balance of the wind tunnel, especially under wind load.
For the experiments, the net panels had to be additionally stabilised. This was realized by building a second 6-axis load balance which was fixed to the traverse-system of the wind tunnel and placed overhead above the measuring section. That way, the bracket holding the net panel could be fixed at the lower and upper end. Furthermore, the measuring section was limited at the bottom by a table covering the lower load balance and by an end plate at the top end of the net panels. Also, the upper load balance has been encased to prevent any influence of the wind flow on it. The final setup is shown in Figure 2.

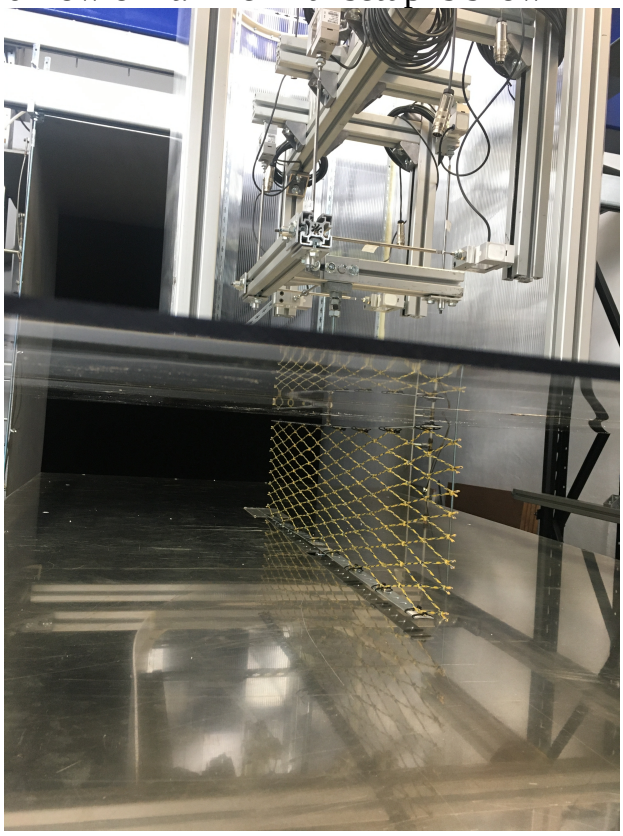

Figure 2
Net panel in measuring section of the wind tunnel with end plate and second load balance

The tests were conducted under Reynolds' law of similarity, which states that the flow field around two geometrically similar objects is similar too when the Reynolds Number in both cases is constant. The Reynolds Number, as seen in Equation (1), expresses the ratio of inertial forces to viscous forces.

$$\mathrm{Re} = \frac{\rho v L}{\eta} \tag{1}$$

For these tests, that means that the flow around a net in water has to be re-created with a similar net in air as the fluid medium.

$$\mathrm{Re} = \frac{\rho_w v_w L}{\eta_w} = \frac{\rho_a v_a L}{\eta_a} \tag{2}$$

The indices w and a in Equation (2) representing the medium water and air respectively. The characteristic length, L in Equation (1) and (2) is here the twine diameter of the netting material. As this is the same for the real life application and the test case, the air speed of the wind tunnel tests can be calculated according to Equation (3).

$$v_a = v_w \frac{\rho_w \eta_a}{\rho_a \eta_w} \tag{3}$$

For convenience reasons, the calculated air speed has been rounded for the speed adjustment of the wind tunnel as shown in Table 1.

Table 1
Towing speed in water and corresponding air speed for wind tunnel tests

Towing speed in water in kn	Calculated air speed in m/s	Set air speed in m/s	Reynolds number
2	15.81	16	~2000
2.5	19.76	20	~2500
3	23.71	24	~3000
3.5	27.67	28	~3500

For each panel and each velocity, the angle of attack has been varied from 0° to 90°. The steps between have been adjusted over the full span. For small angles of attack up to 20 degrees, the step between each measurement was five degrees. Additionally there have been three measurements around the angle of attack that was expected to yield the maximum lateral force with a step of ten degrees between them. The final measurement was then taken at 90° which should represent the angle of attack with the highest drag force.
Furthermore, for each setup there has been a series of measurements with a separated row of meshes in front of the net panel to establish a disturbed flow around the actual panel. For that series, the last angle of attack of 90° has been skipped as the effect was suspected to be marginal and also because the space in the measuring section was not sufficient to place that extra row of meshes.
A summary of the different setups is given in Table 2.
In order to obtain the forces in longitudinal and transverse direction with respect to the flow direction, it was only necessary to record the forces in x- and y-direction in the coordinate system of the load balances in which the x-axis is

aligned with the flow direction, y is parallel to the end plate and at a right angle to the x-axis, and the z-axis is in the vertical direction. The forces were recorded simultaneously at both load balances and combined later in the data processing. The z-component was not recorded since there were no fluid loads expected in this direction.

Table 2
Overview of tested parameters

Variable	values
Angle of attack	0°, 5°, 10°, 15°, 20°, 45°, 55°, 65°, 90°
Hanging ratio u1	0.2, 0.3, 0.4, 0.5
Air speed	16 m/s, 20 m/s, 24 m/s, 28 m/s
Additional row of meshes	with (up to 65°), without

Experimental Results

Exemplary for the collected data, Figure 3 shows the recorded forces in the two relevant directions at a flow velocity of 28 m/s. Likewise, the same forces are depicted in Figure 4 but rather for the constant hanging ratio of 0.3. Based on the coordinate system of the measurement equipment, the force in y-direction is negative.

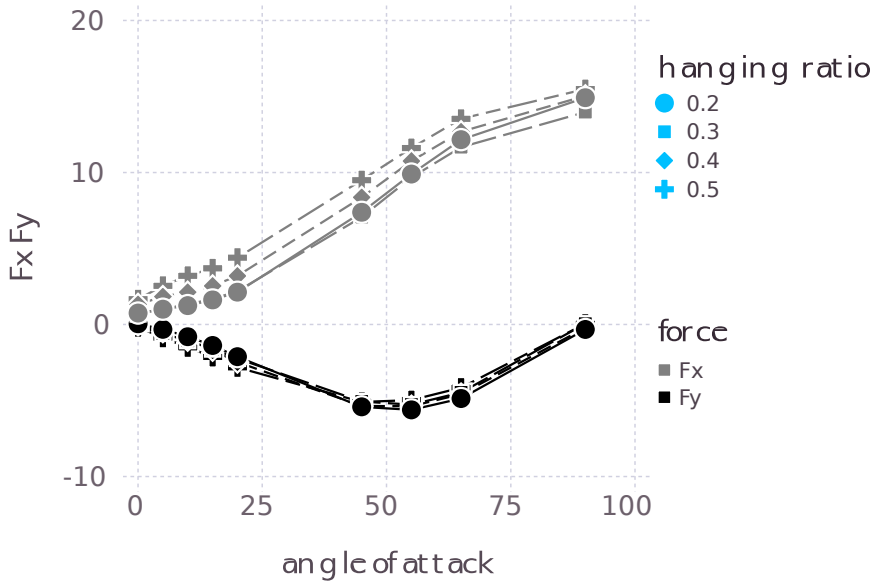

Figure 3
Recorded forces in x- and y-direction for the tested hanging ratios at 28 m/s air speed

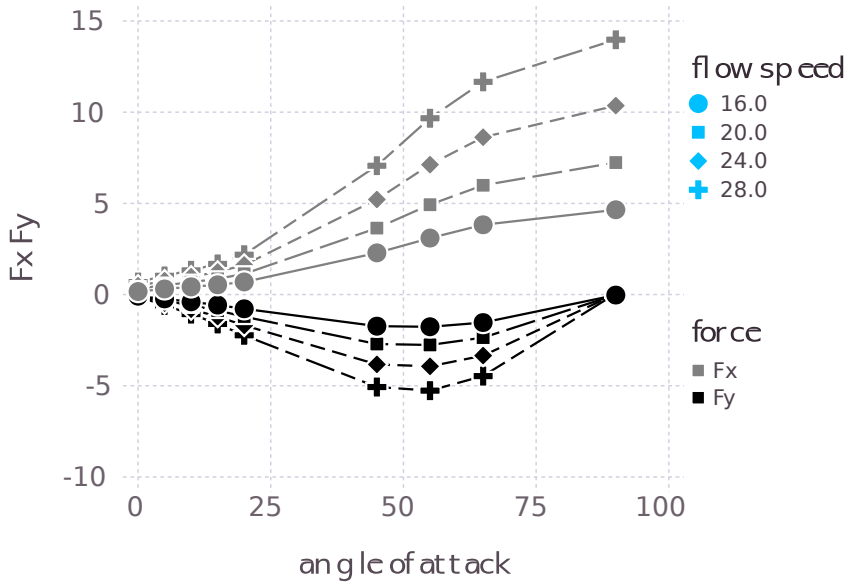

Figure 4
Recorded forces in x- and y-direction for the tested air speeds with a hanging ratio of 0.3

From the formula for the hydrodynamic force, Equation (4), the Equations (5) and (6) for the hydrodynamic coefficients can be derived.

$$F = C\frac{\rho}{2}v^2 A \tag{4}$$

$$C_x = 2\cdot\frac{F_x}{\rho v^2 A} \tag{5}$$

$$C_y = 2\cdot\frac{F_Y}{\rho v^2 A} \tag{6}$$

Here, the indices x and y are representing the direction of the force were x corresponds to the longitudinal or drag and y to the lateral force of the panel.
For the calculation of the hydrodynamic coefficients, the area A is the twine surface area. This is in accordance with the experiments of Bortlik and Hoffmann who gave the formula for the twine surface area as shown in Equation (7).

$$A = 4\cdot mn\pi d\left(a - \frac{d}{2\cdot\sin(2\cdot\alpha)}\right) \tag{7}$$

As a comparison, Figure 5 shows the results from Bortlik and Hoffmann from a grid that came closest to the set-up used for the present experiments together

with some of the recent results. There is a good overlap for the drag coefficients but not so much for the lift coefficients. As the investigated angles of attack were limited to a maximum of 30 degrees, there is no comparison of the shape of the curves possible. However, looking at the results from Madsen et al., the shapes of the curves are very similar with the maxima reached around the same angles of attack. Only the values differ as the material tested was different and the reference area too.

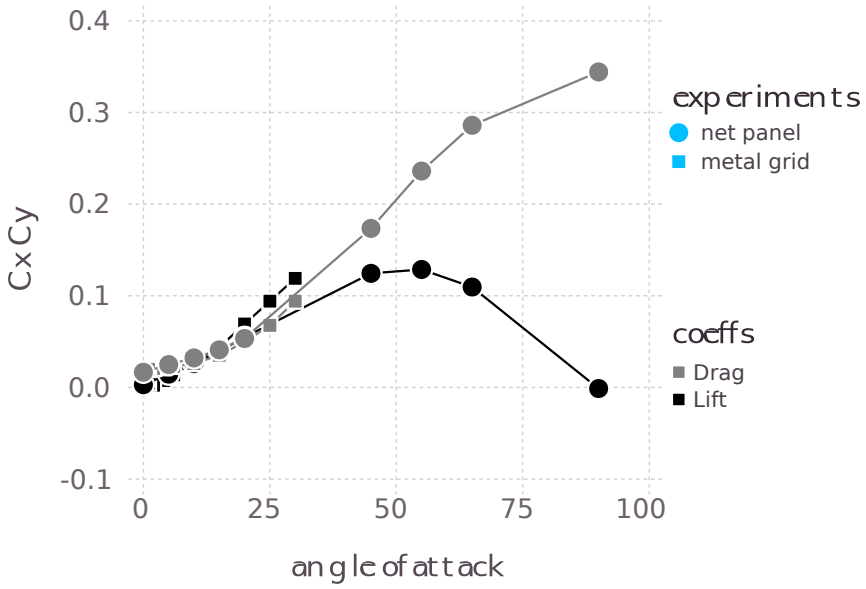

Figure 5
Lift and drag coefficients from Bortlik and Hoffmann compared to the recent results with a hanging ratio of 0.3 at 28 m/s air speed

When looking at Figure 7, it can be clearly seen that there is a Reynolds number independency for the hydrodynamic coefficients at the tested air speeds.
Interestingly, the smallest hanging ratio and therefore highest solidity does not necessarily lead to the highest lift or drag, at least not over the full range of angle of attack (Figure 2 and 6).

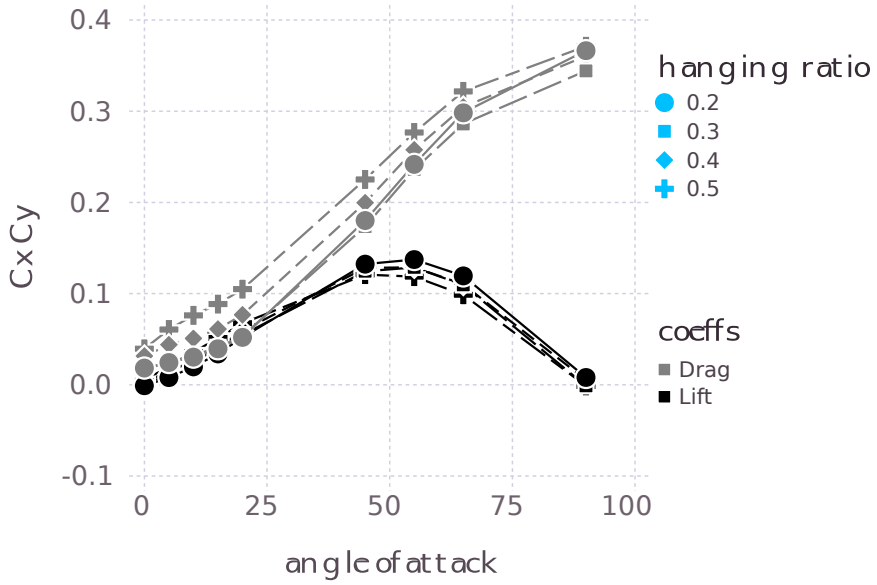

Figure 6
Lift and drag coefficients related to the twine surface area for the tested hanging ratios at 28 m/s air speed

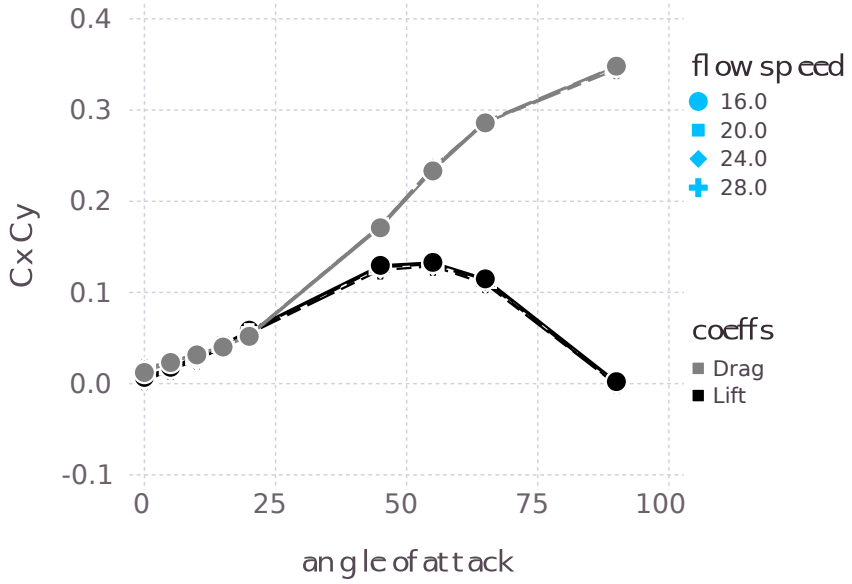

Figure 7
Lift and drag coefficients related to the twine surface area for the tested air speeds with a hanging ratio of 0.3

In contrast to the results from Bortlik and Hoffmann, the measurements with the separated row of meshes placed in front of the net panels did not give any

different results from the measurements without that extra mesh row. It seems, the influence from this kind of material is too little, at least from a single row of meshes. To verify this assumption, further experiments with other flow disturbing objects, like a bigger piece of such material, would be needed.

Conclusions

As a main achievement it was accomplished to create a comprehensive dataset for the tested material. For the ongoing project SimuNet, this will be used to verify the discretisation approach chosen for substituting the net material in CDF-simulations. Furthermore, the procedure to create supplementary datasets for other materials, if needed, was determined.

Acknowledgements

The research described in this paper was funded by the European Maritime and Fisheries Fund and the Federal state of Mecklenburg – Western Pomerania, Germany, under ID no. MV-I.16-LM-002, SimuNet - Ein Werkzeug zur Fanggeräteoptimierung.
The authors would also like to thank the colleagues at the Chair of Ocean Engineering at the University of Rostock for their support during the setup and operation of the wind tunnel facility.

References

1. Bortlik and Hoffmann – Strömungstechnische Untersuchung an Netzgittermodellen – Report, 1989
2. Kruse, W. – Strömungstechnische Untersuchung an ebenen Netzgittermodellen – ein Beitrag zur Ermittlung hydrodynamischer Belastungsfunktionen des Netzteils von Schleppnetzen, Dissertation WPU-Rostock, 1979
3. Madsen, N., Hansen, K. and Enerhaug, B. – Experimental analysis of the hydrodynamic coefficients of net panels in the flume tank in Hirtshals – Contributions on the Theory of Fishing Gears and Related Marine Systems, 7 (Proceedings of the DEMaT 2011), 2011, ISBN 978-3-8440-0468-7, pp. 131-140
4. Paschen, M. and Winkel, H.-J. – Flow investigations of net cones – Contributions on the Theory of Fishing Gears and Related Marine Systems, 1 (Proceedings of the DEMaT 1999), ISBN: 3-929544-95-4, pp. 197-216

EXPERIMENTAL CONSIDERATIONS FOR FLEXIBLE OFFSHORE STRUCTURES

Ignacio León Hernando[1], Sascha Kosleck[2]

Rostock Universität, Lehrstuhls für Meerestechnik, Oskar-Kellner-Institut (OKI), Justus-von-Liebig-Weg 2, 18059 Rostock

Rostock Universität, Lehrstuhls für Meerestechnik, Oskar-Kellner-Institut (OKI), Justus-von-Liebig-Weg 2, 18059 Rostock

Abstract

In this paper the state of the art of the experimental methods used for offshore structures and offshore tools, mainly focusing on tools and constructions related to fisheries and aquaculture, is explored. An overview of the most common types of flexible structures, together with the mathematical models used for their representation is presented. Furthermore, using the main physics of the fluid structure interaction problem and, by relaying in a dimensional analysis of it, the concept of similarity in the classical experimental set-up of flexible structures is criticized.

With all the above, the scope of this paper is to expose the accuracies and flaws of the experimental methods in the field of offshore flexible structures. With the aim to raise the awareness of the limitations and special considerations that need to be taken during the experimental campaigns.

Keywords

Flexible structures, Morison's equation, fishing gear, fluid structure interaction.

Introduction

Most of the constructions of mankind, nowadays even more so, are based on rigid materials such as steel. It is simple to grasp that the usage steel or other metallic materials bring several advantages, they are simple to shape and to join, their availability is worldwide, and most importantly they have outstanding mechanical properties that make them perfect for almost all structural applications. However in the field of offshore engineering there are still points of application where such materials usage is limited, cases of this are fishing gears, cables in general and aquaculture installations.

Due to their great rigidity, or put in another way, low damping, sea loads are less than forgiving in such structures and the engineering requirements heavily intensify. For example, pen-net fish cages, the structures that will be the focus of this paper and that are widely used in the Norwegian seas to grow and harvest salmon, are made of a flexible floating ring from which a half oval net, conformed by

plastic-based threads, hangs. The flexibility of the material translates in a deformation of the structure, following currents and wave motions, which implies low structural loads on the expense of a reduced living space for the fish.

However, these structures are associated with an additional problem in terms of design. This is, that contrary to highly rigid structures which can be easily considered completely rigid from the point of view of the fluid-structure calculations, these flexible structures cannot. Under these circumstances the designer needs to rely on empirical or semi-empirical approaches to the problem and work with simplified mathematical models.

In the following sections some of such experimental approaches will be mentioned and evaluated. In the same manner, the models used for the simulations of such structures will be judged.

Into the concept of scaled model tests

When facing with the problem of designing such a structure, for example a pen-net fish farm, the first most valid approach would be to do model tests of it. With this the designer would theoretically be able to determine the main design parameters. The question remains, however, in how to confront model scale tests, in other words, if a model scale fish cage were to be tested the researcher should know if the model test results are scalable or at least significative of the full scale or not.

To successfully do model test, it is important that the model and the model set-up match the so-called similarity.

Geometric similarity exists when model and net are the same shape and all linear dimensions of the model are related to the corresponding dimensions of the prototype by a constant scale factor [1].

The dynamic similarity is related to how forces cause accelerations. At corresponding points in the flow, identical kinds of forces are parallel for the case of the model and the prototype and are related by a constant scale factor [1].

Finally, the kinematic similarity needs to be complied with. In this case velocities at corresponding points (corresponding points are points of the set-up that are at the same scaled distance in the model as in the prototype) in the two flows (model and prototype) are in the same direction and are related by a constant scale factor in magnitude. Additionally, flow regimes must be the same (laminar, turbulent) [1].

Non-dimensional numbers or coefficients are relations between physical effects that are comparable in units. This allows for the comparison of the effects of different forces types.

In this particular problem the forces that affect the system are viscous, gravitational, inertial forces and internal body forces.

To relate these forces to each other in this paper the chosen dimensionless parameters should be the Reynolds number (R_e), the mass number (M), and the Cauchy number (C_Y).

$$R_e = \frac{\rho_f U_0 L}{\mu} \quad (1)$$

$$M = \rho_f / \rho_s \quad (2)$$

$$C_Y = \frac{\rho_f U_0^2}{E} \quad (3)$$

Let us assume now that we want to engage in an experimental campaign to evaluate the previously mentioned offshore closed fish farm. Our goal should be to archive geometrical, kinematical and dynamic similarities during the process so we can then scale the results by means of the dimensionless parameters. Let us assume that the main parameters of the problem are simple and as presented in Table 1.

Table 1: Example of scale vs full scale model test

Parameter	**Model value required parameter**	**Full scale**
Material	(?)	Nylon
Scale of the model	1:50	1:1
Density [kg/m^3]	1150	1150
Diameter [m]	2.00E-05	0.001
Trawl speed [m/s]	100	2
Density/Young [kg/m^3GPa]	1.59E-10	3.97E-07
Re	1.68E+03	1.68E+03
CY	1.59E-06	1.59E-06
M	8.91E-01	8.91E-01

From the beginning one can appreciate the complexity of the problem, first of all, to archive geometrical similarity the twine diameter would need to be 0.02 micrometres. Also because of this, to archive the same Reynolds number the fluid media would need to be either extremely dense, or if it is towed in salt water extreme speeds would need to be archived.

If the model tests are being taken in salt water and a material with the same density as the nylon in used as well, so that the mass number can be matched. This will keep the relative gravity forces in the same proportion; however, the Cauchy number will be greatly influenced. Because to maintain the same Cauchy number the relation between the density and the young modulus will need to be one hundred orders of magnitude different. Such material simply does not exist.

Experiments with full scale nets or other flexible structures

Once understood that scaling model tests is a challenging matter at best, the designer will either have to do full-scale tests, which defeats the purpose of efficient preliminary design, or relay on numerical methods that can approximate the solution.

For this second option there are two differentiated routes that can be taken, on one hand there is the option of complex numerical tools such as CFDs, on the other are semi-empirical formulas. In the CFD field the state-of-the-art shows that it is feasible to present good results in the fluid domain solution. However, due to the small scale of the netting, it is not feasible to archive a computational mesh accurate enough and that would allow the full cage-mesh problem to be solved in a feasible amount of time[2]. In this case the preferred approach is the usage of porosity models to account for the pressure and velocity reduction of the field, and the usage of FEM models for the deformation of the net [3], [4]. Others implement the semi-empirical formulas in the CFD codes to use the velocity field generated by the numerical codes[4].

At the end, it seems unavoidable to go through the usage of semi-empirical formulas, in particular the usage of the Morison equation [4]. Which depend on experimental values because of the drag and mass coefficients which are needed to describe the physics of the problem.

The option is then to engage in experimental campaigns, trying to test significant pieces of material that could represent by themselves the desired coefficients on the whole structure. Some examples are given below.

Currently, the focus of interest is the determination of the drag coefficient as it is usually assumed that the condition to be of most interest is the fishing gear or fish farm under a constant flow speed. There are several pieces of literature that approach this from a similar way. Reference [5] presented experimental results of a

large model on a fjord, in which deformation of the cage, drag and velocities in different points were measured. A comparison of the results with literature presented is also given in their publication [5], and in such comparison, it can be seen that the Morison approach overestimates the drag force at high flow speeds because of the reasons mentioned above. Moreover, these results can be said to be useful for that specific geometry and size, but scaling the results will lead to dubious results.

In the works of [6] two dimensional sheets of netting at small angles of attack were tested in the wind tunnel. The net is tested horizontally (holes are perpendicular to the flow direction), and it is made of aluminium, therefore the flexibility of the structure is not considered. In the aft of the net different plates with different porosities were tested to study the impact of clogging in the distribution of forces of the grid. The result was a noticeable effect on the drag and lift forces depending on the clogging of the plate. These experimental results are interesting to understand a part of the physics of the problem, however the data found might not be extrapolated to more general cases.

The works presented in [7] show both a screen method and experimental results for a square net in constant flows and at different Kreulegan-Carpenter number (KC). This formulation was however proven by [8] to underestimate the contribution of the drag coefficient at high angles of attack. Because of the specific geometry, these model tests are useful in the context of the screen model approach, but they do not guarantee that the extrapolation of such panels to a complex geometry will generate equivalent results. An interesting part of the experiments of the authors was the oscillatory flow testing, from which it was discovered that the added mass coefficient is large in comparison with single cylinders, tested in [9]. Moreover, the added mass coefficient seems to be independent of twine diameter or net solidity. This is yet another proof of how applying Morison equation or similar methods blindly can deal to great errors in computation. In the work of these authors the oscillatory effects were normalized to an effective thickness and a modified KC number, giving some intuition on the correlation of these values. However, nothing more than an intuition on this relation was presented, leaving the physics of the problem unresolved. Therefore, here it can be observed how the impact of the net on the fluid and the complexity in the interaction make simplistic models unrealistic.

Evaluation of the physics of the problem

The literature shows clear limitations in what seems to be the only method available to approach the design of these structures. However no real explanation behind the physics of Morison's formula is given[10], and it is then difficult to identify the source of error.

Thus, to be able to evaluate the numerical models as well as the experiments being made in the state of the art, a comprehensive look into the physics of the problem is needed. The scope is to understand the main drivers of the forces and interactions, as well as the effect of such interactions between both domains: The solid and the fluid domain.

For the fluid domain the constitutive equations that define the problem are the mass balance and the momentum balance. This set forms the Navier-Stokes equations for incompressible fluids.

$$div\, U = 0 \tag{4}$$

$$\rho \frac{d\underline{U}}{dt} = -\rho \underline{g} e_z - \nabla \underline{p} + \mu \Delta \underline{U} \tag{5}$$

For the solid, it can be considered that the modal approximation formulation represents sufficiently well the movement of the solid. In a single mode approximation, the displacement of the body $\xi(x,t)$, can be represented by a modal displacement function $q(t)$ and a modal shape $\varphi(x)$ as shown in. Additionally, it is fairly common to use the equation of the spring mass model, as it is applicable to most oscillatory problems

$$\rho \underline{\xi(x,t)} = \underline{q(t)} \varphi(x) \tag{6}$$

$$\rho m \frac{d^2 \underline{q}}{dt^2} + k \underline{q} = \underline{f} \tag{7}$$

Next, the interconnection between the fluid and solid domain. Such connection is given by the kinematic and the dynamic conditions. In the first place, the kinematic condition connects the velocities of both domains, making them the same at the interface. This reads:

$$\underline{U}(\underline{x},t) = \frac{\partial \underline{\xi}(t)}{\partial t} = \frac{d\underline{q}(t)}{dt} \underline{\varphi(\underline{x})} \tag{8}$$

The second condition, the dynamic condition, equals the forces in the domain. On the fluid side we have the pressure and viscous forces acting on the free surface, meanwhile in the solid side we have the quantity called modal force f. The dynamic condition reads:

$$\int_{interface} \left(\left(-p\underline{\underline{I}} + \mu(\nabla \underline{U}) \right) \underline{n} \right) \varphi dS = \underline{F_{FS}} \quad (9)$$

$$F_{FS} = \underline{f} \quad (10)$$

This gives a simple overview of the physics involved in the FSI (Fluid-Structure-Interaction) problems, due to the multiple correlations and the unknowns in the equations, such problems are not simple to solve.

Morison's equation: A look into the correlation with complex models

As mentioned above, such formula is the most used approach to tackle flexible slender structures. However, there is little critic or analysis of such equation, and even though one can find some literature that proves that there exist certain limits of application industry and researches use it comfortably in almost any scenario. The reason is that, the equation does not only produce good results in most cases, but it is also intuitive. The total force is a subdivision of damping forces and inertial forces, which are characterized by two experimental coefficients C_D and C_M.

$$F_{Morison} = \rho C_M V \underline{\ddot{x}} + 0.5 \rho C_D A (\underline{\dot{x}_{flow}}^2 - \underline{\dot{x}}_{body}^2) \quad (11)$$

Such equation was specifically made for oscillatory flows and slender structures, but in practice it is widely used for a wide range of shapes, sizes and flows.

Morison's equation can be understood as a simplification of the conservation of fluid momentum. From such equations, the Morison equation is equivalent to the volume and surface integral of the velocities around the body. Pressure and gravity forces are not considered and need to be included separately.

The mathematical formulation of the momentum theorem, [11]:

$$\frac{\partial}{\partial t} \int_V (\rho \underline{U}\, dV) + \int_S (\rho \underline{U}\, (\underline{U}\, \underline{n}) dS) = -\underline{F_e} - \int_S \underline{p} n dS + \int_V \rho \underline{g} dV \quad (12)$$

In the Morison equation the force due to density and pressure differences need to be included separately. The Morison equation can then be seen as a simplification of such integrals in the way:

$$-\underline{F_e} = \frac{\partial}{\partial t} \int_V (\rho \underline{U}\, dV) + \int_S (\rho \underline{U}\, (\underline{U}\, \underline{n}) dS) = \rho C_M V \underline{\ddot{x}} + 0.5 \rho C_D A (\underline{\dot{x}_{flow}}^2 - \underline{\dot{x}}_{body}^2) \quad (13)$$

This shows that the Morison equation premise of inertia and drag forces is more than a simple intuition of how the physics of the problem should work. In fact, the momentum equation shows that the fluid will suffer and transmit forces based on those two terms. In the Morison equation, however, the forces are only being received by the solid while assuming a flow velocity field.

A better way to approach the Morison equation might be by means of the dynamic condition on the interphase. It can be approached with a multivariable Taylor approximation by assuming that it is a function F_{FS} that depends on the position, velocity and acceleration of the body as variables. Leaving the following relation:

$$\underline{FS} \approx \underline{F_{(FS)}}_0 + \frac{\partial \underline{F_{FS}}}{\partial \underline{q}}_0 \underline{q} + \frac{\partial \underline{F_{FS}}}{\partial \underline{\dot{q}}}_0 \underline{\dot{q}} + \frac{\partial \underline{F_{FS}}}{\partial \underline{\ddot{q}}}_0 \underline{\ddot{q}} \quad (14)$$

$$\underline{F_{(FS)}}_0 + \frac{\partial \underline{F_{FS}}}{\partial \underline{q}}_0 \underline{q} + \frac{\partial \underline{F_{FS}}}{\partial \underline{\dot{q}}}_0 \underline{\dot{q}} + \frac{\partial \underline{F_{FS}}}{\partial \underline{\ddot{q}}}_0 \underline{\ddot{q}} = m\frac{d^2\underline{q}}{dt^2} + k\underline{q} \quad (15)$$

In the Morison equation only the third and fourth terms are being presented. The first term relates to the initial loads of the system, and the first term is the so-called induced stiffness. Such induced stiffness might also play a role, for example, the usage of an oscillator equation considering only the induced stiffness is a common approach to determine flow induced instability in air-foils.

If velocity and acceleration of the body are significant, and so they are the damping and added mass terms when compared with the induced stiffness, then those two terms dominate. And only if the impact of the body on the fluid can be neglected, Morison's equation will thrive. Additionally, because the acceleration and the velocity have different phase the linear superposition of both forces follows a logic.

The Morison equation simplifies the intermediate stages by assuming that the variation depends only on the flow velocity and acceleration, and that the domain integrals remain the same.

The previous analysis allows to conclude that Morison's equation has significant limitations that need to be considered:

First, at intermediate ranges of velocities between maximum acceleration and maximum velocity is not guaranteed to be accurate. Even less so if the integral of the body and surface over the domain changes due to flow changes. This is a common and known problem of this equation, and it derives from the empirical nature of the drag and mass coefficients, which is usually a scalar value, and denotes an average over a range of oscillations.

Second, neglecting the dynamic condition and not resolving the velocity flow field results in the known errors in the Morison codes which include the excessive drag in successive panel's configuration and for the net deformed in large angles of attack, as the fluid velocity is reduced due to the twines and this is not considered in such codes.

Third, because the velocity field is not being resolved, and the induced stiffness is not included, instabilities of the system are not considered. Such instabilities may include flutter and effects such as lock in or galloping. In general, the larger the velocity of the fluid compared with the movement of the body the greater of the dominance of such induced stiffness.

Conclusions and final considerations

As presented in this paper, the fluid structure interaction problem is highly complex. A Taylor expansion approach to the problem of a solid-fluid interface, plus the fundamental equations of the problem show how the physics of the system are related to each other and the induced effects that the movement of a body in a fluid has. Because of this, the usage of semi-empirical approaches such as the Morison equation can be justified, but only in specific cases. The user of the formula shall always acknowledge the implications and limitations of it.

Consequently, model test and other approaches to the prediction of response of flexible bodies and their key empirical coefficients shall be undertaken with care. So far it is thought impossible to be able to scale results from a model test to a full-scale structure due to the impossibility of archiving similarity in any of its forms.

The proposed methodology to test and predict the behaviour of flexible structures is then to proceed with model tests, but rather than using them to obtain the final results, as a mean to develop and perfect efficient numerical methods that will apply to the full-scale model.

Acknowledgements

The authors of this paper want to give special thanks to the New Zealand company Plants and Food Research for the support with the ongoing project.

References

[1] Y. A. Cengel and J. M.Cimbala, *Fluid mechanics fundamentals and applications*. 2006.

[2] G. Wang, T. Martin, L. Huang, and H. Bihs, "NUMERICAL SIMULATION OF HYDRODYNAMICS AROUND NET MESHES USING

REEF3D," 2020. [Online]. Available: http://asmedigitalcollection.asme.org/OMAE/proceedings-pdf/OMAE2020/84362/V005T05A002/6606402/v005t05a002-omae2020-18355.pdf

[3] O. Patursson, "Flow through and around fish farming nets," University of New Hampshire, 2008. [Online]. Available: https://scholars.unh.edu/dissertation

[4] T. Martin, A. Kamath, and H. Bihs, "Numerical modelling of net motion in waves and current using CFD," in *Proceedings of the International Conference on Offshore Mechanics and Arctic Engineering - OMAE*, 2019, vol. 6. doi: 10.1115/OMAE2019-95154.

[5] L. C. Gansel, F. Oppedal, J. Birkevold, and S. A. Tuene, "Drag forces and deformation of aquaculture cages—Full-scale towing tests in the field," *Aquacultural Engineering*, vol. 81, pp. 46–56, 2018, doi: 10.1016/j.aquaeng.2018.02.001.

[6] M. Paschen and K. Breddermann, "HYDRODYNAMIC LOADS ON TWO-DIMENSIONAL SHEETS OF NETTING WITHIN THE RANGE OF," no. October, 2011.

[7] C. Balash, B. Colbourne, N. Bose, and W. Raman-Nair, "Aquaculture Net Drag Force and Added Mass," *Aquacultural Engineering*, vol. 41, no. 1, pp. 14–21, Jul. 2009, doi: 10.1016/j.aquaeng.2009.04.003.

[8] H. Cheng, L. Li, K. G. Aarsæther, and M. C. Ong, "Typical hydrodynamic models for aquaculture nets: A comparative study under pure current conditions," *Aquacultural Engineering*, vol. 90, no. March, p. 102070, 2020, doi: 10.1016/j.aquaeng.2020.102070.

[9] S. K. Chakrabarti, *The Theory and Practice of Hydrodynamics and Vibration.* 2002.

[10] J. R. Morison, M. P. O'brien, J. W. Johnson, and S. A. Schaaf, "THE FORCE EXERTED BY SURF'ACE W AVES ON PILES THE FORCE EXERTED BY SURF ACE WAVES ON PILES," 1950. [Online]. Available: http://onepetro.org/JPT/article-pdf/2/05/149/2238818/spe-950149-g.pdf/1

[11] A. M. Kuethe and C. Y. Chow, *Foundations of aerodynamics: bases of aerodynamic design. 3rd ed.* 1976.

A NEW TECHNOLOGICAL APPROACH FOR SUSTAINABLE SEAGRASS REFORESTATION USING TEXTILE PLASTIC-FREE GROWING MEDIA

Mathias PASCHEN[1,2], Daniela GLÜCK[1,3], Reinhard HELBIG[1,4]

[1] MariKom GmbH, Friedrich-Barnewitz-Str. 5, Rostock, 18119, Germany
[2] University of Rostock, Department of Maritime Systems, A.-Einstein-Str. 21, Rostock, 18059, Germany
[3] University of Rostock, Department of Bio-Sciences, A.-Einstein-Str. 3, Rostock, 18059, Germany
[4] Saxon Textile Research Institute, Annaberger Str. 240, Chemnitz, 09125, Germany

Abstract

It has now been sufficiently proven that the existence of extensive seagrass respectively eelgrass fields in coastal areas has positive economic and ecological as well as health-promoting effects. Eelgrass meadows of the species *Zostera marina* largely dissipate the energy of fluid flow close to the sea bed. This prevents, for example, scour formation of coastal structures or sanding-up of traffic channels. The oxygen-carbon balance of seaweed is many times better than that of rainforests. Likewise, recent research results say that eelgrass meadows significantly limit the spread of harmful bacteria of the species *Vibrionidae*.

On the other hand, a significant decline in eelgrass meadows in the northern hemisphere has been noted for years.

In this light, the authors set themselves the goal of designing a technology for efficient and sustainable reforestation of seagrass beds and testing it in the southern Baltic Sea. The basis of their technological approach is the well-known principle of "rolled turf".

The seeds or young plants are placed on specially developed textile, plastic-free growing media. They are cultivated under controlled conditions, e.g. in greenhouses. After a few days to weeks, the growth media including plants will be fixed on the previously determined location on the seabed by means of diving operations. The paper presents the technological concept as well as initial results.

Keywords

Seagrass, eelgrass, seagrass reforestation, technology development, textile plastic-free growing media

Introduction

At the internet address Seagrass and Seagrass Beds | Smithsonian Ocean (si.edu), numerous important publications are available that deal in particular with specific issues on the biology of seagrasses in the oceans and marginal seas and their ecological importance for both the health of the marine environment and the world's climate.

REUSCH [7] points out for example the importance of a stable seagrass stock for the oxygen and carbon dioxide balance. Unlike the flora in tropical rainforests, seagrasses are able to transport the climate-damaging CO_2 via their roots to the seabed, where it is permanently deposited. In addition, according to REUSCH [7], fewer Vibrio bacteria are found in the vicinity of seagrass meadows in the Baltic Sea.

A recent report by the German government also shows that a stable seagrass population has a positive effect on the greenhouse effect, see [2].

Seagrass beds also have a positive effect on stabilising the seabed against sediment movements (erosion and scouring) by significantly dampening the energy of near-bottom currents, see PASCHEN & WRANIK [6], HARBRECHT [4] as well as MENZEL & PASCHEN [5].

Last but not least, healthy seagrass beds guarantee ideal spawning and nursery conditions for a large number of marine species.

The seagrasses *Zostera marina* and *Zostera noltii* occurring in the Baltic Sea region are listed as endangered species. Both nutrients entering the coastal areas of the Baltic Sea via inflows from the terrestrial zone and rising water temperatures due to climate change, especially in the summer months, are significant stress factors for these seagrasses and have a negative impact on the population and the spread of the natural seagrass meadows, as BOBSIEN [1] shows.

A natural recolonization of seagrass beds has already been observed in recent times due to an improvement in water quality caused by a measurable decrease in nutrient inputs in the western and southern Baltic Sea. However this natural recolonization takes place on large time scales. In this context, REUSCH [7] says that it can take decades even on suitable areas. In this respect, supportive measures are necessary to sustainably push the process of reintroducing seagrass meadows at manageable costs.

In many countries, efforts can be observed, especially among young marine scientists, to accelerate the spread of plants by manually replanting plants removed from one site in another. Some of these efforts have produced satisfactory results.

Nevertheless, this is, in the long term, a time-consuming manual process and therefore a costly method.

GLÜCK [3] succeeded in providing experimental proof that seagrass plants can develop just as well on artificial habitats as on natural sediments. On that note the chance were given to develop a technological concept for seagrass field's restoration on the basis of the proven method of rolled turf to significantly reduce the manual effort under water.

The aim of the project is a validated technical concept for a technology that is suitable and acceptable for the afforestation of seagrass beds from both an ecological and a commercial point of view. The tasks associated with this are inevitably complex. Only individual steps are explained below.

Material and Methods

Explanation of the concept

The concept pursued is based on the rolled turf principle. Textile, plastic-free growing media are the basis for planting seagrass meadows. Healthy seagrass plants collected as flotsam from the beach after storms or seagrass seeds are put into suitable plant carriers. In this way prepared carriers, will be kept in basins onshore until the plants start growing or the seeds germinate under controlled conditions.

When the plants reached an adequate size as well as a sufficient robustness against mechanical loads divers are going to spread the plant carrier including the seagrass plants on the seabed. In the same time the growing media will be fixed on the seabed by ground spikes. All these operations have to be done in one step.

In this context it is important to pay attention that there is a close contact between seabed and carrier. In other case the roots of the young seagrass plants will not have the possibility to grow into the sediment.

Subsequently, all parts of the installation have to be checked regarding correct workmanship and to be documented typically by underwater photographs and videos.

In order to be able to observe both the progress of growth of the seagrass and the process of successive degradation of the growth carrier, monitoring should be done by means of ROV's or by divers.

Material and design of the textile plastic-free growing media

The material textile, plastic-free growth carriers should be made from has to be compatible with the marine environment as well as the seagrass. The growth carriers themselves can be practically designed in a strand, mesh or grid shape.

Shape of carrier is not so important whether netlike or grid structure. Much more important is the design of the strand which keeps the seed respectively the young plants and it is the basis for manufacturing the carrier. On the one hand, material and design of the strand must ensure the required strength of the growth carrier to withstand current and wave induced loads until the seagrass plants are firmly anchored to the seabed. On the other hand, the strand should have such a structure that provides sufficient support to the plant without hindering its growth.

It is in the interest of the project to use such materials which are available in the region in sufficient quantities and at low costs. For this reason, experiments were carried out in particular with dead seagrass, hemp and flax fibres for manufacturing the strand. In addition, viscose fibres made of wood were also tested as a supplementary material.

The general construction of the strands is shown in fig. 1. An example of a rope made from seagrass can be seen in fig. 2.

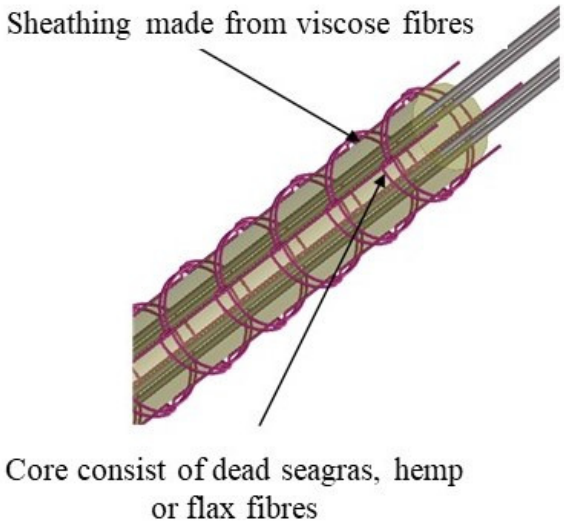

Figure 1
Structure of the textile strands developed

Figure 2
Finished strand, made from seagrass

The conceptual structure of a grid-shaped growth carrier is shown in fig. 3. One example of a produced growing media is depicted in fig. 4. In this case, the weft is manufactured from hemp. The warp consist of viscos fibre.

The growing media consisting of rhombic meshes are similar in structure to the grid-like ones. Two mesh bars of each mesh are comparable to the warp threads in terms of their structure. The other two mesh bars consist of a strand that is comparable to the weft thread of the grid construction. The net-like growth medium shown in fig. 4 is made of hemp and flax.

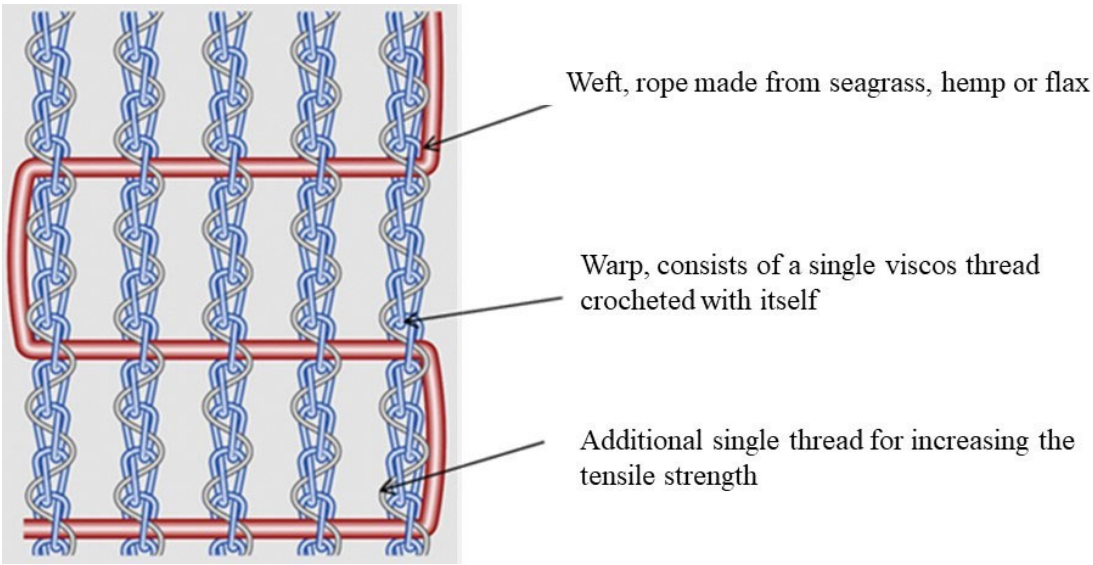

Figure 3
Detail design of the growing media in grid shape developed and used for the project

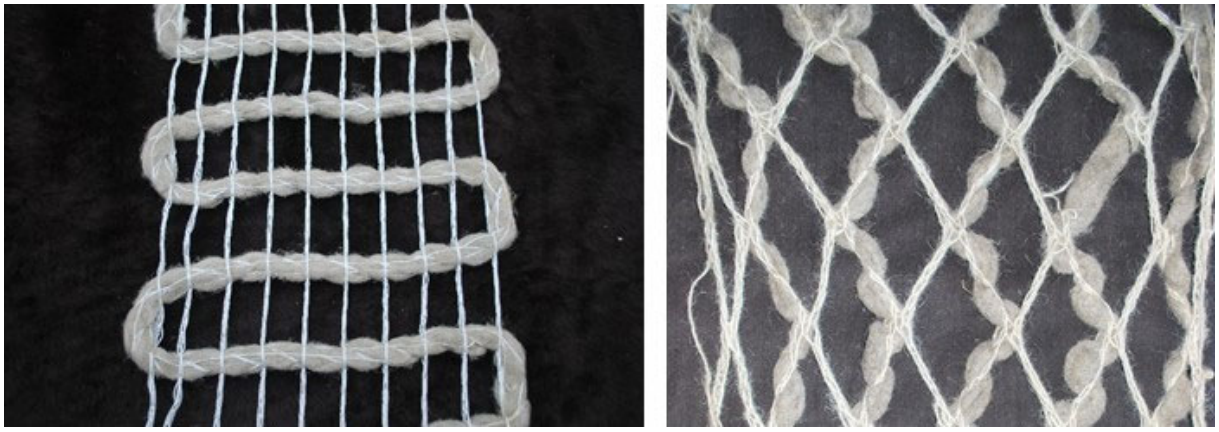

Figure 4
Example of a growth carrier in both grid shape (left) and net-like shape (right)

Results and Conclusion

First results

In mid-February 2022, the first trials began according to the concept described above. For this purpose, several basins filled with seawater (length: 4 m, width 1.25 m, height of the water column: approx. 35 cm) were installed in a greenhouse by an air temperature between 6°C to 8°C, later up to 20°C.

Healthy seagrass plants collected from the beach after a storm were placed in different types of growing media by hand. The distance between the plants was about 20 cm by 20 cm.

The growth mediums and plants prepared in this way were kept in the greenhouse for 10 weeks. During this time, the condition of both the plants and the growth carriers was regularly checked. Selected parameters of the water body were measured.

About every 10^{th} plant was marked with special markers to precisely follow its development. This way, it could be determined that more than 50 percent of the plants developed well. They showed recognisable root and leaf growth, see fig. 5. Individual plants already developed seeds during this period. The rest of the plants died.

On 13 April 2022, the growth carriers including plants were deployed to a previously determined location with sandy soil in the Baltic Sea close to Rostock in approximately 7 metres depth (Rosenort reef) by two research divers.

For this purpose, the growth mediums and plants were placed in trough-like transport containers before.

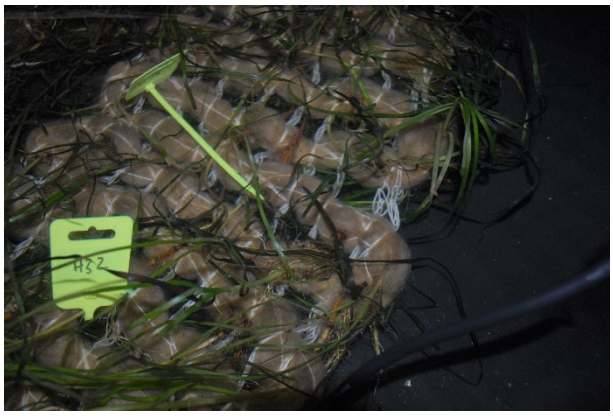

Figure 5
Seagrass plants placed in the growth carrier, two markers are visible.

The installation went well due to good weather conditions, see fig. 6. However, everyone involved was sceptical whether the plants would survive the heavy drop in temperature well (Baltic water temperature was below 6°C).

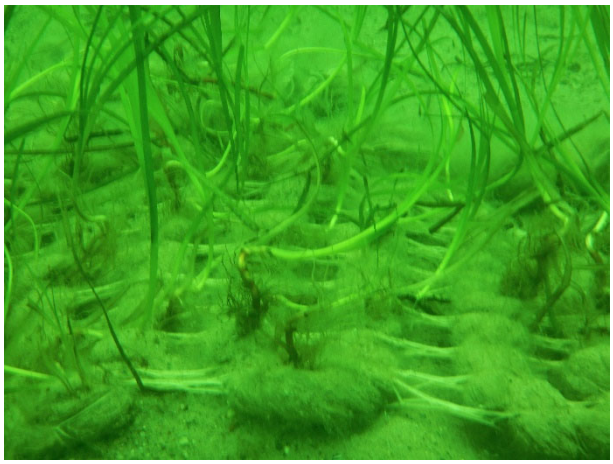

Figure 6
Photographic image immediately after installation

On 18 May 2022, i.e. approximately five weeks after installation, the first monitoring took place. It could be seen that

- a great number of plants took a good development with regard to growth of roots and leaves, see fig. 7 and 8,
- the viscous threads of the growth media were already partly in the process of degradation,
- unfortunately, the growing carrier also form a good habitat for green algae,
- a less number of plants didn't survive the procedure.

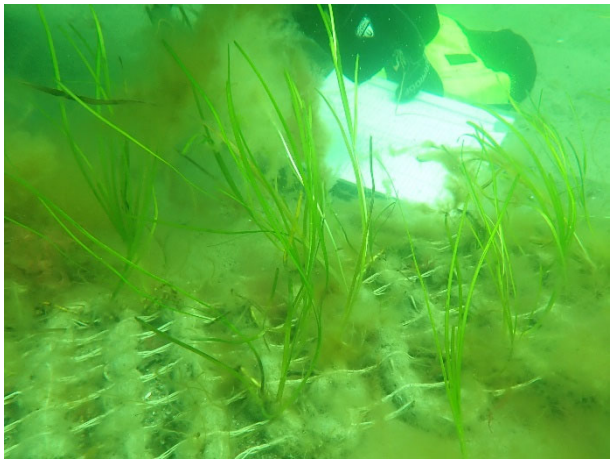

Figure 7
Monitoring on 18 May 2022, condition of the plants and growth medium is satisfactory

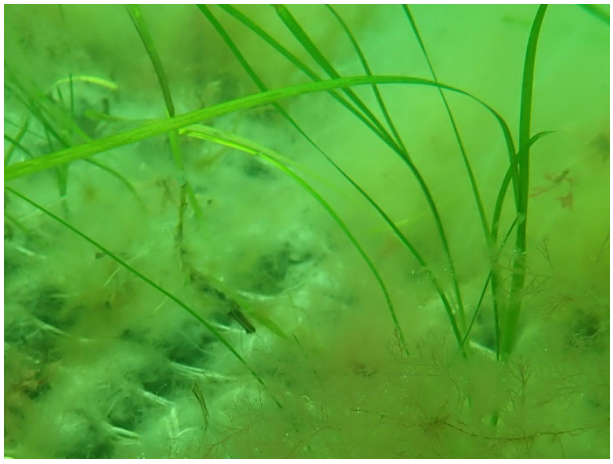

Figure 8
Monitoring on 18 May 2022, view on individual plants

At the beginning of August 2022, there were days of very stormy weather with corresponding rough seas in the southern Baltic Sea. The monitoring on 16 August made the extent of this weather event clear. Numerous plants and growth mediums were destroyed. Of course, this was an unpleasant result. In terms of research, it led to further gains in knowledge.

Conclusion

It is internationally proven that the worldwide protection of seagrass meadows in general and the restoration of seagrass beds in the Baltic Sea in particular is of

high priority under the aspect of "climate protection". In addition, there are numerous other reasons to do everything possible to protect and increase seagrass meadows. These have already been mentioned in the introduction to the paper.

With this project, the authors are taking up the challenge of developing a promising technology for the sustainable reforestation of seagrass beds based on textile, plastic-free growth media.

The results so far have clearly shown that the concept as a whole leads to the specified goal.

It must also be accepted that there is still a need for further optimisation, particularly in the construction of the strands, which are important for seed germination and seedling development.

Likewise, the existing hydrological and meteorological conditions must be substantially taken into account in the choice of a suitable location.

Acknowledgement

The authors would like to thank the Climate and Environment Foundation Mecklenburg - Western Pomerania (CEF) for funding this research and development project.

Thanks are equally due to the members of the project advisory board Dr. Heike Illing-Günther (STFI), Christin Klinger (CEF), Petra Mahnke (GMT) and Prof. Dr. Hendrik Schubert (University of Rostock) for their fruitful support.

References

1. Bobsien, I.: Mögliche Auswirkungen des Klimawandels auf den Blasentag (Fucus vesiculosus) und das Gewöhnliche Seegras (Zostera marina) in der Ostsee (*Possible impacts of climate change on bladder wrack (Fucus vesiculosus*) and common seagrass (Zostera marina) in the Baltic Sea). Report. RADOST-Berichtsreihe 24. Landesamt für Landwirtschaft, Umwelt und ländliche Räume Schleswig-Holstein, Flintbek, 2014
2. Die Bundesregierung: Seegraswiesen gegen den Treibhauseffekt (*Seagrass beds against the greenhouse effect*), 2021
3. Glück, D.: Keimungsverhalten von Seegras auf künstlichen Substraten (*Germination behaviour of seagrass on artificial substrates*)**.** M.Sc.-Thesis, University of Rostock, Faculty of Mathematics and Natural Sciences, Institute of Biosciences, 2020
4. Harbrecht, G.: Untersuchungen zur Kolkbildung an Monopiles und zur Migration von Objekten am Meeresboden (*Investigations on scouring of monopiles and migration of objects on the seabed*). B.Sc.-Thesis, University of Rostock, Faculty of

Mechanical Engineering and Marine Technology, Chair of Ocean Engineering, 2017

5. Menzel, P.; Paschen, M.: Kolkbildung und Kolkschutz an Monopile-Fundamenten (*Scouring and scour protection on monopole foundations*). Lecture at the 112th Annual General Meeting of the Schiffbautechnische Gesellschaft in Potsdam in November 2017, published in: Yearbook of the Schiffbautechnische Gesellschaft, Vol. 111, pages 208 - 213
6. Paschen, M.; Wranik, H.: Beurteilung der Wirksamkeit technischer Maßnahmen zur Verhinderung von Kolkbildung an zylindrischen Gründungsstrukturen von Offshore-Bauwerken auf Grundlage numerischer und experimenteller Analysen. Maritime Competence Centre for Industrial Research of Ocean Engineering GmbH, Report on the R&D project „Scour protection“, 2016
7. Reusch, T.: Unterwasserwiesen im Klima-Labor speichern 30 Mal mehr CO_2 als die Tropen (Underwater meadows in the climate lab store 30 times more CO_2 than the tropics). Interview vom 7. Oktober 2021, abgedruckt in **ntv**

FIXED MESH CONSTRUCTIONS ARE REQUIRED TO REDUCE VARIABILITY IN CODEND SIZE SELECTION

Zita BAK-JENSEN[1*], Bent HERRMANN[1,2,3], Juan SANTOS[4], Valentina MELLI[1], Jordan P. FEEKINGS[1], Daniel STEPPUTTIS[4]

[1]DTU Aqua, Technical University of Denmark, 30, Niels Juelsvej, Hirtshals, 9850, Denmark
[2]SINTEF Ocean, Brattørkaia 17C, N-7010 Trondheim, Norway
[3]The Arctic University of Norway, UiT, Breivika, N-9037 Tromsø, Norway
[4]Thünen Institute for Baltic Sea Fisheries, Alter Hafen Süd 2, Rostock, 18069; Germany

Abstract

In demersal trawls the most commonly used codends are diamond-mesh. However, diamond-mesh codends is discovered to vary in mesh geometry which lead to a less well-defined size selection process. One alternative often adopted to reduce variability in mesh geometry, and thereby obtain a sharper size selection, is to force the meshes to adopt a square geometry by turning the codend netting 45 degrees (T45 standard square-mesh). Therefore, we tested the size selectivity of a standard square-mesh and a standard diamond-mesh codend and a fixed diamond-mesh codend whose mesh geometry was optimally defined to suite the morphology of cod. Using Atlantic cod (*Gadus morhua*) as a case study, we found no evidence that the square-mesh codend had lower variability in size selection than a standard diamond-mesh codend with same mesh size. Moreover, we demonstrated that the square-mesh codend had significantly larger variability in size selection compared to what was obtained with a codend where the mesh geometry was kept fixed during the fishing process. These results demonstrate that the use of square-mesh codends is not a sufficient strategy to reduce the variability in codend size selection. On the contrary, this would need a codend construction where the mesh geometry is kept constant during fishing, thus providing a new engineering challenge for the development of commercial trawl gears.

Keywords

Codend size selectivity, fixed mesh openness, diamond-mesh, square-mesh, mesh opening angle

Nomenclature

DOF – Degrees of freedom (number of independent values in the data set)
L50 – The size at which there is 50 % retention probability [cm]

SR – The difference in length between fish with a 75% probability of retention and the length of fish with a 25% probability of retention [cm]
SR_B – The baseline SR [cm]
SR_T – SR value for treatment design [cm]
deviance – measure of deviation of the data points and the model
p-value – quantifies the probability of by coincidence obtaining at least as large a discrepancy between the experimental data and the model
ΔSR – Percentage change in SR value for treatment compared to baseline [%]

Introduction

Selectivity is a keystone in the aim for sustainable fisheries (Vasilakopoulos et al., 2015) Selectivity is defined by Wileman et al. (1996) as "*the probability of a fish of a given species and size being retained by a gear once it has encountered it*". In towed fishing gears, the majority of the selection occurs in the catch accumulating part, i.e. the codend (Wileman et al., 1996). Selection across sizes (i.e. size selection) is often described by a sigmoid curve with retention probability as a function of length of the fish. The ideal size selection curve would be knife-edged with a critical length, corresponding to the minimum landing size, at which all fish below would be released, and all above would be retained, (Wileman et al., 1996; Andersen, 2019). The advantage of a sharp size selection would be to maximize economic yield and minimize undersized discard. To define the sharpness of the curve, and thereby the variation in sizes retained, the selection range (SR) is used. SR is the difference in length between fish with a 75% probability of retention (L75) and the length of fish with a 25% probability of retention (L25) (Wileman et al. 1996). Therefore, optimal size selection aims at obtaining an SR as close to zero as possible.

Diamond-mesh are the most commonly used codend design and have traditionally been applied due to their simplicity in structure and operation (He, 2007; Wienbeck et al. 2011; Sistiaga et al. 2021). However, a variety of studies have concluded that diamond-mesh codends do not maintain a constant mesh openness during trawling (e.g., Robertson and Stewart, 1988; Reeves et al. 1992; Herrmann, 2005). During the catch process, as the catch develops in the codend, the mesh openness becomes more heterogeneous, whereby meshes close to the catch build-up zone become more open and meshes further forward in the codend become more elongated and thereby closed (Jones, 1963; Herrmann, 2005; Herrmann and O'Neill, 2005). These variations in the mesh openness have been associated to large SR values and therefore to a large variation in the size selection of the codend (Fryer, 1991; Herrmann and O'Neill, 2005; Herrmann, 2005). This leading to an unwanted catch structure i.e. retention of undersized fish and release of valuable large individuals. One alternative, often

adopted in an attempt to reduce variability in mesh geometry, is the use of square meshes, as they have shown less variability compared to diamond meshes (e.g., Robertson and Stewart, 1988; Broadhurst et al, 2004). However, former research has raised doubts regarding the size selection variability in square-mesh codends (Wienbeck et al., 2014).

The effect of variability in mesh openness on the sharpness of codend size selection was first quantified experimentally by Bak-Jensen et al. (2022). The study found a significant difference between a codend where mesh openness was kept constant and a simple diamond-mesh codend where the mesh and thereby the openness was flexible. By using the same approach, we aimed at answering the two questions:

- *Does a square-mesh codend produce a sharper selection curve than a diamond-mesh codend?*
- *Does a square-mesh codend produce a shaper selection curve than a diamond-mesh codend with a fixed mesh opening angle?*

Materials and methods

The experimental fishing trials were conducted in the Baltic Sea onboard the German FRV Solea (42.40 m LOA, 1780 kW), during September 16th to 27th 2021 (diamond-mesh) and June 13th to 27th 2022 (fixed mesh codend and square-mesh codend). The covered codend method according to Wilemann et al. (1996) was applied. Individuals escaping from the experimental codends were collected using a cover surrounding the entire codend (Wilemann et al., 1996; Wienbeck et al. 2011, 2014). The three experimental codends were tested one at a time for a number of hauls. The catches obtained at each haul were treated for each compartment separately. The total length of all cod individuals was measured using measuring boards and the lengths were rounded to the centimetre below.

For the fixed mesh codend, a rigid steel frame setup was used, according to Bak-Jensen et al. (2022). The four rectangular surfaces of the frame were covered with diamond-mesh angled at 60° opening angle instead of the 40° mesh opening angle used by Bak-Jensen et al. (2022). The angle was obtained by using a measured angle of 60° to test the netting during fixation. The angle of 60° was chosen according to the design guide in Herrmann et al. (2009), it would have a larger L50 close to the L50 expected with square-mesh. The rigid frame codend is hereafter referred to as “OA60”. The diamond-mesh and the square-mesh codend were made of the same netting as the netting used for the OA60 made of 5 mm Euroline single twine. The mesh size for the codend was measured to 110.4 cm ± 4.0 cm, 112.4 cm ± 2.7 cm and 113.9 cm ± 2.1 cm for the square-

mesh, diamond-mesh and the OA60 respectively. The square and the diamond mesh were made of two panels with 24 and 43 meshes respectively. The four panels in the OA60 were each 11 meshes wide. The cover was made of single 2.5 mm-PE twine with a nominal mesh size of 55 mm and had a diameter of ~3 m (Bak-Jensen et al., 2022). All the codends are pictured below in Figure 1.

Figure 1
The three codends. From left square-mesh, diamond-mesh and OA60.

The statistical analysis was conducted according to Bak-Jensen et al. (2022). All the experimental codends were analysed using the methodology described in Wileman et al. (1996). The codend retention probability was modelled by simple mathematical functions with parametric structures leading to non-decreasing, s-shaped selectivity curve asymptotically restricted to values between [0.0, 1.0] (Wileman et al. 1996). The logistic, probit, gompertz, and Richard selectivity models (Model descriptions in Bak-Jensen et al. 2022) were fitted to the experimental data and the best model was chosen based on the AIC value (Akaike, 1974). The collected data was bootstrapped with 1000 repetitions and analysed using the chosen model to obtain 95% confidence bands. If the variation in mesh geometry is contributing to the variability in size selection and the variability is reflected on the SR, then the average SR estimated by pooling the hauls should maintain the same variability across hauls (Fryer 1991; Herrmann, 2005; Herrmann and O'Neill 2005). By testing the selective properties of a square-mesh codend and an experimental codend with the geometry of the meshes fixed or a diamond-mesh codend, the contribution of geometric mesh variation to the variability in selectivity is quantified by the following statistics:

$$\Delta SR[\%] = 100\,\frac{(SR_T - SR_B)}{SR_B} \qquad (1)$$

Where SR_T is the selection range estimated for treatment which in this case is either the diamond-mesh codend or OA60. SR_B is the selection range estimated for the square-mesh codend and is used as baseline. Therefore, ΔSR quantifies the contribution of the variability in mesh geometry in percentage (%). A value of ΔSR ~ 0 would imply that the variation in selectivity obtained experimentally could not be related to the flexible nature of the codend meshes. Conversely, the larger the value of ΔSR, the larger the contribution of geometric mesh variation is to the overall selectivity variation. To evaluate if ΔSR is significantly different from zero, 95% confidence intervals are estimated from a bootstrap distribution of ΔSR obtained from a previously estimated bootstrap distributions for SR_B and SR_T (Larsen et al. 2018; Herrmann et al. 2018). Thus, significant differences would be found when the 95% confidence intervals around ΔSR did not overlap the value associated to the null hypothesis Ho: ΔSR = 0.0. This procedure is equivalent to methodologies often applied to assess differences between selectivity and catch comparison curves (Herrmann et al. 2018; Larsen et al. 2018; Melli et al. 2020).

Results

The result from size selection estimates and fit statistics of the models picked by AIC is shown in Table 1. In the table the number of hauls and the number of cod individuals measured is listed. The hauls were only used if they contained more than 20 individuals. The models presented in Table 1 were fitted to the data for the three codends (Figure 2). The SR was found to be lowest for the OA60 (5.51cm) compared to the square-mesh codend and diamond-mesh codend (7.42 cm and 8.75 cm, respectively) (Figure 3). Eq. 1 was used to calculate the difference in SR between square-mesh codend and diamond-mesh codend to 17.88 % (Table 2). The variation in size selection between square-mesh codend and diamond-mesh codend was not significant. However, a significant 25.69 % less variation in the size selection was found in the square-mesh codend compared to the OA60.

Table 1

Fit statistics obtained from the covered codend analysis showing the L50 and SR for the four different trawl configurations tested. Values in parentheses represent 95% CI's. The fit statistics in terms of the p-value, deviance, and DOF. Number of hauls and number of fish measured is listed last. For number of fish the first number is the total count and the count in the cover in brackets.

	Square	**Diamond**	**OA60**
Model	Richard	Logit	Richard
L50 (cm)	38.25(37.56-39.28)	27.79 (25.21-30.70)	33.57(33.03-34.12)

SR (cm)	7.42(6.35-8.70)	8.75 (6.80-11.62)	5.51(4.97-6.12)
***p*-value**	0.86	0.17	0.98
Deviance	35.66	38.56	28.64
DOF	46	31	46
No. hauls	14	15	6
No. fish	3937 (3409)	566 (485)	3629 (2414)

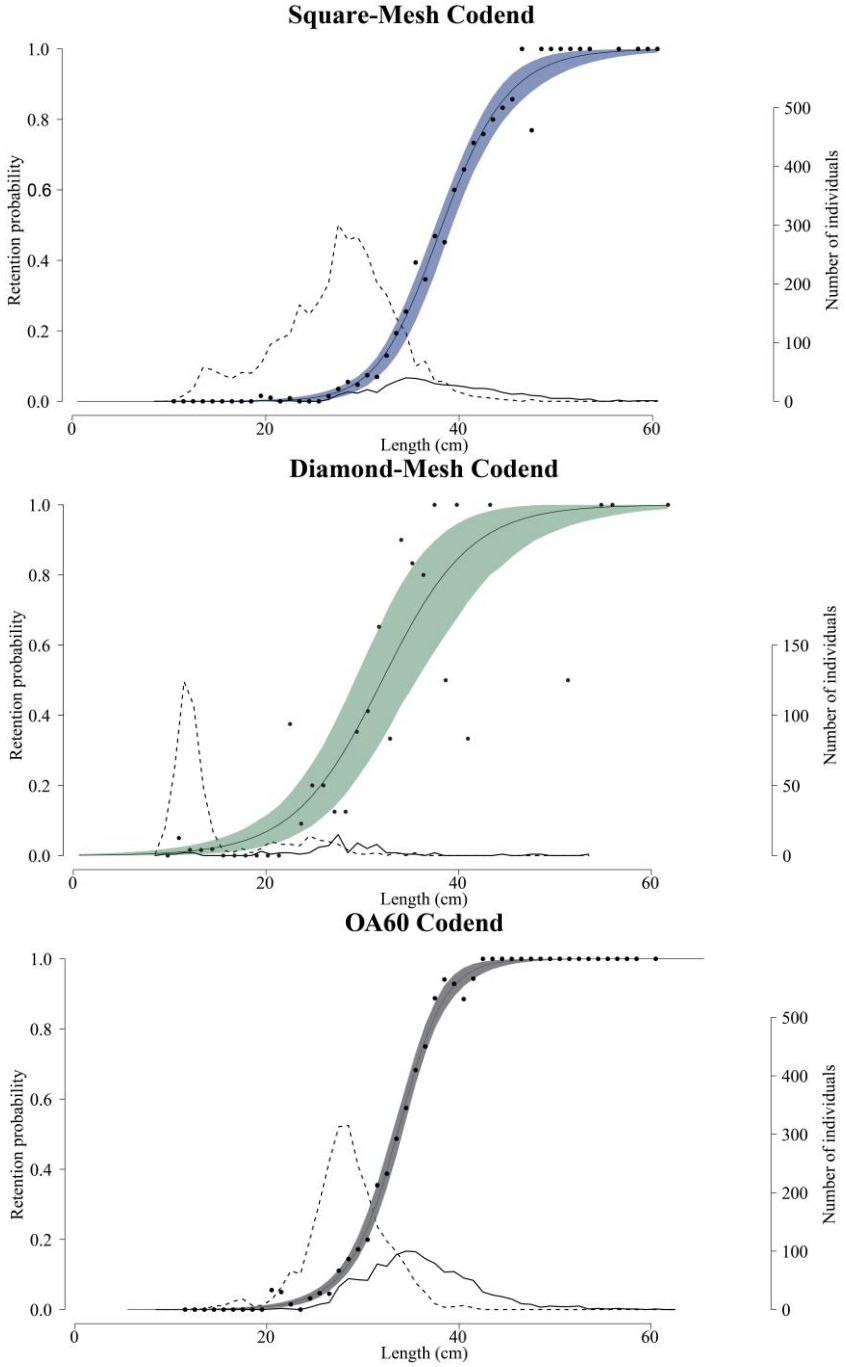

Figure 2

Length-dependent probabilities of escape in the OA60 and square- and diamond-mesh codends respectively. The solid curves represent the models fitted to the data (points) with the 95% CIs (shaded area). The frequency curves represent the number of fish caught in each length class in the codend (solid) and cover (dashed). The data for the diamond-mesh codend is collected in fall 2021 (Bak-Jensen et al., 2022).

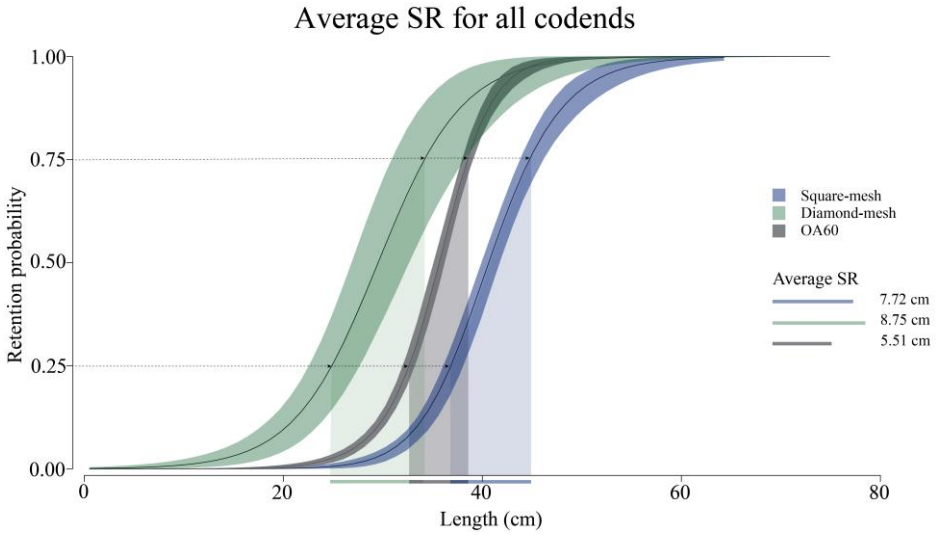

Figure 3
Length-dependent retention probabilities of escape in the square-, diamond-mesh codends and OA60. The solid curves represent the selected model with the 95% CIs (coloured area). The horizontal lines denotes the points for the L25 and L75 which marks the interval for the SR (showed with shadowed colours from the model curve to the x-axis). The data for the diamond-mesh codend was collected in fall 2021 (Bak-Jensen et al., 2022).

Table 2
The ΔSR for between the two other codends compared with square-mesh codend. * denotes value with significant difference.

ΔSR for square-mesh codend comparison	
Diamond-mesh codend [%]	17.88 (-13.53; 63.96)
OA60 [%]	-25.69 (-38.67; -10.65) *

Discussion

We assessed and compared the size selectivity results from a standard square-mesh codend to a standard diamond-mesh codend. We also tested the variability in selectivity in a standard square-mesh codend and compared it with a diamond-mesh construction that ensured mesh openness remained constant. Our results showed no evidence that a square-mesh codend has less variation in size

selectivity than a diamond-mesh codend. That no significance was found could be a result of the less cod caught in the fall 2021 where the data for the diamond-mesh was collected compared to the catch from summer 2022. The square-mesh codend which has been assumed to have stable mesh openness and low variability (i.e. Robertson and Stewart, 1988; He, 2007) was found to have a significant higher SR and thereby lower variability compared to the OA60. Similarly to diamond meshes, the flexible meshes in the square-mesh codend are at some level affected either in the catch build-up process or during haul back, which affects the risk of losing valuable catch or increasing retention of unwanted catch. According to our results using square-mesh codends is not an effective strategy to reduce the issue of selectivity variation caused by variation in mesh geometry.

Therefore, we propose a change in the way we think trawl codend design towards a focus on stabilization of the meshes. As the construction used in this experimental trial is not feasible for commercial fisheries due to the large unhandy structure that can be a hazard risk, and limitation in catch volume, a new design should be developed. The need for a functional codend with high selective properties is more relevant than ever. However, the solution requires maintaining of the mesh openness regardless the difference in tension for example caused by changing catch size and during haul back. The design keeping a constant mesh openness cannot be inflexible as the need for storage and handling onboard the vessel makes it necessary for a construction that it is somehow easy managed.

Acknowledgements

The authors would like to thank the crew onboard the “R/V Solea”, as well as Kerstin Schöps, Beate Büttner, Annika Brüger and Lennart Hannawald, for their valuable help during the sea trial periods. This work has received funding from the European Maritime and Fisheries Fund (EMFF) and the Ministry of Food, Agriculture and Fisheries of Denmark (Ministeriet for Fødevarer, Landbrug og Fiskeri) as part of the projects (FastTrack II – Sustainable, cost effective and responsive gear solutions under the landing obligation (33112-P-18-051) and Udvikling af SELEKTive redskaber og teknologier til kommercielle fiskerier (SELEKT))

References

1. Akaike, H., – A new look at the statistical model identification – IEEE Trans. Automat.Contr. 19, 6, 1974, 716–723.
2. Andersen, K. H. – Fish Ecology; Evolution and Exploitation: A New Theoretical Synthesis – Oxfordshire: Princeton University Press, 2019
3. Broadhurst M. K., Millar R. B., Kennelly S. J., Macbeth W. G., Young D. J., Charles A., and Gray C.A. – Selectivity of conventional diamond- and novel square-mesh codends in an Australian estuarine penaeid-trawl fishery – 2003
4. Fryer, R.J. – A model of between-haul variation in selectivity – ICES J. Mar. Sci., 48, 1991, 281–290.
5. He, P. – Selectivity of large mesh trawl codends in the Gulf of Maine: I. Comparison of square and diamond mesh – Fisheries Research, 83, 1, 2007, 44-59
6. Herrmann, B. – Effect of catch size and shape on the selectivity of diamond mesh cod-ends. II. Theoretical study of haddock selection – Fish. Res., 71 2005, 15-26
7. Herrmann, B. and O'Neill, F.G. – Theoretical study of the between-haul variation of haddock selectivity in a diamond mesh cod-end – Fish. Res. 74, 2005, 243-252
8. Herrmann, B., Krag, L.A., Frandsen, R.P., Madsen, N., Lundgren, B., and Stæhr, K.J. – Prediction of selectivity from morphological conditions: methodology and a case study on cod (Gadus morhua) – Fish. Res. 97, 2009, 59-71
9. Herrmann, B., Krag, L. A., and Krafft, B. A. – Size selection of Antarctic krill (Euphausia superba) in a commercial codend and trawl body – Fisheries Research, 207, 2018, 49– 54.
10. Jones, R. – Some theoretical observations on the escape of haddock from a codend – ICNAF Spec. Publ., 5, 1963,116-127
11. Krag, L. A., Herrmann, B., Iversen, S. A., Enga°s, A., Nordrum, S., and Krafft, B. A. – Size selection of Antarctic krill (Euphausia superba) in trawls – PLoS One, 2014
12. Larsen, R. B., Herrmann, B., Sistiaga, M., Brinkhof, J., and Grimaldo, E. – Bycatch reduction in the Norwegian Deep-water Shrimp (Pandalus borealis) fishery with a double grid selection system – Fisheries Research, 208, 2018, 267–273
13. Melli, V., Herrmann, B., Karlsen, J. D., Feekings, J. P., and Krag. L. A. – Predicting optimal combinations of by-catch reduction devices in trawl gears: A meta-analytical approach – Fish and Fisheries, 21, 2, 2020, 252-268
14. Millar, R. B. – Incorporation of between-haul variation using bootstrapping and nonparametric estimation of selection curves – Fisheries Bulletin, 91, 1993, 564–572
15. Reeves, S.A., Armstrong, D.W., Fryer, R.J., and Coull, K.A. – The effects of mesh size, cod-end extension length and cod-end diameter on the selectivity of Scottish trawls and seines – ICES J. Mar. Sci., 49, 1992, 279-288

16. Robertson, J.H.B. and Stewart, P.A.M. – A comparison of size selection of haddock and whiting by square and diamond mesh codends – J. Cons. lnt. Explor. Mer., 44, 1988, 148-161
17. Santos, J., Stepputtis, D., Oesterwind, D., Herrmann, B., Lichtenstein, U., Hammerl, C., and Krumme, U. – Reducing cod bycatch in flatfish fisheries – Ocean and Coastal Management 220, 2022, 106058
18. Sistiaga, M., Brinkhof, J., Herrmann, B., Larsen, R. B., Grimaldo, E., Cerbule, K., Brinkhof I. and Jørgensen, T. – Potential for codends with shortened lastridge ropes to replace mandated selection devices in demersal trawl fisheries – Canadian Journal of Fisheries and Aquatic Sciences, 2021
19. Sistiaga, M., Herrmann, B., Grimaldo, E., and Larsen, R. – Assessment of dual selection in grid based selectivity systems – Fisheries Research, 105, 2010, 187–199
20. Vasilakopoulos, P., O'Niell F. G., and Marshall. T. – The unfulfilled potential of fisheries selectivity to promote sustainability – Fish and Fisheries.
21. 17, 2, 2015, 399-416
22. Vasilakopoulos. P.; Maravelias. C. D., and Tserpes. G. – The alarming decline of mediterranean fish stocks – Current Biology, 24, 14, 2014, 1643-1648.
23. Wienbeck, H., Herrmann, B., Feekings, J. P., Stepputtis, D., and Moderhak, W. – A comparative analysis of legislated and modified Baltic Sea trawl codends for simultaneously improving the size selection of cod (*Gadus morhua*) and plaice (*Pleuronectes platessa*) – Fish. Res., 150, 2014, 28-37.
24. Wienbeck, H., Herrmann, B., Moderhak, W., and Stepputtis D., Effect of netting direction and number of meshes around on size selection in the codend for Baltic cod (Gadus morhua). Fish. Res., 109, 2011, 80-88.
25. Wileman, D. A., Ferro, R. S.T., Fonteyne, R., and Millar, R. B. (Eds.). Manual of Methods of Measuring the Selectivity of Towed Fishing Gears. ICES Cooperative Research Report No. 215. 1996, 126

A BIOLOGICAL APPROACH TO BOTTOM IMPACT; THE CASE OF DEMERSAL TRAWLING IN THE AEGEAN SEA

Ozan SOYKAN[1], Adnan TOKAÇ[1]
[1], Ege University, Faculty of Fisheries, 35100, Bornova, İzmir, Turkey

Abstract

The impact of demersal trawling on species diversity along the Turkish coast of the Aegean Sea was emphasized in the present study. Samplings were carried out with commercial trawlers from 2010 to 2012. While a total of 68 species was landed, the discarded catch was composed of 191 species; 110 fish (59 always discarded), 26 crustaceans (19 always discarded), 25 molluscs (15 always discarded) and 30 other invertebrates (all discarded). Total discarding rate for pooled data was calculated to be 33 ± 20 %. Among the obtained taxonomic groups, fish composed the majority of the discarded fraction in terms of number and weight. It was found that the most abundant discarded species in terms of number were *Serranus hepatus* (13%), *Capros aper* (8%), *Citharus linguatula* (6%), *Parapenaeus longirostris* (5%), *Lepidotrigla cavillione* (5%), *Munida ruttlanti* (4%), *Argentina sphyraena* (4%), *Diplodus annularis* (4%), *Chlorophthalmus agassizi* (3%) and *Lampanyctus crocodilus* (3%). It was also determined that undersized commercial species are subject to discarding. Our study indicated that discards generated by bottom trawling in the Aegean Sea constitute an important fraction of the total catch and that the number of affected species is very high. The area is the most efficient trawling zone among Turkish Seas thus requiring long-term monitoring in terms of fish stocks and trawl discards to maintain a sustainable fishery. Therefore, discarding features (species composition, discard ratio, CPUE values and etc.) of Aegean Sea trawl fishery should be more seriously considered during decision making and ecosystem friendly innovations must be implemented to the Aegean Sea trawl fishery.

Keywords

Discard, trawl, Aegean Sea, Impact

Introduction

Trawl fishery has been recognized with high discarding features in the Mediterranean. Aegean Sea, a shared water between Turkey and Greece, has been under a big trawl fishing pressure for many years. Multispecies character of Mediterranean aquatic environment is probably the most important reason of trawl dis-

cards in the area. Discards of trawl fisheries are composed of unwanted species (noncommercial species), by-catch species (low commercial value), and undersized individuals of commercial species. The discard rate of 10.8% (discards/total catch), estimated for the world's marine fisheries, is equivalent to 9.1 million tonnes discarded annually (Gilman et al., 2020). Discarding and its effects in the Mediterranean and in the Aegean Sea were emphasized in many studies (Machias et al., 2001; Allain et al., 2003; Sanchez et al., 2004; Yemişken et al., 2014; Soykan et al., 2016). Although coastal areas in the Turkish part of the Aegean Sea are rich in terms of gulfs and bays, there is a narrow continental shelf with hilly and jagged bottom structures that limit fishing activities in the area (Soykan et al., 2016). Total fisheries production of Turkey was given to be 785811 tonnes and 46% of this amount belonged to capture fisheries (TUIK, 2020). Purse seiners and trawlers contributed to the majority of this amount, with bottom trawlers providing 90% of the demersal resources. Although there are many studies addressing some aspects of trawl fishery including selectivity, catch composition and catch per unit effort values in Turkey, discarding features are less mentioned. In the present study, discarded trawl catches in the three main fishing areas of the Turkish coasts of the Aegean Sea were emphasized using data from commercial trawlers. The main features of discarding process were considered such as species composition, discard ratios and catch per unit effort values (CPUE).

Materials and Methods

This study was performed in the legal trawling areas of Turkish coasts of Aegean Sea from Saros Bay (North) to Güllük Bay (South) between 2010 and 2012 by commercial trawlers (Figure 1A). Study area was divided into 3 subareas as North Aegean, middle Aegean and South Aegean Sea. Depth of the trawl hauls ranged from 40 m in the south to 450 m in the north. Study was carried out by 9 commercial trawlers having typical engine powers of 400-500 hp. Samplings were carried out by 1200 mesh trawl net with a stretched mesh size of 44 mm (Figure 1B). A total of 311 trawl hauls were performed; 49 in the north, 141 in the middle and 121 in the south. Species were divided into 2 categories as commercial and discarded. Estimating the total catch, recording the commercial composition of the catch which was identified at the species level and listed as fish, cephalopods, crustaceans and finally sampling the discarded portion of the catch comprised the on board works. Researchers didn't interfere with the normal fishing practices of the crew. After the marketable species were sorted by the fishermen, the number of boxes was counted and their weight calculated. Depending on the quantity of discarded catch, either the total or a sample was retained to be investigated in detail in the laboratory to determine the specific composition of the haul discard and weight by species. The number of discarded

species (S) was counted for each haul in the laboratory. The diversity indices were computed using the number of specimens (N). Total hauling time for each area was standardized according to the time spent in North, where had the minimum total hauling time. The estimations were made using the Species Richness, evenness diversity index, Brillouin diversity index, Fisher diversity index, Shannon-Wiener diversity index and Simpson diversity index. The SIMPER test was performed to determine the level of dissimilarity according to trawl fishing areas; north, middle and south of the Aegean Sea. Computation of diversity indices and SIMPER analysis were performed using the PRIMER 5 statistical package program. Data such as position and depth (start and the end of each haul), duration of the haul, percentage of marketable and discarded fractions of the catch were recorded for each haul. Data on the species composition of the landings and discards, by haul, were standardized to hourly yields (kg/h). Calculation of discard rate was performed according to Kelleher (2005) by the mentioned formula below with standard deviation values:

$$dr = \frac{d}{d+l} x100$$

Where d represents discarded catch and l landings.
Catch per unit effort (CPUE) and standard error were calculated according to Phiri and Shirakihara (1999) as follows:

$$CPUE = \frac{\sum \frac{Ci}{nh}}{\sum \frac{t}{nh}}$$

Where C_i is the catch amount per operation (kg); t is hauling time (min/hour) and nh: number of trawl operations (hauls).

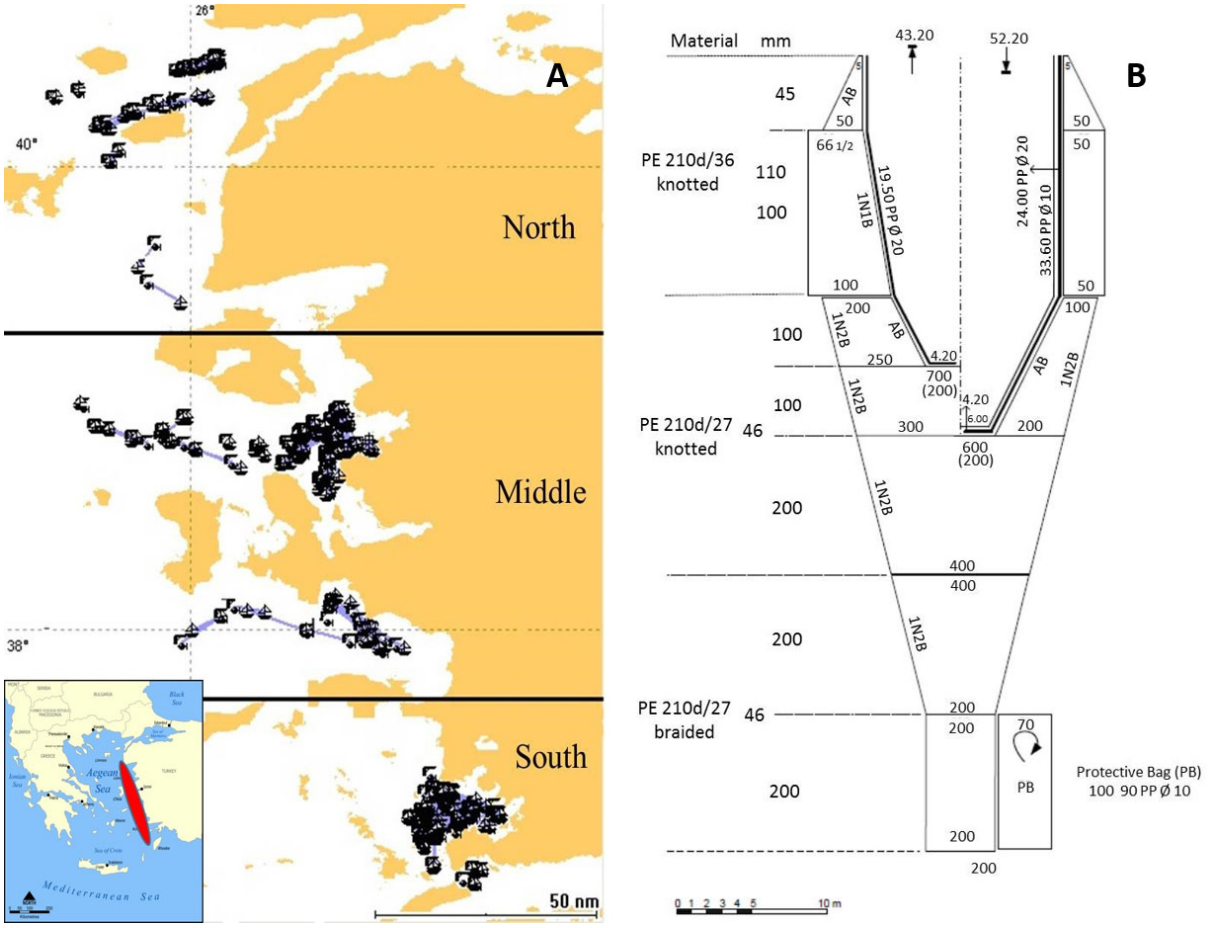

Figure 1
(A) Study area and total of 311 fishing hauls, from 2012 to 2014 in the Aegean Sea. (Length of trawling varied from 50 to 430 minutes, trawling speed from 2.4 to 2.6 knots; water depth ranged from 40 to 450 m (B) Technical plan of trawl net (Tosunoğlu&Aydın., 2007).

Results

A total of 311 hauls were conducted during the seasonal samplings. The average depths according to the region were 284, 155 and 71 m. for north, middle and south part of the Aegean Sea respectively. The typical duration of a trip was 1 day and the haul duration ranged between 50 to 430 minutes with an average of 178 (3 hours) ± 63 minutes (SD). It was found that the mean hauling time was 156 ± 63 minutes (SD) for north, 189 ± 71 minutes (SD) for middle and 175 ± 47 minutes (SD) for south. A total of 925 hours (128 hours for north, 444 hours for middle and 353 hours for south) were spent during trawl operations. A total of 23560 kg total catch was obtained from the samplings and of those 16840 kg was marketed and the rest 6720 kg was discarded. The total number of discarded individuals was found to be 465740. The minimum discard ratio was obtained from north part of the Aegean Sea with 1% while the maximum rate was 90% in

the south. Discard ratios were found to be 22 ± 19.9 %, 27.3 ± 17.4 % and 44.2 ± 18.2 % for north, middle and south respectively. ANOVA analysis indicated a significant difference between the discard ratios of each subarea ($p<0.05$). Total discarding rate for pooled data was calculated as 33 ± 20 %. Furthermore, it was found that "depth" and "discard ratio" didn't show any relationship ($r=0.18$). Discard CPUE values according to subareas were determined to be 6.8±0.9 (S.E) kg for north, 7.4±0.5 (S.E) kg for middle and 8.2±0.5 (S.E) kg for south. No statistical significant difference was observed between the discarded CPUE values of each subarea (ANOVA, $p>0.05$). No statistical relation was found between the depth and CPUE values ($r=0.24$). A total of 68 species was landed and 200 discarded. Species composition of the study was given in Soykan et al., 2019. Within the commercial fraction, 60 were fishes, 5 molluscs (cephalopods) and 3 crustaceans. The discarded catch was composed of 200 species belonging to eight taxonomic groups (Porifera, Cnidaria, Annelida, Arthropoda, Mollusca, Echinodermata, Tunicata, Chordata). Among them, the most abundant phylum was Chordata with 116 species. The second dominant group was molluscs (30 species), followed by arthropods (28 species) and echinoderms (16 species). The rest of the taxonomic groups were represented with 10 species.

The most affected species in terms of weight were *S. hepatus* (11%)*, D. annularis* (9%)*, C. linguatula* (7%)*, L. cavillione* (5%)*, C. aper* (4%)*, S. canicula* (4%)*, S. mantis* (3%)*, S. flexuosa* (3%)*, N. sclerorhynchus* (3%)*, A. sphyraena* (2%). According to number based order, *S. hepatus* (13%), *C. aper* (8%), *C. linguatula* (6%), *P. longirostris* (5%), *L. cavillione* (5%), *M. ruttlanti* (4%), *A. sphyraena* (4%), *D. annularis* (4%), *C. agassizi* (3%), *L. crocodilus* (3%) and they composed more than 50% of the discarded fraction. *Hoplostethus mediterraneus*, *Nezumia* sp. and *Scyliorhinus canicula* dominated the discards in the North in terms of weight and number. For middle Aegean Sea, *Capros aper*, *Parapenaeus longirostris* and *Argentina sphyraena* were represented with the maximum number of individuals respectively. Dominant discarded species of the South in terms of weight and number are *Serranus hepatus, Diplodus annularis* and *C. linguatula.* The ecological indices of discarded fish for each subarea are shown in Table 1.

Table 1

Ecological parameter means for the subregions (North, Middle, South) in the Agean Sea. S: Species number (S), N (Total specimens), d (Species Richness), J´ (Evenness Diversity index), Ĥ (Brillouin Diversity index), α (Fisher Diverstiy index), H' (Shannon-Wiener Diversity Index), 1-λ (Simpson Diversity Index).

	S	N	d	J'	Ĥ	α	H'	1-λ
North	82	35958	7.722	0.7008	3.081	10.02	3.088	0.9254
Middle	145	77761	12.79	0.6975	3.466	17.23	3.471	0.9498

South 134 57763 12.13 0.5534 2.705 16.41 2.71 0.8629

The species richness (d) was estimated as 7.72 in the north and 12.79 in the middle Aegean Sea. Evenness diversity index (J´) was found to be minimum with a value of 0.55 in the South. The Shannon - Weiner diversity index had the maximum value (3.471) in the middle and minimum (2.71) in the south. The SIMPER analysis indicated that *C. aper and S. hepatus* displayed highest average dissimilarity among discarded fish (Table 2). Dissimilarity between north and middle was computed to be 64 % by the leading of *C. aper* with 13 %. *S. hepatus* showed the highest contribution (21 %) on the dissimilarity between north and south which was estimated to be 93 %. Dissimilarity of middle and south was found to 77 % and the greatest contributions belonged to *S. hepatus* (15 %) and *C. aper* (10 %).

Table 2
SIMPER analysis results of discarded species according to their number (The total duration of trawl hauls for each subarea was standardized to 128 hours). Av. Ab.; Average of abundance, Av. Diss.; Average of Dissimilarity, Contrib.; Contribution Percentage, Cum.; Cumulative Percentage.

	North	**Middle**	**average dissimilariy:**		**63.79**
Species	Av.Ab.	Av.Ab.	Av.Diss	Contrib%	Cum. %
Capros aper	774	10561	8.61	13.49	13.49
Coelorhynchus coelorhynchus	5369	0	4.72	7.40	20.89
Argentina sphyraena	663	4869	3,7	5.80	26.69
Chlorophtalmus agassizi	229	4199	3.49	5.47	32.16
Lepidotrigla cavillione	44	3781	3.29	5.15	37.32
Lampanyctus crocodilus	445	4094	3.21	5.03	42.35
Cithaurus linguatula	77	3589	2.81	4.84	47.19
Hymenocephalus italicus	3941	745	2.78	4.41	51.59
	North	**South**	**average dissimilariy:**		**93.03**
	Av.Abund	Av.Abund	Av.Diss	Contrib%	Cum. %
Serranus hepatus	95	18028	19.13	20.57	20.57
Diplodus annularis	23	6004	6.38	6.86	27.43
Cithaurus linguatula	77	6009	6.33	6.80	34.23
Coelorhynchus coelorhynchus	5369	0	5.73	6.16	40.39

Spicara flexuosa	0	4672	4.99	5.36	45.75
Lepidotrigla cavillione	44	4177	4.41	4.74	50.49
	Middle	**South**	**average dissimilariy:**		**76.73**
	Av.Abund	Av.Abund	Av.Diss	Contrib%	Cum. %
Serranus hepatus	2582	18028	11.40	14.85	14.85
Capros aper	10561	0	7.79	10.16	25.01
Diplodus annularis	225	6004	4.26	5.56	30.57
Parapenaeus longirostris	5736	593	3.79	4.95	35.51
Argentina sphyraena	4869	0	3.59	4.68	40.20
Spicara flexuosa	64	4672	3.40	4.43	44.63
Munida ruttlanti	4522	18	3.32	4.33	48.96
Chlorophtalmus agassizi	4199	0	3.10	4.04	53.00

Discussion and Conclusion

Fishing has significant direct and indirect effects on the habitat, diversity, and community productivity (Machias et al., 2001). Discard practices are very important for fisheries management especially for multispecies trawl fishery. Discard studies require onboard performance usually under rough weather conditions and hard laboratory work which makes it difficult to practice. Machias et al., (2001) supported this idea by indicating the need for special effort and financing for long-term monitoring of the discarded yield. On the other hand discard information is essential for ecosystem based fisheries management. Trawling was reported to be one of the most responsible fishing activity for the bulk of the discards (Stergiou et al., 1999). Eastern Mediterranean fisheries was reported to have four distinct characters compared to those of other areas (Stergiou et al., 1997b): (1) Highly oligotrophic conditions; (2) higher diversity in comparison to other northern temperate environments, but lower than tropical regions; (3) greater number of marketable species than in temperate waters, lower than tropical regions; (4) the small size of species, captured with small mesh sized trawl net increase the diversity as well as the number of discards (Stergiou, 1999).

A total of 311 trawl hauls were done; 49 in the north, 141 in the middle and 121 in the south. Less hauls conducted in the north in comparison to other areas were due to tough sea and weather conditions. Because while there are many bays which are geographically prevented from rough winds, also available and legal to operate in the middle and south of the Aegean Sea, such areas are very limited in the north. The results of our study show average discard ratio (2010-2012) in the Aegean Sea as 33 ± 20 % including 191 species. Yemişken et al., (2014) reported the discard rate to be 32.2 ± 16.5% with 69 discarded species from the

North-eastern Mediterranean. Soykan et al., (2016) stated the discard ratio as 33.2 % from the middle Aegean Sea including 84 discarded species in one legal fishing season (autumn, winter and spring). Sanchez et al, (2004), declared the discard ratio to be 26% covering 309 species in the northwest Mediterranean. Machias et al., (2001) reported the discard ratio from the northeastern Mediterranean as 44%. The results of our study on discard ratios are in accordance with those of performed in the Mediterranean region indicating that multispecies character of Mediterranean ecosystem enables the formation of discards. The main reason for discarding is the lack of commercial value of some of the caught species (Sanchez et al, 2004). Presence of 68 commercial species within the discarded catch composition is very high which means more than 1/3 the discarded fraction were composed of undersized or unmarketable (due to its condition) commercial species. In the present study no species were specifically targeted, but all marketable individuals were separated for sale by the fishermen. It is difficult to nominate a target species in multispecies fishery areas, especially for bottom trawls. Therefore, the term 'commercial catch' may be used instead of 'target catch' to clarify the classification of the total catch for multispecies bottom trawl fishery (Soykan et al., 2016).

Regarding the species composition, north was represented by 82 discarded species while middle (145 species) and south (134 species) were more diverse. SIMPER analysis revealed that *C. aper* and *S. hepatus* were the main species for dissimilarities among regions. The greatest dissimilarity (93 %) between regions occurred in between north and south. Beside This discrepancy is attributable to difference in depths of trawl hauls. Difference is attributable to "depth" factor, because the mean depth (288 m) of the legal trawling zones was almost two times and four times more than the middle (155 m) and south (71 m) respectively.

It was also found that discard ratio was almost two times greater in the south (mean depth 71m, discard ratio 44.2%) than in the north (mean depth 288 m, discard ratio 22%). Yemişken et al. (2014) reported the discarded biomass ratios as 44% for the shallower than 60m depth, and its value was 75% of all the discarded catch. Authors explained this situation with the higher fish productivity of shallow waters than deeper (>60 m) waters. This opinion was also supported by Sanchez et al. (2004) as they stated more discards in shallowest waters than that of deeper areas. This case was revealed by the concentration of the appreciated juveniles at certain time of the year (Aldebert et al., 1998). Furthermore, it was stated that the structure of the coastal fish community varies in the Mediterranean because of new immigrant species entering from the Red Sea (Yemişken et al., 2014). Our study included 6 lesepsian fish species; *Lagocephalus spadiceus, Saurida lesepsianus, Siganus rivulatus, Stephanolepis diaspros, Sphyraena chrysotaenia* and *Uponeus mollucensis*. While four of them were captured only

from the south, *S. lesepsianus* was obtained from both middle and south Aegean Sea. Yemişken et al. (2014) reported 27 lessepsian fish species in the İskenderun Bay (North-eastern Mediterranean).

From the other side, discards are also known to provide nutrition to the ecosystem and enhance productivity, as discards returned to the water can be recycled by the food web (Rijnsdorp and van Beek 1991; Groenewold and Fonds 2000; Bozzano and Sarda 2002; Cabral et al. 2002). Nevertheless, discard material is rapidly consumed by opportunistic scavenging species, such as crabs, starfish and fish among others (Kaiser and Spencer, 1994; Ramsay et al., 1997; Fonds and Groenewold, 2000; Demestre et al., 2000b; Sanchez et al., 2004). It was also mentioned in many studies that scavenging seabirds also benefit the discarded material not only in supporting their populations, but also in their breeding performance in the western Mediterranean (Oro and Ruiz, 1997; Sanchez et al., 2004). From this point of view Reducing discards may not be always beneficial but could potentially cause some negative impacts on the ecosystem at least in the short term, in contrast to the objectives of ecosystem based fisheries management (EBFM) (Zhou, 2008).

Our study showed that discards generated by bottom trawling in the Aegean Sea constitute an important fraction of the total catch and that the number of species affected is very high. The area is the most efficient trawling zone among Turkish Seas thus requiring long-term monitoring in terms of fish stocks and trawl discards to maintain a sustainable fishery. Therefore, discarding features (species composition, discard ratio, CPUE values and etc.) of Aegean Sea trawl fishery should be more seriously considered during decision making.

References

1. Aldebert, Y., Sánchez, P., Demestre, M. - Scale of temporal variability of groundfish landings in Northwestern Mediterranean - Rapp. Commun. Int. Mer. Médit. 35, 1998, 364–365.
2. Allain, V., Biseau, A., & Kergoat, B. - Preliminary estimates of French deepwater fishery discards in the Northeast Atlantic Ocean - Fisheries Research, 60 (1), 2003,185-192.
3. Demestre, M., Sánchez, P., Kaiser, M.J. - The behavioural response of benthic scavengers to otter-trawling disturbance in the Mediterranean - In: Kaiser, M.J., de Groot, S.J. (Eds.), Effects of Fishing on Non-tar get Species and Habitats. Blackwell Scientific Publications, Oxford, 2000, 121–129.
4. Fonds, M., Groenewold, S. - Food subsidies generated bythe beam-trawl fisheries in the southern North Sea - In: Kaiser, M.J., de Groot, S.J. (Eds.), Effects of Fishing on Non-target Species and Habitats. Blackwell Scientific Publications, Oxford, 2000, 130–150.

5. Gilman, E., Perez Roda, A., Huntington, T., Kennelly, S. J., Suuronen, P., Chaloupka, M., & Medley, P. A. H. - Benchmarking global fisheries discards - Scientific reports, 10(1), 2020, 1-8.
6. Hall, S.J. - The effects of fishing on marine ecosystems and communities - Blackwell Science, London, 1999, 274 pp.
7. Kaiser, M.J., Spencer, B.E. - Fish scavenging behaviour in recently trawled areas - Mar. Ecol. Prog. Ser. 112, 1994, 41–49.
8. Kelleher, K. - Discards in the World's Marine Fisheries: An update - FAO Fisheries and Technical Paper. No: 470. Rome, 2005, 134 pp.
9. Machias, A., Vassilopoulou, V., Vatsos, D., Bekas, P., Kallianiotis, A., Papaconstantinou, C., & Tsimenides, N. - Bottom trawl discards in the northeastern Mediterranean Sea - Fisheries research, 53(2), 2001, 181-195.
10. Oro, D., Ruiz, P. - Exploitation of trawler discards by seabirds in the northwestern Mediterranean: differences between the Ebro Delta and the Balearic Islands areas - ICES J. Mar. Sci. 54, 1997, 695–707.
11. Phiri, H. & Shirakihara, K. - Distribution and seasonal movement of pelagic fish in southern Lake Tanganyika - Fisheries Research, 41, 1999, 63–71.
12. Ramsay, K., Kaiser, M.J., Hughes, R.N. - A field study of intraspecific competition for food in hermit crabs (*Pagurus bernhardus*) - Estuar. Coast. Shelf Sci. 44, 1997, 213–220.
13. Sánchez, P., Demestre, M., & Martí, P. - Characterisation of the discards generated by bottom trawling in the northwestern Mediterranean - Fisheries Research, 67(1), 2004, 71-80.
14. Soykan, O., Akgül, Ş. A., & Kınacıgil, H. T. - Catch composition and some other aspects of bottom trawl fishery in Sığacık Bay, central Aegean Sea, eastern Mediterranean - Journal of Applied Ichthyology, *32*(3), 2016, 542-547.1
15. Stergiou, K.I. - Effects of changes in the size and shape of codend on catch of Aegean Sea fishes - ICES J. Mar. Sci. 56, 1999, 96–102.
16. Stergiou, K.I., Christou, E.D., Georgopoulos, D., Zenetos, A. and Souvermezoglou, C. - The Hellenic Seas: Physics, chemistry, biology and fisheries. - Ocean. Mar. Biol. Ann. Rev. 35, 1997, 415–538.
17. Stergiou, K.I., Economou, A., Papaconstantinou, C., Tsimenides, N. And Kavstdas, S. - Estimates of discards in the hellenic commercial trawl fishery - Rapp. Comm. Int. Mer Medit., 35, 1998, 490-491.
18. Tosunoğlu, Z. & Aydın, C. - Technical characteristics of demersal trawl nets recently used in the Turkish coast of the Aegean Sea - J Fish. Sci. Com 1, 2007, 184–187.
19. TUIK - Available at: http://www.tuik.gov.tr/PreHaberBul- € tenleri.do?id=10863 (accessed on 25 July 2020)
20. Yemisken, E., C. Dalyan, and L. Eryilmaz. - Catch and discardfish species of trawl fisheries in the Iskenderun Bay (Northeastern Mediterranean) with emphasis on lessepsian and chondricthyan species - Mediterranean Marine Science 15(2), 2014, 380-389.

21. Zhou, S. - Fishery by-catch and a discards: a positive perspective from ecosystem-based fishery management - *Fish And Fisheries,* 9, 2008, 308-315.

A DATA-BASED STUDY ON THE COMPARISON OF FISHING GEAR SELECTIVITY AND FISHERS' SELECTIVITY IN THE BOTTOM TRAWL FISHERIES

Adnan TOKAÇ[1], M. Hakan KAYKAÇ[1]
[1]Ege University Faculty of Fisheries 35150, Bornova, İzmir, Turkey

Abstract

The improvement of trawl codend selectivity and discard rates is crucial for sustainable trawl fisheries and management. Some technical improvements to increase selectivity on the trawl codend such as increasing the mesh size and reducing the number of meshes around the codend may cause a very little amount of loss from the economical fish to be caught. This is one of the most undesirable situations for fishers and generally it is not possible to agree on this point at the first stage with the fishers'. However, in traditionally used trawl nets, a second selection procedure is also applied once more to the species caught on the deck by the fishers, and the species are separated mainly into two groups as will be marketed and discarded. In this study, a comparison was made between gear selectivity versus fisher's selectivity for hake (*Merluccius merluccius*) in three different trawl codend using the previous selectivity studies data. For this purpose, fishers' selectivity data were used which were recorded in previous fishing gear-focused selectivity studies. Thus, it has been possible to make a comparison between previously published fishing gear selectivity results and fisher's selectivity results. The results indicated that when the fishing gear selectivity is improved, the selectivity is coming closer to the fisher's selectivity, and the amount of discarded fish decreases as well. The main goal should be to ensure the fisher's selectivity in the trawl codend. Thus, numerous advantages such as cost reduction, use of unnecessary labor and time, and most importantly, protecting the ecosystem will be achieved.

Keywords

Selectivity, fishers, bottom trawl, Mediterranean Sea

Introduction

Conventionally, selectivity trawl fisheries has been regulated by means of a legally defined minimum codend mesh size. However, it is apparent that many other aspects of gear design also influence gear selectivity (Reeves et al., 1992). Many researchers have therefore suggested increasing the mesh size and ⁄ or changing the mesh shape in the codend (Tokaç, et al., 2004, 2010; Bahamon et al., 2006; Sala et al., 2008; Sala and Luchetti, 2010). In addition, the General Fisheries Commission for the Mediterranean (GFCM) has encouraged studies aimed at improving selectivity and reducing discards of the Mediterranean demersal trawl fleet (GFCM, 2007). The Council Regulation of the European Commission concerned with management measures for sustainable exploitation of fishery resources in the Mediterranean Sea also requires EU countries that use towed nets, i.e. demersal trawls, to replace the 40 mm diamond mesh with a square mesh at the codend, or, if the ship owner makes a justified request, with a 50 mm diamond mesh (E.C., 2006).

However, the size selection in the sea by the gear is followed by a fisher selection process on the vessel resulting in that only a proportion of the catch reaching the deck on the fishing vessel will be landed in the harbour. The fishers sort the catch on the deck of the fishing vessels into landings and discards (Mytilineou, 2018). In this study, a comparison was made between gear selectivity versus fisher's selectivity for hake (*Merluccius merluccius*) in three different trawl codend using the previous selectivity studies data. For this purpose, fishers' selectivity data were used which were recorded in previous fishing gear-focused selectivity studies. Thus, it has been possible to make a comparison between previously published fishing gear selectivity results and fisher's selectivity results.

Material and methods

The 26.2 m LOA, 294 kw commercial trawler was chartered for a 15-day sea trial from 5 to 27 August 2004. Trawling was carried out in international waters of the Aegean Sea at depths of 274–426 m. All tows were carried out during daytime. Towing duration varied between 130 and 430 min, and towing speed varied from 2.1 to 2.2 knots. Fishing was conducted using a conventional bottom trawl with 900 meshes around the mouth. Three different codends were used to study the overall selection process. The first one had 300 meshes around its circumference (three seams of 100 mesh panels) as in commercial practice (300 MC). The second had 200 meshes (33% reduced, two seams of 100 mesh panels) around its circumference (200 MC). Finally, the third was constructed as 150 diamond meshes on the lower and 75 square meshes on the top panel

(SMTPC) (Figure 1). Three codends were constructed of netting which was made of 40 mm nominal mesh size PE material. The covered codend method was used to collect the selectivity data (Wileman et al., 1996). The cover used was 10.15 m in length and made of 24 mm nominal mesh size knotless PA (polyamide) netting. It was supported by two hoops 1.9 m in diameter. Selectivity and discard data were collected for hake. At the end of each tow, first the cover catch was taken and target species were separately sorted from the rest of the catch and weighed. Meanwhile, the crew of the fishing boat sorted the marketable codend catch and left the discards on deck. Thus, the fisherman performs a second selection process on the deck. Full or sub-samples were taken and weighed separately for marketable catch and discards. For the target species, length measurements were taken to the cm below. Before the data analysis 0.5 cm was added to each length class. Data from the sub-sampled catch were raised prior to the estimation of the selection parameters. Selectivity parameters were calculated by fitting a logistic equation using the maximum likelihood method as given in Wileman et al. (1996). CC 2000 software (ConStat, 1995) was used in the analysis. Selection parameters for hake were calculated using a less rigorous approach of stacked haul method (Millar et al., 2004), which does not incorporate an explicit modelling of the between haul variation.

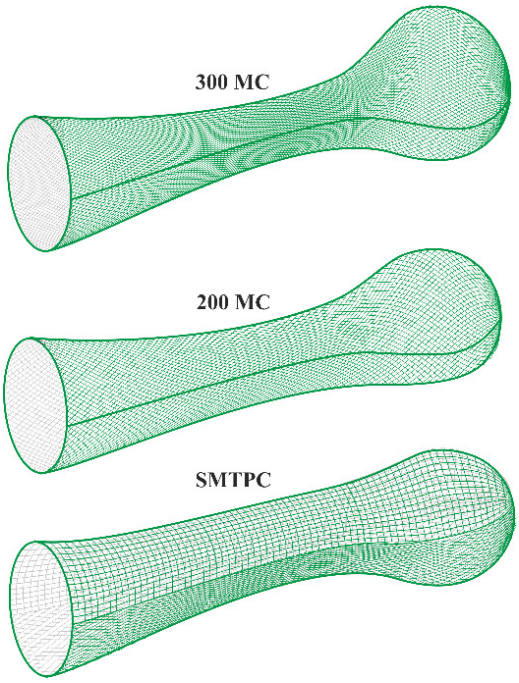

Figure 1
Illustration of tested codends: 300 MC_conventional type; 200 MC_ 33% reduced and SMTPC_square mesh top panel codend

Codend Selectivity

Selectivity data were collected using the covered codend method and selection curves of the pooled data were obtained by fitting a logistic function:

$$r(l) = \exp(v_1 + v_2 l) / \left[1 + \exp(v_1 + v_2 l)\right]$$

where *r(l)* is the retained proportion of length class *l*, given that it entered the codend (Wileman et al., 1996), and $\nu=(\nu_1, \nu_2)T$ is the vector of the selectivity parameters. The values of L_{50} were estimated from the expressions:

$$L_{50} = \frac{-v_1}{v_2}$$

Fisher's Selectivity

Selectivity data on board were collected using the marketed (codend) discard (cover) method and selection curves of the pooled data were obtained by fitting a logistic function:

$$r(l) = \exp(v_1 + v_2 l) / \left[1 + \exp(v_1 + v_2 l)\right]$$

where *r(l)* is the retained proportion of length class *l*, given that it obtained on board like cover codend (Wileman et al., 1996), and $\nu_f=(\nu_{1f}, \nu_{2f})T$ is the vector of the selectivity parameters. The values of L_{50} were estimated from the expressions:

$$L_{50} = \frac{-v_1}{v_2}$$

All these parameters were calculated by maximum likelihood using the software CC 2000 (ConStat, 1995).

Results

Selection curves of 300 MC, 200 MC, and SMTPC codends were found to be significantly different when considering gear and fisher's selectivity for each codend type (Figure 2, 3 and 4). L50 values of 10.81 and 18.71, and SR values of 6.12 and 1.61 cm for 300 MC; 11.60 and 25.01, and SR values of 4.07 and 2.95 cm for 200 MC; 12.89 and 19.33 and SR values of 7.44 and 2.97 cm for SMTPC were estimated for gear and fisher's selectivity, respectively (Table 1).

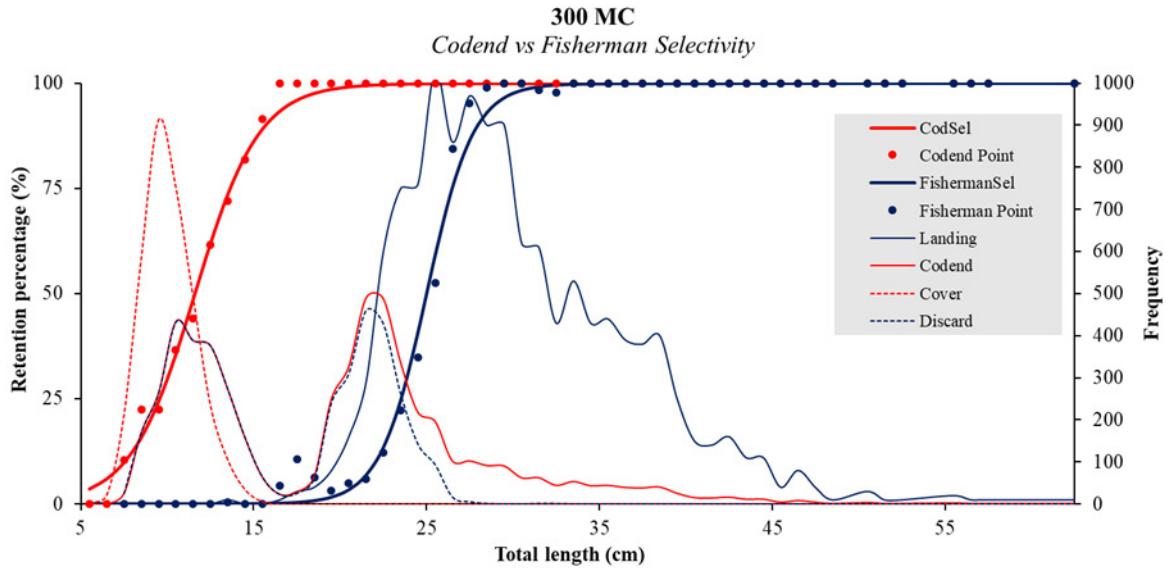

Figure 2
300 MC. Selection curves and length frequency distributions of the population entering and escaping from the codends (gear-codsel) on the left (red) and selection curves and length frequency distributions of the codend population seperated by fisher's as marketed (codend) and discard (cover) (fisher's sel) on the right (blue).

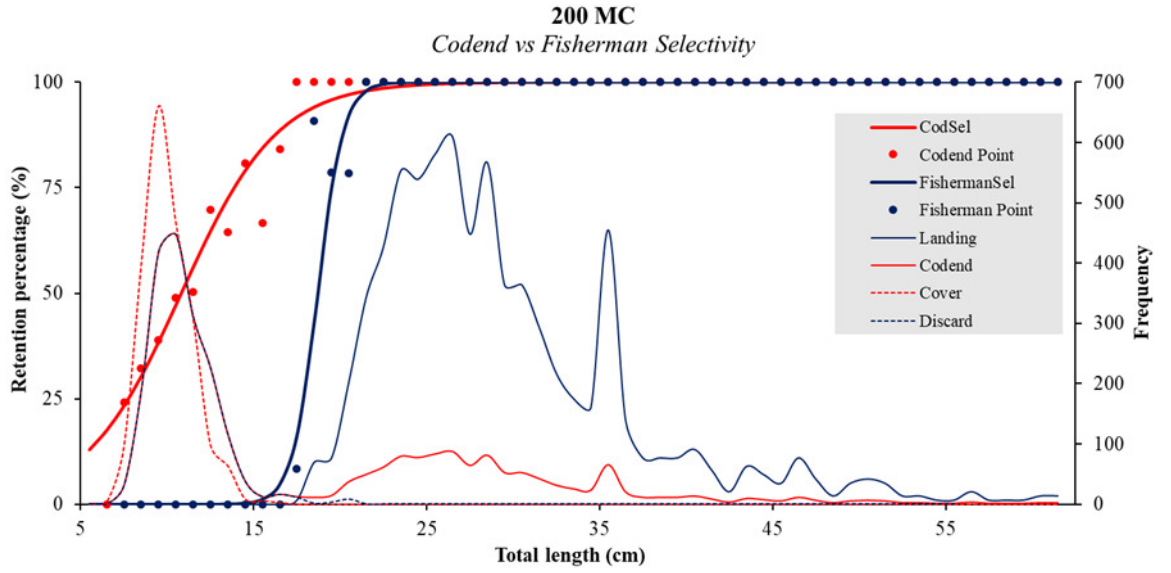

Figure 3
200 MC. Selection curves and length frequency distributions of the population entering and escaping from the codends (gear-codsel) on the left (red) and selection curves and length frequency distributions of the codend population seperated by fisher's as marketed (codend) and discard (cover) (fisher's sel) on the right (blue).

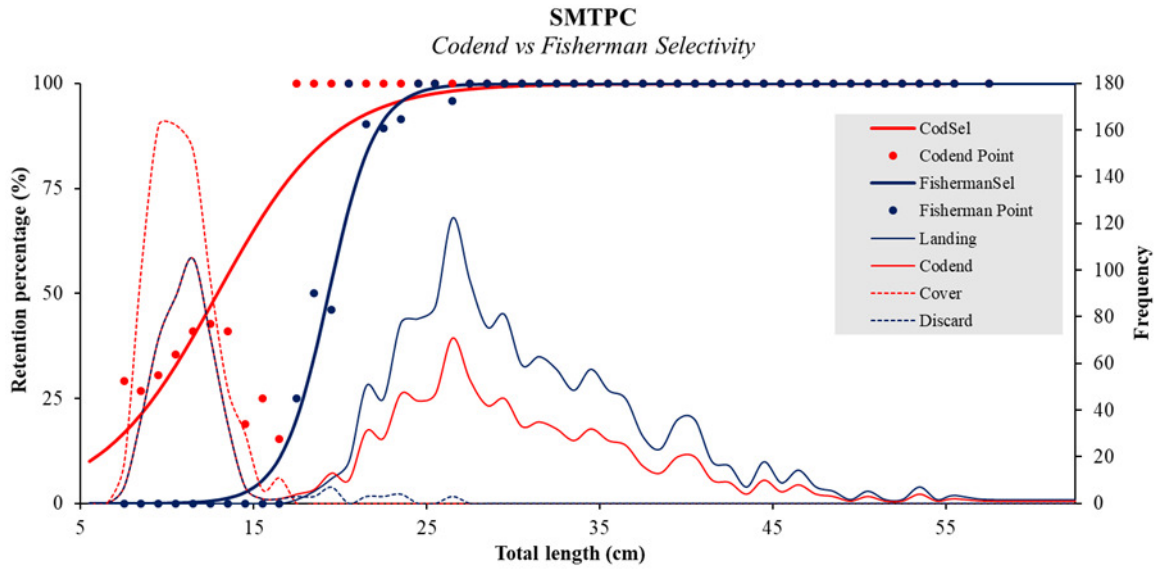

Figure 4
SMTPC. Selection curves and length frequency distributions of the population entering and escaping from the codends (gear-codsel) on the left (red) and selection curves and length frequency distributions of the codend population seperated by fisher's as marketed (codend) and discard (cover) (fisher's sel) on the right (blue).

Discussion

The obvious problems for both target and by-catch species in the Mediterranean are the small sizes of the retained individuals and the multi-species nature of the fisheries. Hake escape probability through bottom trawl codend was generally low for the species population structure in the fishing grounds examined, where commercial trawl fishery is practiced (Mytilineou et al., 2018). When considering the results of the square mesh top panel codend (SMTPC) in the present study show higher mean L50 values than that of the commercial codend (300 MC) and 33% reduced codend (200 MC) for hake. In case of considering the codend selectivity, the results of the square mesh top panel codend (SMTPC) have higher mean L50 values than the 300 MC and 200 MC for hake. On the contrary, when considering the fisher's selectivity, it is seen that 300 MC has the highest L50 value (Table 1). This is a pretty expected result because of the amount of discard of this codend is much higher than the other codends. Conventional bottom trawling is a fishing methods producing high quantities of discards. Historically, trawl selectivity studies were always focussed on modelling only the gear selectivity occurring in the sea. However, the size selection in the sea by the gear is followed by a fisher selection process on the vessel resulting in that only a proportion of the catch reaching the deck on the fishing vessel will be landed in the harbour (Mytilineou et al., 2018).

Table 1
Selectivity parameter estimates [L50 (cm), length at 50% retention; SR (cm), selection range; CI, confidence interval; SF, selection factor; v1 and v2, maximum likelihood estimators of selectivity parameters; R11, R12, and R22, variance matrix measuring within-haul variation; d.f., degrees of freedom]; number of specimens in codend and cover for 300 MC and SMTPC.

													Codend		Cover
	L_{50}	SE	R	SE	v_1	v_2	R_{11}	R_{12}	R_{22}	Deviance	d.f.	*p-Value*	$N_{landing}$	$N_{discard}$	N_{cover}
200 MC CODEND	**10.81**	0.09	6.12	0.31	-3.882	0.359	0.0369	-0.0034	0.0003	40.82	54	0.907	**2899**		2112
200 MC FISHERMAN	18.71	0.22	1.61	0.19	-25.508	1.364	9.2178	-0.4767	0.0249	24.27	53	1.000	1071	1828	2112
300 MC CODEND	**11.60**	0.07	4.07	0.14	-6.253	0.539	0.0423	-0.0037	0.0003	67.49	49	0.041	**5497**		3362
300 MC FISHERMAN	25.01	0.11	2.95	0.14	-18.633	0.745	0.7539	-0.0312	0.0013	78.67	47	0.003	1281	4216	3362
SMTPC CODEND	**12.89**	0.31	7.44	0.65	-3.816	0.296	0.0994	-0.0078	0.0007	101.8	50	0.000	**1215**		784
SMC FISHERMAN	19.33	0.33	2.97	0.28	-14.306	0.740	2.1123	-0.0999	0.0048	25.69	50	0.998	764	451	784

Conclusion

Improving of a larger mesh size by ensuring the mesh opening during trawling is essential to improve size selectivity. Not only gear selectivity but also fisherman selectivity needs to be studied.The number of studies on this subject needs to be increased, and this remarkable difference between gear selectivity and the fishers own selectivity needs to be explained to fishermen very well.

References

1. Bahamon, N., Sarda, F., Suuronen, P. 2006. Improvement of trawl selectivity in the NW Mediterranean demersal fishery by using a 40 mm square mesh codend. Fish. Res., 81, 15–25.
2. E.C. 2006. Council Regulation (EC 1967 ⁄ 2006) concerning management-measures for the sustainable exploitation of fishery resourcesin the Mediterranean Sea, amending Regulation (EEC) No 2847⁄93 and repealing Regulation (EC) No 1626⁄94. Off. J. E.U. 409, 75.
3. GFCM, 2007. FAO Report of the tenth session of the Scientific Advisory Committee, Nicosia, Cyprus, 22–26 October 2007. Fish. Res. 856, 1–157.
4. Mytilineou, C., Herrmann, B., Mantopoulou-Palouka, D., Sala, A., and Megalofonou, P. 2018. Modelling gear and fishers size selection for escapees, discards, and landings: a case study in Mediterranean trawl fisheries. – ICES Journal of Marine Science, 75: 1693–1709.
5. Reeves, S. A., Armstrong, D. W., Freyer, R. J., Coull, K. A. 1992. The effects of mesh size, cod-end extension length and cod-end diameter on the selectivity of Scottish trawls and seines. ICES J.Mar. Sci. 49, 279–288.
6. Sala, A., Lucchetti, A. 2010. The effect of mesh configuration and codend circumference on selectivity in the Mediterranen trawl Nephrops fishery. Fish. Res. 103, 63–72.
7. Sala, A., Lucchetti, A., Piccinetti, C., Ferretti, M. 2008. Size selection by diamond- and square-mesh codends in multi-species Mediterranean demersal trawl fisheries. Fish. Res. 93, 8–21.
8. Tokaç, A. Özbilgin, H., Kaykaç, H. 2010. Selectivity of conventionaland alternative codend design for five fish species in the AegeanSea. J. Appl. Ichthyol. 26, 403‑409.
9. Tokaç¸ A., Özbilgin, H., Tosunoğlu, Z. 2004. Effect of PA and PE material on codend selectivity in Turkish bottom trawl. Fish. Res.67, 317–327.

Wileman, D. A., R. S. T. Ferro, R. Fonteyne & R. B. Millar (Eds.), 1996. Manual of methods of measuring the selectivity of towed fishing gears. ICES Cooperative Research Report, 215: 1-126. (Copenhagen).

HYDROGRAPHY ON FISHING VESSELS – A FEASABILITY STUDY LEADS TO AN OPEN SOURCE DEVELOPMENT

Andreas Hermann[1], Daniel Stepputtis[1], Frederik Furkert [1], Mathis Björner[2], Michael Naumann[2]
[1]Thünen Institute of Baltic Sea Fisheries, Alter Hafen Sued 2; 18069 Rostock, Germany
[2]Leibniz Institute for Baltic Sea Research Warnemünde, Seestraße 15, 18119 Rostock, Germany

Abstract

The knowledge of hydrographic conditions is of central importance for the assessment of the state of marine ecosystems – with all its implications on climate or usage of the sea. Currently, data collection is mainly carried out by environmental monitoring programs and very costly. Spatial and temporal resolution is insufficient and data validation is mostly hand-operated before it can be stored in scientific databases. Therefore, we urgently need new monitoring strategies. More efficient data collection not only contributes to a better understanding of the marine ecosystem, but is relevant to issues such as:

- Fish stock forecasts
- Monitoring of the marine environment e.g. North and Baltic Sea (HELCOM)
- State on ocean acidification, oxygen deficiency and eutrophication
- Implementation of sustainable development goals (e.g. MSRL in Europe)

Ships of opportunity could play an important role here. Today, ferries and cargo ships can be equipped with FerryBox systems 1 to collect hydrographic data, but they are limited to surface water measurements and ferry routes or sea lanes. In contrast, fishing vessels deploy their gear deep below the surface. Here we present a method for using fishery as ships of opportunity in data collection and our results from a feasibility study on a fleet of commercial fishing vessels over the period of nine weeks. We show our experience with existing systems, the collected data, feedbacks from fishermen and a fine granulated list of necessary system features, which are not yet offered by existing systems. Therefore we started to develop HyFiVe (Hydrography on Fishing Vessels) - an autonomous measurement system to be installed on board of fishing vessels. We show that this can carry out a significant increase in the temporal and spatial data collection density at a

relatively low cost. Further we present the development status, the results of which will be published under open source licenses.

Introduction

Isaac Newton said; "What we know is a drop, what we don`t know is an ocean". Even though much has changed since this quote, it is still true for the oceans themselves, especially below sea surface. The temporal and spatial resolution of physical and chemical parameters of the water body (hydrography) is insufficient to follow its increasing process dynamic. Therefore, we need to intensify data measurement density and improve the process of validation for important forecasts on climate development and the evolution of underwater flora and fauna. This is especially true for coastal and marginal seas with limited water exchange, which represent a particularly sensitive ecosystem such as the Baltic Sea. Inflows of oxygen-rich water masses from the North Sea and North Atlantic represent an important control process for its overall state. In marine research, hydrography provides important foundations not only in the field of oceanography, but also in the areas of marine biology, marine chemistry, geological processes and marine ecology. Here it plays a prominent role in a variety of processes that have a decisive influence on the development of fish stocks and other living aquatic resources.

At present, data collection is mainly carried out by research vessels, moored platforms and drifting Argo-Floats 15. Research vessels visit determined positions a few times per year to collect measurement profiles with very precise profiling CTD instruments and water samplers during their research cruises; but the spatial and temporal resolution is very low. Moored measuring stations continuously collect data at a few strategic positions; their temporal resolution is high, but their spatial resolution is low. Floats use sea currents at different depths for navigation and can increase the density of data collection, but are limited to suitable areas. However, all these methods are very cost-intensive and can increase data collection density only at considerable expense. For this reason, ferries and cargo ships are equipped as ships of opportunity with FerryBoxes, which are measurement systems that collect hydrographic data along the way. However, they only measure close to sea surface. The same applies to data collected by satellites that reveal physical parameters. However, the fields of climate research as well as marine and fishery research require physical and geochemical parameters with their dynamics in the entire water column.

In this context, fishing vessels are ideal ships of opportunity, as they operate widely distributed in time and space and regularly profile their gear through the water column. However, the data collection systems on board commercial fishing vessels need to operate fully autonomously and transmit their data without disturbing any fishing operations. Key features of HyFiVe include autonomous recording of hydrographic data, transmission and visualisation of data from a large number of vehicles to a shore-based server, remote maintenance access from shore, automatic validation algorithms, intelligent power supply and advanced trigger functions.

Feasibility study and requirements

In contrast to research vessels, fishing vessels operate almost all year round in wide areas. A system to increase the data acquisition density for hydrographic parameters for autonomous use on fishing vessels has special requirements. On a trawler, a typical deployment position is at one of the trawl doors.

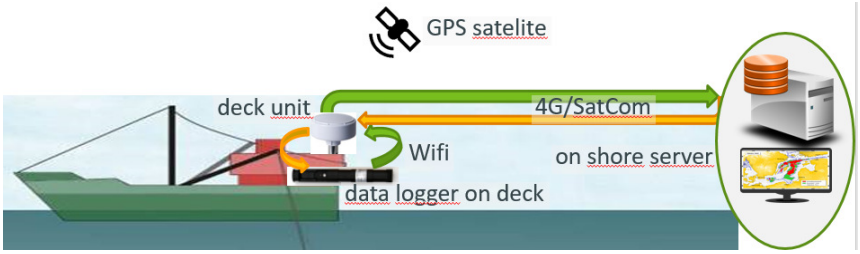

Figure 1
HyFiVe system: autonomous hydrographic data acquisition for fisheries above: non fishing mode below. fishing mode

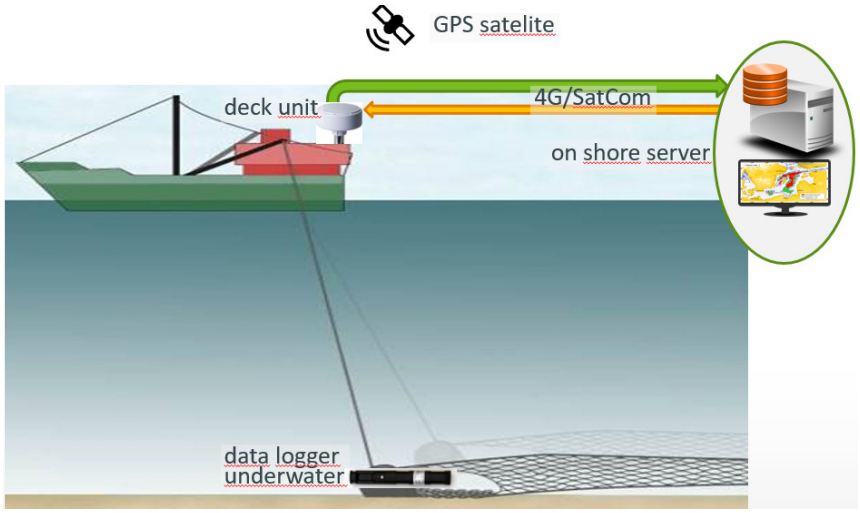

We use three system components for data collection, position allocation and data transmission, processing and visualisation:

- data logger for underwater use at the fishing gear,
- deck unit on the vessel for data read from the data logger on air, record of the vessel positions via GPS and on shore data transmission,
- on shore server including web service package to collect, validate and process data from all vessels towards international databases,

Figure 1 illustrates the functioning of HyFiVe system in its two operating modes. Our main focus is on optimised data formats and protocols for the bidirectional data flow between all components and towards national and international databases.

A feasibility study with four commercial German fishing trawlers (demersal trawler with a length of 20-30 m) was carried out in the period from April 2016 to June 2016, in which semi-autonomous data loggers were installed on the trawl doors and recorded hydrographic parameters there. The recording was limited to temperature, salinity, dissolved oxygen content, water turbidity and water pressure. All parameters in conjunction with depth, time and global coordinates of the measuring positions. We used a system from the company NKE Instruments, which can record at least parts of the data in a synchronised way. We procured this system and critically tested it under real conditions in the German Baltic Sea commercial fishery fleet, deployed in the region of Arkona Sea to Bornholm Sea. In the period from 20.4.2016 to 16.6.2016 on four fishing vessels: Christin Bettina (25m), Blauwal (26m), Antares (21m) and Crampas (18m) from Sassnitz. Figure 2 shows the mounting of the data loggers at a trawl door and the position logger and data synchronisation unit on deck.

Figure 2
mountings: data logger at trawl door (left) and GPS logger on deck (right)

During the nine-week test period, 198 hauls were recorded. One system failed during the functional test and two vessels had longer downtimes due to technical problems or crew illness. The other vessels showed an average of 10 hauls per week, which corresponds to 20 vertical profiles and 120 hours of underwater data collection per week and vessel.

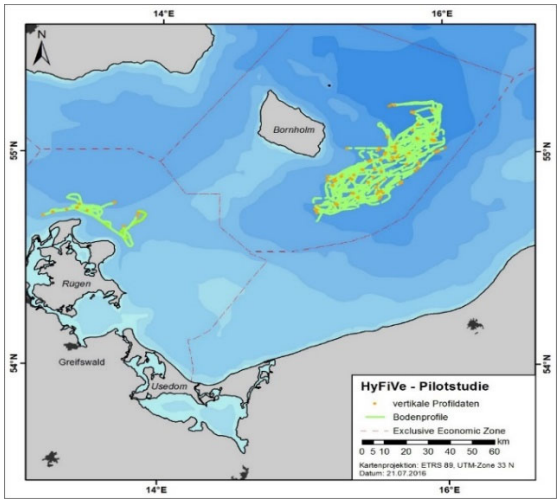

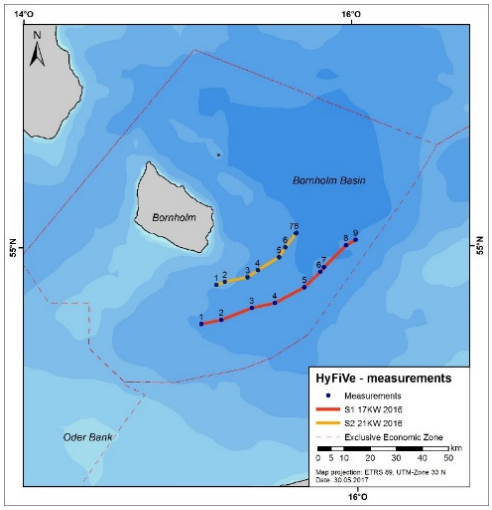

Figure 3

left: positions of hydrographic measurements during test phase; profiles (yellow dots) underwater tracks (green lines)

right: positions for two exemplary hydrographic sections (Figure 4 left and right)

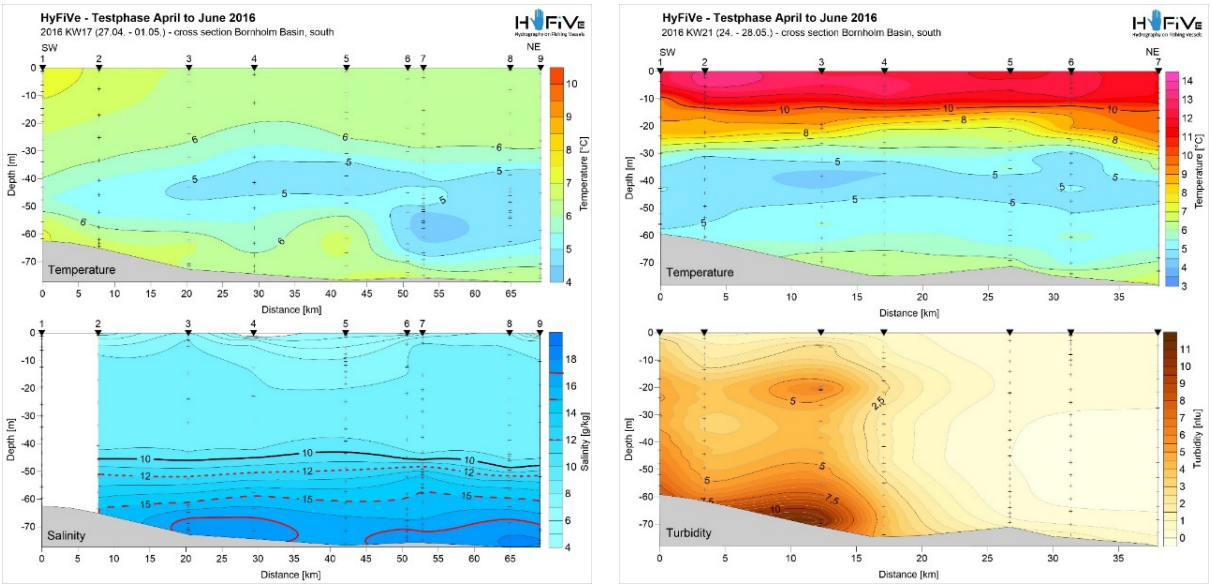

Figure 4
left: Bornholm Sea section1; temperature and salinity 27.4.- 1.5.16; right: Bornholm Sea section 2; temperature and turbidity: 24.-28.5.16

The result is a very high-resolution data set in the areas south of Bornholm island and northeast of Ruegen island. We computed the measured data by example from the area south of Bornholm along two vertical lines shown in Figure 3 right. It is presented in form of two hydrographic sections each on its own time slot and target parameters. The graphs are shown in **Figure 4**.

From feasibility study to system development

Even if the system in the test phase did not meet the basic requirements for this application, the study showed that a system introduced as HyFiVe:

- can collect considerable amounts of hydrographic data,
- can be implemented with current technology,
- cannot be setup from any available technical system worldwide yet,
- has a high acceptance by the fishermen (when local data visualisation is available)

Furthermore, the study delivered a large number of important system requirements for autonomous operation at commercial fishing vessels. For implementation, it is necessary to develop innovative and universal solutions and concepts. In addition to the basic functionality of existing logger systems, a number of functions are required that enable the system to be used on a large scale. In particular, modularity in sensor assembly, remote maintenance, long battery

life and easy recharging of the data logger, special trigger management of the sensors (e.g. parameter dependent trigger intervals) and reliable bidirectional data transmission across all components are essential components for this application. Finally, after intensive market research, it became clear that such a system would only be possible through a new development in form of a third-party funding project. First project application was in 2016, with positive funding decision in 2021.

HyFiVe project

HyFiVe project has three local project partners: Hensel Elektronik, Leibnitz-Institute for Baltic Sea Research Warnemuende and Thuenen Institute of Baltic Sea Fisheries and is funded by the Federal Ministry of Food and Agriculture. Project duration is 3 years from September 2021 to August 2024. The general project outline is:

1. determination of the specification of the overall system,
2. development of a multi-parameter data logger,
3. development of a deck unit,
4. development of server architecture including a web service package for storage,
5. storage, administration, analysis and visualization of the data,
6. integration and validation of the overall system,
7. and exploitation and publication.

The project philosophy is to use open concepts, open standards and open sources and to be modular, future-proof and modifiable. All results, sources and construction plans will be published under open source licenses to achieve sustainability and connectability. We use MPL 2.0 2 for software, CERN OHL W 3 for hardware and CC-BY-SA 4 for documentation with weak copyleft and commercial usability.

First results

So far, functional samples of the three main components data logger, deck unit and land-based server have been developed and tested in their basic functions to be able to determine the overall functionality of the system. The wireless dataflow between data logger and deck unit based on WiFi is shown in **Figure** 5. The transfer between the deck unit and the land-based server is via mobile phone network.

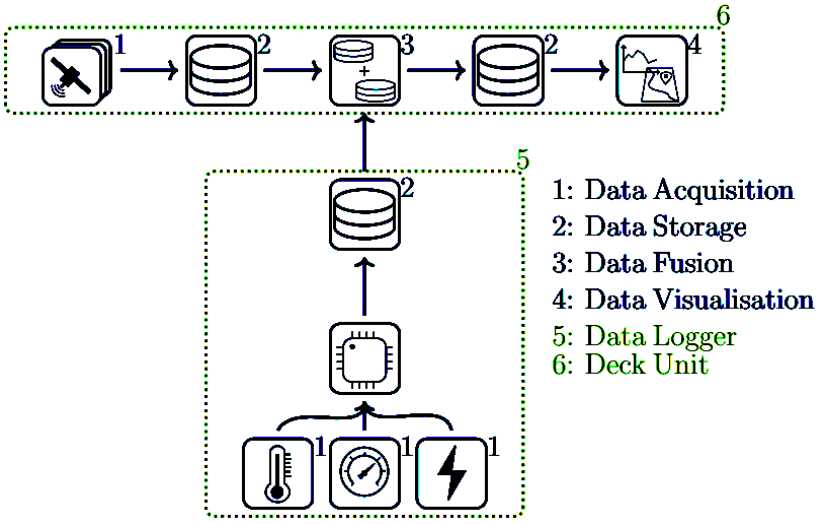

Figure 5
Dataflow between data logger and deck unit

The data logger uses an ESP32 microcontroller [5] and integrates the conductivity probe K0.1 from Atlas Scientific 6, the temperature probe TSYS01 7 and the pressure sensor MS5837-30BA 8 to measure CTD. While in the water, it stores the measured data on an SD card and sends it to the deck unit after surfacing. Figure 6 left shows it attached to the CTD of the RV Elisabeth Mann Borgese [14] for validation tests.

The deck unit consists of a Raspberry Pi 9 and a router RUT955 by Teltonika 10. The router provides WiFi, global position data and a link to mobile network. A multiband antenna on the cover enables the external connections. The deck unit software stores GPS data, merges it with the CTD data from the data logger, visualize the data and transfers it to the onshore server. For these steps we use the open source software Node-Red (data fusion) 11, InfluxDB (data storage) 12 and Grafana (data visualisation) 13.

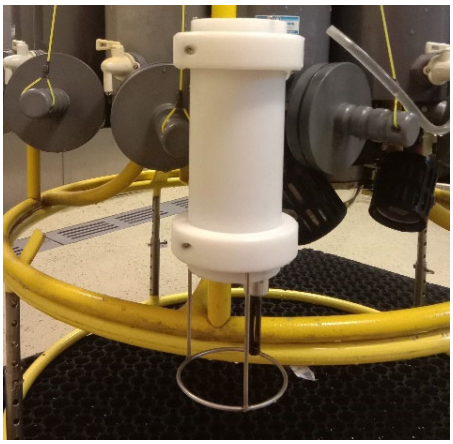

Figure 6
left: data logger on CTD

right: data logger at plankton sampler

The system had been tested in two typical deployment scenarios of fishery trawls at on the cruise EMB295 in July 2022. First, it was attached to the CTD sampler (figure 6 left) to collect down- and up-cast data: profiles at 1 Hz with depths of up to 230 meters. The parallel CTD measurements are suitable for validation. Second, it was attached to a dragged plankton net to collect data on a horizontal track (figure 6 right): trawl data over 700 meters at about 3m depth were collected. The data logger autonomously started the measurement of the profile when immersed in water and detected its end after surfacing, transmitting the data to the deck unit. The deck unit added the GPS positions to each measurement and transmitted the data onshore where we visualized and evaluated the data. More detailed information about accuracy and reliability will be published later. Figure 7 shows the measured temperature and conductivity over depth at 7.7.2022, 16:13 (UTC) in position 57.191°N, 20.072°E. It indicates the different stratified water layers between surface and seafloor. At around 20 m water depth a typical sharp summerly thermocline from 18°C sea surface temperature to 5°C in the intermediate layer is shown, which develops in calm weather conditions. The conductivity diagram shows the same rapid decrease in 20 m water depth between both water layers but a strong increase in about 60-70 m water depth. It detects the pycnocline between surface water layer of lower salinity (fed by freshwater runoff) and higher salinities of the deep water layer (fed by saline inflows from the north Atlantic). The plot in figure 8 exemplary displays the collected temperature data along the plankton sample track in global positions.

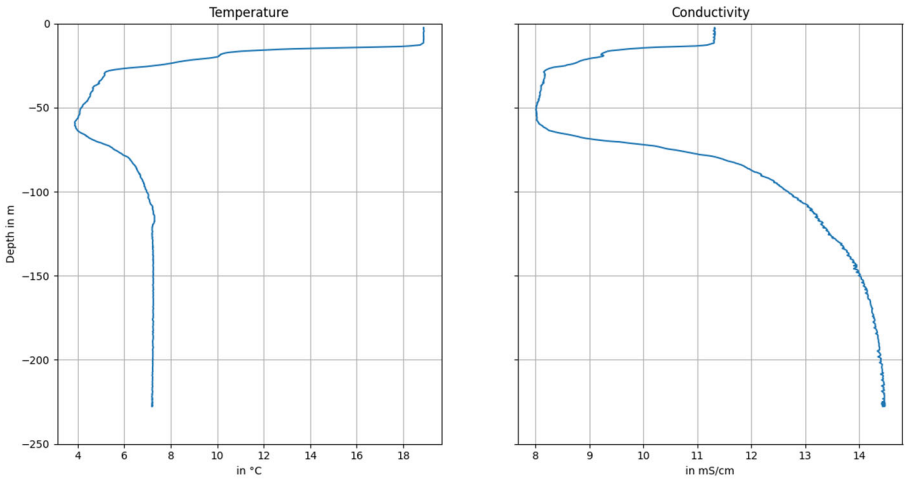

Figure 7
Autonomously measured profiles for temperature and conductivity

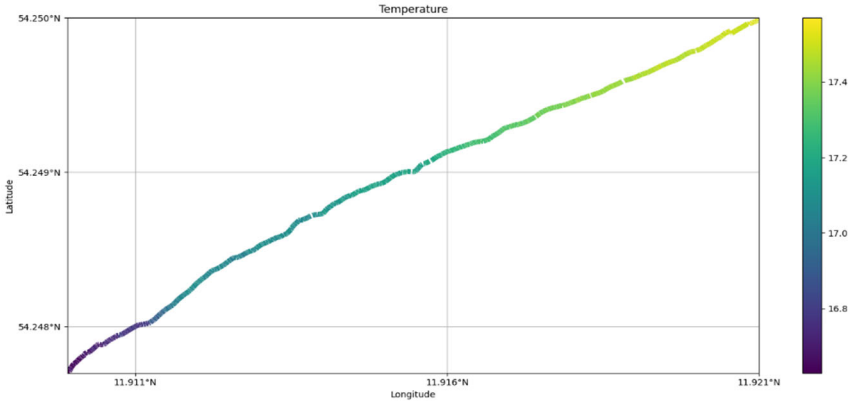

Figure 8
Autonomously measured temperature on a trawl over 700 metres

Next steps

Until now, the system has been tested with a unidirectional dataflow from the logger to the onshore server. Next steps will be the integration of the bidirectional data flow for maintenance from shore and a test on a real fish trawler. The cruise has shown a good functionality of the overall system. Further objectives lie in automated data evaluation algorithms and the integration of different sensors and sensor types to the data logger such as dissolved oxygen, pCO_2, turbidity and others.

References

1. EuroGOOS Ferrybox Whitepaper 2017; https://eurogoos.eu/download/publications/EuroGOOS_Ferrybox_whitepaper_2017.pdf
2. Mozilla Public License Version 2; https://www.mozilla.org/en-US/MPL/2.0/
3. CERN Open Hardware Licence Version 2 -Weakly Reciprocal; https://ohwr.org/cern_ohl_w_v2.pdf
4. Creative Commons Attribution-ShareAlike 3.0 German (CC BY-SA 3.0 DE); https://creativecommons.org/licenses/by-sa/3.0/de/deed.en
5. Microcontroller Espressif ESP32 datasheet; https://www.espressif.com/sites/default/files/documentation/esp32_datasheet_en.pdf
6. Conductivity sensor Atlas Scientific K0.1 datasheet: https://files.atlas-scientific.com/EC_K_0.1_probe.pdf
7. Temperature sensor TSY01 BlueRobotics underwater integration: https://bluerobotics.com/store/sensors-sonars-cameras/sensors/celsius-sensor-r1/
8. Pressure sensor MS5837-30BA BlueRobotics underwater integration: https://bluerobotics.com/store/sensors-sonars-cameras/sensors/bar30-sensor-r1/
9. Microcomputer Raspberry Pi 4 Model B: https://www.raspberrypi.com/products/raspberry-pi-4-model-b/specifications/
10. WiFi and LTE router Teltonika RUT955: https://teltonika-networks.com/de/product/rut955/
11. Node-Red, programming for event-driven applications: https://nodered.org/
12. InfluxDB, open source database system to collect, query and process data: https://docs.influxdata.com/influxdb/v1.8/
13. Grafana, open source data visualization software: https://grafana.com/
14. Campaign list of RV Elisabeth Mann Borgese: https://www.pangaea.de/expeditions/bybasis/Elisabeth%20Mann%20Borgese
15. The Argo Program - Argo and the ocean observing system: https://argo.ucsd.edu/about/observing-system/

DEVELOPMENT OF A BLUE BIOECONOMY FOR SUSTAINABLE PRODUCTION OF MARINE CARBO-HYDRATES FROM BALTIC SEA MACROALGAE

Christian PORSCHE[1] & Hendrik SCHUBERT[1]
[1]University of Rostock, Institute for Biosciences, Aquatic Ecology, A.-Einstein-Str. 3, 18059 Rostock, Germany

Abstract

Blue bioeconomy offers options for the development of innovative products. In the ongoing project (Plant³ – MarZucker), technologies for producing high-quality carbohydrates from marine algae by enzymatic pre-treatment are developed, focussing on the production of fine chemicals for pharmaceutical applications. This aim requires a high degree of quality control all along the production chain, including the source of biomass. To allow sustainable production of standardized quality biomass, aquaculture approaches are developed and tested. An important further aspect of this strategy is to establish a source of additional income for local fishermen.
The development of aquaculture production started on a laboratory scale and lead to on- and inshore prototype facilities. The onshore aquaculture was built in an old cooling channel of the former atomic power plant in Lubmin as a flow-through system. The inshore prototype was constructed in the Wieker lagoon on the island Rügen. Both aquaculture prototype facilities should mainly produce biomass of the green algae *Ulva* sp. Two major issues emerged during the development and running of these facilities. First, administrative complications occured to obtain permission for the installation and operation of on- as well as inshore aquaculture facilities. And secondly biological implications occurred caused by competing species overgrowing the target organism *Ulva* sp. The measures effectively reducing competing species differed between approaches and became more difficult under field conditions because of the higher complexity of the environment. The work for this project is still in progress and will be optimized in the approaching project period.

Keywords

Aquaculture, *Ulva*, onshore cultivation

Introduction

Marine resources are highly influenced by the intensive usage by human society, especially for the food industry. To cope with ongoing and future problems it is important to reduce the impact on the marine ecosystems. Worldwide approaches to developing sustainable and economical marine resources are an ongoing process (Potts et al., 2016; Carballeira Braña et al., 2021; Cochrane, 2021). One approach is the development of ecologically sustainable aquaculture facilities. Here, we focus on cultivating marine macroalgae as a source of specific high-quality carbohydrates like ulvans (Reisky et al., 2019; Tziveleka et al., 2019) in the Western-Pomeranian coastal region. Using this resource for the production of carbohydrates a regional value-added chain shall be established.
The green algae *Ulva* sp. has been chosen as the main target organism because of its fast growth and widespread occurrence along the Western-Pomeranian coast. First, different methods for cultivation on a laboratory scale were tested to optimize cultivation conditions employing physiological parameters assessed. Because of the high morphological plasticity of the genus *Ulva,* the determination on species level was omitted, respecting the ongoing taxonomic debate (Steinhagen et al., 2019; Tran et al., 2022, Wichard, 2015). Using lab-grown strains for inoculation, the exact taxonomic evaluation of them can be determined after the debate is settled. For this work, the parameters of interest are growth characteristics and ulvan content of the isolated strain, as strain-specific parameters are independent of taxonomic affiliation. Secondly, a prototype facility for onshore aquaculture, with the potential for simple scale-up to a production level, was designed and installed. This prototype facility was used to gather reliable data about biomass yield and installation as well as maintenance efforts. These data are crucial concerning the installation of a start-up facility with focus on its applicants, mainly fishermen. In a third approach an inshore aquaculture facility of *Ulva* sp. in a natural habitat without land-based infrastructure was tested. This attempt increases the risk of losses due to natural events such as e.g. overgrowth by other algae or storm events while reducing installation and maintenance costs. To obtain data about the balance of pros and cons, irrespective of administrative problems, especially for industrial-scale installations, such an inshore facility was installed too.

Materials and Methods

The aim of laboratory cultivation of *Ulva* sp. is to find cultivation conditions suitable for *Ulva* sp. in terms of long-term survival and growth of biomass. In the laboratory, the availability of coastal habitat water as a medium for

aquaculture is limited. Furthermore, the composition of habitat water could differ with each acquisition. Therefore, we produced the Ulva cultivation medium (UCM) as described in Stratmann et al. (1996) for the laboratory cultivation.
The first cultivation experiment consisted of 1 l glass beakers with 800 ml UCM and an aeration system (Fig. 1). This cultivation method leads to sufficient growth in short time periods of about 2 to 4 weeks before the growth of epiphytes suppressed the *Ulva* sp. These overgrowing by epiphytes was the main issue of the laboratory cultivation, which elevates with increasing time periods. Additionaly, the cost of the UCM is quite high, so the volume of the UCM was reduced to 250 ml. This cultivation method allows short-term experiments to optimize the cultivation conditions almost without influence of phytoplankton.

Figure 1
Cultivation of *Ulva* sp. in artificial light, in 1 l glass beakers (left) and 250 ml Erlenmeyer flasks (right) with aeration.

The dependencies between growth rate of *Ulva* sp. and levels of salinity and nutrient concentrations (nitrate and ammonium) of the UCM were tested. Therefore, the UCM was modified corresponding to a central composite design, with different salinity (4, 8, 16, 24, 32) and nutrient (21.25, 42.5, 85, 170, 340 mg l^{-1} $NaNO_3$; 1.65, 3.3, 6.6, 13.2, 26.4 mg l^{-1} $(NH_4)_2SO_4$) levels. The experimental setup is further depicted in Fig. 2.
For each combination of factor levels, 250 ml of the respective UCM was filled in an Erlenmeyer flask and placed under artificial light for fourteen days with a photoperiod 16 h day and 8 h night cycle. To calculate the growth rate of each *Ulva* sp. individual, its surface area was determined by photogrammetric survey with the software ImageJ (Wayne Rasband, Maryland, USA) at the start and end of the experiment.

Nut. \ Sal.	-2	-1	0	+1	+2
-2			1		
-1		1	1	1	
0	1	1	4	1	1
+1		1	1	1	
+2			1		

Figure 2
Central composite design (ccd) of the experiment for testing the influence of salinity (Sal.) and nutrient concentration (Nut.) levels (-2, -1, 0, +1, +2). Left: scheme with number of replicates per combination of factor levels: salinity (4, 8, 16, 24, 32) and nutrients (21.25, 42.5, 85, 127.5, 170 mg l^{-1} $NaNO_3$; 1.65, 3.3, 6.6, 9.9, 13.2 mg l^{-1} $(NH_4)_2SO_4$). Right: photography of the implementation of the ccd.

The establishment of onshore installations allows the large-scale production of high amounts of *Ulva* sp. biomass. And the advantages of these onshore installations include the controllability of the environmental conditions. Nevertheless, a suitable location to build these onshore aquaculture installations has to be found. A key factor is hereby the access to coastal water and an electrical connection. For this project, it was possible to rent a small area at the EWN (Entsorgungswerk für Nuklearanlagen GmbH) in Lubmin, Western-Pomerania, Germany (Fig. 3). The planned prototype facility itself consisted of 3 × 4 intermediate bulk containers (IBC) with a flow-through installation (~1 m^3 h^{-1}) accessing the coastal water as the medium (Fig. 4). Different types of hard substrates were placed inside these IBCs to provide a foundation for the spores to attach on. Additionally, several Ulva sp. individuals were cut into small pieces (< 5 mm) to trigger the sporulation process (Hiraoka and Oka, 2008; Gao et al., 2010) and deployed into the IBCs.

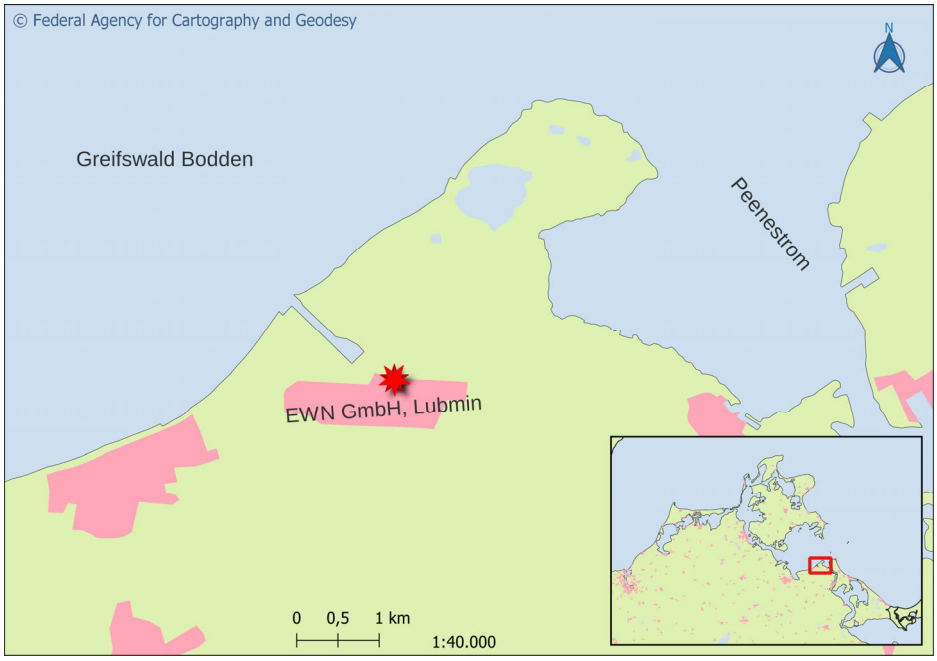

Figure 3
Location of the onshore aquaculture prototype installation at the EWN (Entsorgungswerk für Nuklearanlagen GmbH) in Lubmin, Western-Pomerania, Germany.

Figure 4
Aquaculture prototype installation with 3 × 4 IBCs containing water from the channel which is pumped to the first IBC of each row and flowing in a cascade through the other IBCs back to the channel.

For biomass production of *Ulva* sp. in natural habitat and under natural conditions another prototype installation was built inshore. The site where to install this inshore aquaculture prototype is in the western part of Wieker Bodden at northern Rügen (Fig. 5). The prototype installation consisted of 2 × 2 long ropes made of sisal with a length of about 6 m respectively. Each pair of ropes was connected multiple times to shorter ropes of about 0.8 m in length. The construction was anchored in shallow waters of about 1 m depth with stones connected to the two bottom ropes. The two top ropes are held near the surface by buoys (Fig. 6). The ropes were impregnated with small pieces (~5 mm) of *Ulva* sp. to enhance the sporulation of *Ulva* sp. and to provide a nearby hard substrate for the attachment of the spores. Furthermore, some individuals of *Ulva* sp. were fixated on the ropes as additional starter organisms (Fig. 6).

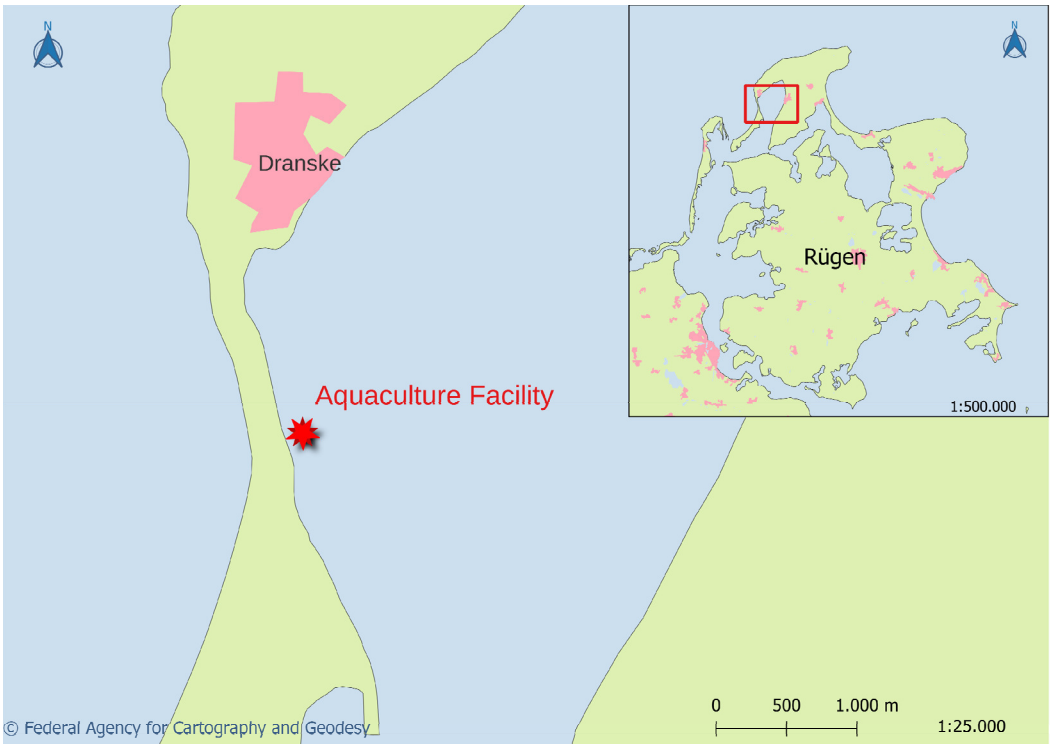

Figure 5
Location of the inshore aquaculture prototype installation in Wieker Bodden at northern Rügen, Germany.

Figure 6
Inshore aquaculture prototype installation in the Wieker Bodden at northern Rügen, Germany.

Results

Figure 7 shows the main results of the laboratory acclimation experiments conducted to optimize cultivation conditions of the *Ulva* sp. strain regarding salinity and nutrient (nitrate and ammonium) content. No significant impact of salinity on the relative growth rate was found; however, the oligohaline conditions expected at the field sites (~8 psu) were clearly suitable for cultivation. Also concerning N-compounds the given concentrations (Figure 7 shows $NaNO_3$), which fell into the range observed at the sites, were found to be suitable.

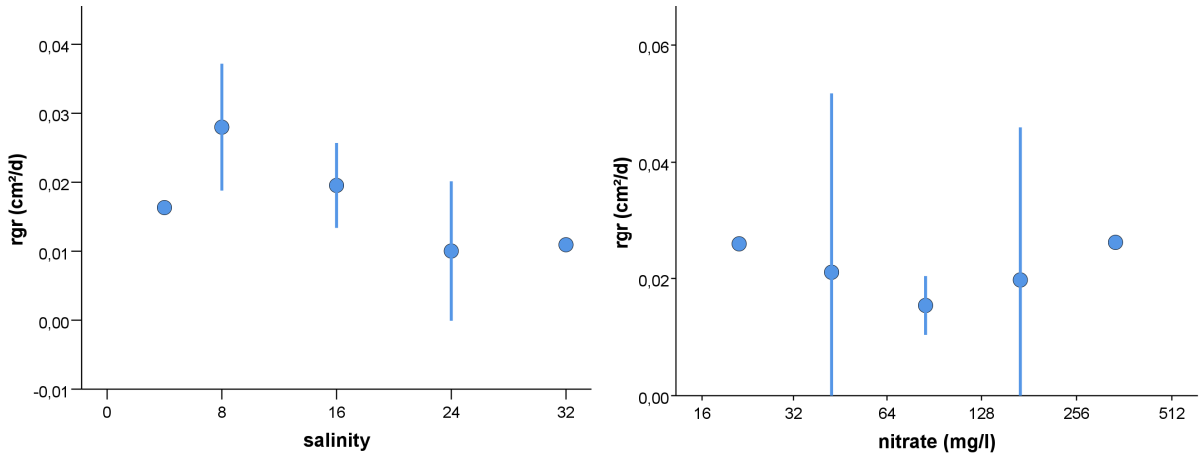

Figure 7
Dependencies of the growth rate of *Ulva* sp. area (rgr) from salinity (left) and nitrate ($NaNO_3$, right). The points represent the mean growth rate of the algae area and the vertical lines are the confidence bands of 95 %.

Production of high amounts of *Ulva* sp. biomass in IBCs as an onshore facility were not as successful as planned. Biomass production of the target species occurred only directly at the water inlet, the remaining part of the vessels were soon overgrown by opportunistic species (Fig. 8).

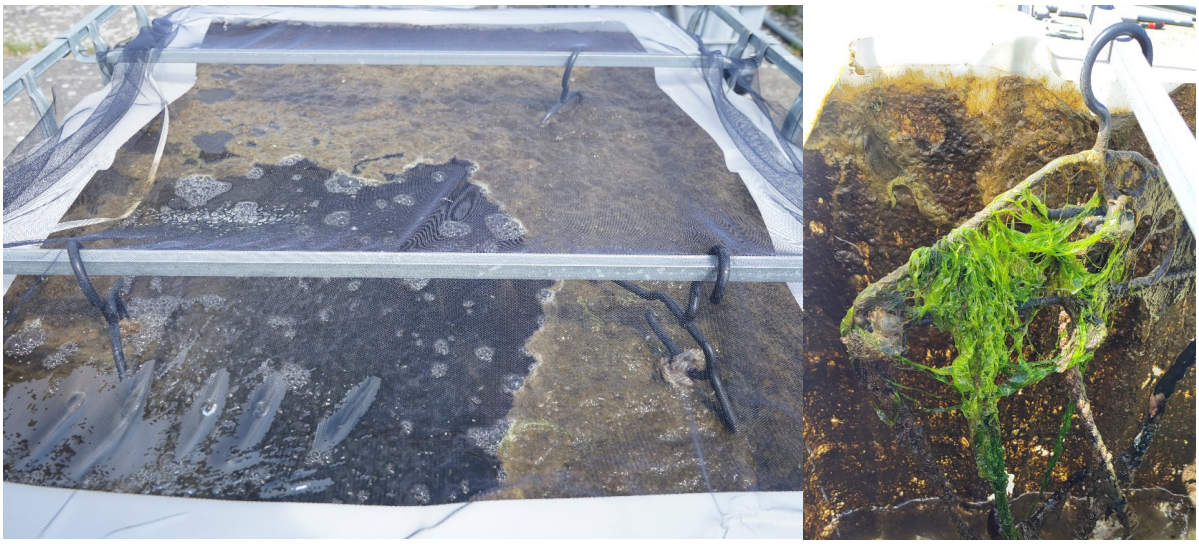

Figure 8
Some scattered individuals of *Ulva* sp. on the water surface of the IBC (left) and several on the clamp holding the settlement ropes (right). Growth of *Ulva* sp. biomass was observed only in the zone exposed to the incoming water.

Moreover, the effluent tubes were colonized within a few weeks by red algae (*Rodomela* sp.) resulting in flooding the concrete floor. This flooded concrete floor provided a suitable habitat for *Ulva* sp. (Fig. 9), which developed high biomass especially after the main efflux tube broke and the basement was flooded continuously (Fig. 9). Because of the harvested amount of biomass and the approximate period in which the flooding appeared, it was possible to estimate a production rate of about 0.5 kg fresh weight per square meter and week. This event will give rise to an altered design, consisting of shallow compartments with continuous and intense water flow instead of the voluminous vessels that were used so far.

Figure 9
Blocked tubes by a red algae (*Rodomela* sp., top-left) leading to an overflow of the IBCs (middle) and flooding of the concrete floor on which high amounts of *Ulva* sp. grew (middle-left). The damaged main afflux tube (bottom-left) resulted in massive growth of *Ulva* sp. algae on the ground (right). Half of the biomass was harvested, whereas the other half was left to function as a starter population for the next harvest. Some of the individuals were over 2 m long (right).

The experiment with the prototype aquaculture facility for inshore cultivation of *Ulva* sp. was operating for one month prior to growth estimation of *Ulva* sp. on ropes. So far, the operation time was limited to one month and further modifications will be established until the end of the project period. Hence, the following results should be regarded as preliminary. Within this month of field incubation, the ropes consisting of sisal and hemp, were fully overgrown with

algae, mainly *Ceramium* and *Cladophora* species. The ropes made of polyamide – used for the anchorage – were free of algae. As a result, the utilization of ropes made from natural resources is suitable for aquaculture installations. The implemented *Ulva* sp. were still present and several additional attached individuals could be observed. This method did not result in the production of large amounts of *Ulva* sp. biomasses within the evaluated time period of one month because of the large amount of competitive species (Fig. 10).

Figure 10
Part of the inshore prototype installation after one month. The implanted *Ulva* sp. are still on the ropes as well as some additionally grown individuals of *Ulva* sp. Several other algae like *Ceramium* sp and *Cladophora* sp. are additionally growing on the ropes which decreased the possible attachment of *Ulva* spores and prevented further growth of *Ulva* sp. individuals.

Discussion

Al-Hafedh et al. (2015) described that a high discharge of water benefits the growth rate of *Ulva* sp. in onshore installations such as the IBCs, which were used in this project. Unlike their approach, we did not install aeration systems in the tanks leading to the movement of the algae. Such aeration could provide better conditions for the growth of *Ulva* sp. and may prevent the overgrowth of competitive species, but would also cause additional costs. The overgrowth of opportunistic species is a common problem in aquaculture facilities for

macroalgae cultivation and there is no general solution for prevention measures established (e. g. Haglund and Pedersén, 1993; Kerrison et al., 2016).
The results from the onshore prototype facility are used to improve this prototype and also the laboratory constructions. The design will be further developed to allow the water to flow over the *Ulva* sp. algae. Consequently, preventing *Ulva* sp. to be overgrown by opportunistic species while still allowing the settlement of spores as well as the growth of *Ulva* sp. This system and the fast growth rate of *Ulva* sp. should provide a high production of *Ulva* sp. biomasses. These works are still in progress and further positive results are anticipated, especially with this cultivation method.
Chemodanov et al. (2019) used aerated cages for the successful cultivation of *Ulva* sp. Here, an energy source is necessary to operate the air pumps but the needed area for such a cultivation of *Ulva* sp. biomasses is reduced compared to cultivation installations with long ropes. Nevertheless, inshore aquaculture for *Ulva* sp. with ropes still looks feasible but must be further improved. In the foreseen future, ropes will be incubated beforehand in the laboratory to allow seedlings to grow prior to inshore facility installation. It is anticipated that this method will lead to the domination of *Ulva* sp. individuals and thus decrease the growth of other opportunistic species. Noteworthy, it is feasible to place this installation at sites where *Ulva* sp. is the dominant species, which would reduce the probability of overgrowth with opportunistic species. This requirement however limits the possible places for a set-up and shows a great disadvantage concerning the administrative management involved, and therefore it is necessary to find other solutions as proposed in this project.

Acknowledgments

We thank the Federal Ministry of Education and Research for funding the project. Also, we want to thank the team of the MarZucker project and all involved persons and institutions.

References

1. Al-Hafedh, Y.S., Alam, A., Buschmann, A.H., 2015. Bioremediation potential, growth and biomass yield of the green seaweed, *Ulva lactuca* in an integrated marine aquaculture system at the Red Sea coast of Saudi Arabia at different stocking densities and effluent flow rates. Reviews in Aquaculture 7 (3), 161–171. doi:10.1111/raq.12060.
2. Carballeira Braña, C.B., Cerbule, K., Senff, P., Stolz, I.K., 2021. Towards Environmental Sustainability in Marine Finfish Aquaculture. Front. Mar. Sci. 8. doi:10.3389/fmars.2021.666662.

3. Chemodanov, A., Robin, A., Jinjikhashvily, G., Yitzhak, D., Liberzon, A., Israel, A., Golberg, A., 2019. Feasibility study of *Ulva* sp. (Chlorophyta) intensive cultivation in a coastal area of the Eastern Mediterranean Sea. Biofpr 13 (4), 864–877. doi:10.1002/bbb.1995.

4. Cochrane, K.L., 2021. Reconciling sustainability, economic efficiency and equity in marine fisheries: Has there been progress in the last 20 years? Fish Fish 22 (2), 298–323. doi:10.1111/faf.12521.

5. Gao, S., Chen, X., Yi, Q., Wang, G., Pan, G., Lin, A., Peng, G., 2010. A strategy for the proliferation of *Ulva prolifera*, main causative species of green tides, with formation of sporangia by fragmentation. PloS one 5 (1), e8571. doi:10.1371/journal.pone.0008571.

6. Haglund, K., Pedersén, M., 1993. Outdoor pond cultivation of the subtropical marine red alga *Gracilaria tenuistipitata* in brackish water in Sweden. Growth, nutrient uptake, co-cultivation with rainbow trout and epiphyte control. J Appl Phycol 5 (3), 271–284. doi:10.1007/BF02186230.

7. Hiraoka, M., Oka, N., 2008. Tank cultivation of *Ulva prolifera* in deep seawater using a new "germling cluster" method. J Appl Phycol 20 (1), 97–102. doi:10.1007/s10811-007-9186-3.

8. Kerrison, P.D., Le, H.N., Twigg, G.C., Smallman, D.R., MacPhee, R., Houston, F.A.B., Hughes, A.D., 2016. Decontamination treatments to eliminate problem biota from macroalgal tank cultures of *Osmundea pinnatifida*, *Palmaria palmata* and *Ulva lactuca*. J Appl Phycol 28 (6), 3423–3434. doi:10.1007/s10811-016-0873-9.

9. Kessler, R.W., Alsufyani, T., Wichard, T., 2018. Purification of sporulation and swarming inhibitors from *Ulva*: Application in algal life-cycle controlling, in: Charrier, B., Wichard, T., Reddy, C.R.K. (Eds.), Protocols for macroalgae research. CRC Press, Boca Raton, London, New York, pp. 139–157.

10. Potts, J., Wilkings, A., Lynch, M., MacFatridge, S., 2016. State of sustainability initiatives review: Standards and the blue economy. International Institute for Sustainable Development; Canadian Electronic Library, Winnipeg, Manitoba, Ottawa, Ontario, 205 pp.

11. Reisky, L., Préchoux, A., Zühlke, M.-K., Bäumgen, M., Robb, C.S., Gerlach, N., Roret, T., Stanetty, C., Larocque, R., Michel, G., Song, T., Markert, S., Unfried, F., Mihovilovic, M.D., Trautwein-Schult, A., Becher, D., Schweder, T., Bornscheuer, U.T., Hehemann, J.-H., 2019. A marine bacterial enzymatic cascade degrades the algal polysaccharide ulvan. Nature chemical biology 15 (8), 803–812. doi:10.1038/s41589-019-0311-9.

12. Steinhagen, S., Barco, A., Wichard, T., Weinberger, F., 2019. Conspecificity of the model organism *Ulva mutabilis* and *Ulva compressa* (Ulvophyceae, Chlorophyta). J. Phycol. 55 (1), 25–36. doi:10.1111/jpy.12804.

13. Stratmann, J., Paputsoglu, G., Oertel, W., 1996. Differentiation of *Ulva mutabilis* (Chlorophyta) gametangia and gamete release are controlled by extracellular inhibitors. J Phycol 32 (6), 1009–1021. doi:10.1111/j.0022-3646.1996.01009.x.

14. Tran, L.-A.T., Vieira, C., Steinhagen, S., Maggs, C.A., Hiraoka, M., Shimada, S., van Nguyen, T., Clerck, O.D., Leliaert, F., 2022. An appraisal of *Ulva* (Ulvophyceae, Chlorophyta) taxonomy. J Appl Phycol. doi:10.1007/s10811-022-02815-x.

15. Tziveleka, L.-A., Ioannou, E., Roussis, V., 2019. Ulvan, a bioactive marine sulphated polysaccharide as a key constituent of hybrid biomaterials: A review. Carbohydrate polymers 218, 355–370. doi:10.1016/j.carbpol. 2019.04.074.

16. Wichard, T., 2015. Exploring bacteria-induced growth and morphogenesis in the green macroalga order Ulvales (Chlorophyta). Frontiers in plant science 6, 86. doi:10.3389/fpls.2015.00086.

OPENAQUASENSE – AN OPEN-SOURCE SENSOR PROTOTYPING PLATFORM FOR TAILOR-MADE MARINE SENSING

Christoph STREHSE[1], Henrik LANGOSCH[1], Heiko BETZ[2], Sascha KOSLECK[1]

[1]University of Rostock, Faculty of Mechanical Engineering and Marine Technology, Chair of Ocean Engineering, Albert-Einstein-Straße 2, Rostock, 18059, Germany
[2]Nautilus Marine Service GmbH, Alter Postweg 30, 21614 Buxtehude

Abstract

To meet the requirements of increasingly complex and specialized marine monitoring, highly specialized sensor systems adapted to the respective measuring task are required. The setup of such systems with commercially available sensors often poses a great challenge to the user due to the lack of standards regarding data formats and interfaces, a lack in technical expertise and significant cost implications. Another limitation is the lack of adaptability of sensor systems for specific applications, because most commercially available products are not open-source systems.

Our goal is to develop and evaluate a library of methods and tools for developing application-specific sensor networks for water quality monitoring in marine applications. The presented open-source sensor prototyping platform “OpenAquaSense” is a tool for the development of tailor-made sensor systems for in-situ measurement of a variety of water quality parameters. To ensure the adaptability and expandability of the systems, a special focus was placed on a modular system character. Due to the pressure-tolerant design of the system, sensor manufacturing can be realized in a 3D-printing process. In addition to significantly reduced costs, this offers a high design flexibility, which in turn has a positive effect with regard to integration and usability. Functionality and application are demonstrated using the example of turbidity monitoring for two different scenarios.

Keywords

Turbidity Sensor, Photonic Sensing, Marine Monitoring, Environmental Monitoring, Open-Source, Rapid Prototyping

Nomenclature

CAN – controller area network
GPS – global positioning system

I^2C – inter-integrated circuit
I_{LED} – LED current
IR – infrared
JSON – java script object notation
LED – light emitting diode
OR – operating range
PC – polycarbonate
PCB – printed circuit board
PETG – polyethylene terephthalate glycol
PWM – pulse-width modulation (duty cycle)
SD – secure digital
SPI – serial peripheral interface
T_i – integration time
UART – universal asynchronous receiver transmitter
USB – universal serial bus

λ – wavelength

Introduction

The sustainable utilization and protection of ocean environments combined with an efficient use of ocean resources is becoming more and more important and is one of the most crucial challenges of the 21st century. The dependency of mankind on ocean resources will continue to increase as the world's population grows. Thus, the ability not only to monitor ocean environments but also the impact of man-made marine facilities is becoming increasingly important.

An example for the need of comprehensive monitoring are on- and off-shore aquaculture facilities at an industrial scale. Here, it is essential to detect potentially dangerous changes in water quality at an early stage to initiate appropriate counter measures. One crucial water quality parameter is turbidity. It is verified, that a high turbidity can have a significant impact on the feeding behaviour (Zingel and Paayer, 2010) and the stress (Kathyayani et al., 2019) of the cultured organisms. Furthermore, high dissolved sediment can cause bad gill conditions and reduce the grow rate of fish (Sutherland and Meyer, 2007). Besides of that, high levels of dissolved solids have significant impacts on the physical, chemical and biological characteristics of the water body (Bilotta and Brazier, 2008). Thus, Parra, Rocher et al. (2018) developed a tailor-made low-cost sensor system for turbidity monitoring in fish farm inlets. The presented system is able to distinguish between

sedimentary and planktonic turbidity, providing important information about the water quality.
Comprehensive monitoring is not only necessary to observe the condition of the marine facilities, it also enables the study of the long-term consequences that these facilities potentially cause for the environment. This allows proactive measures to be taken for a more sustainable operation. One major impact is the input of to much food into the environment. To address the problem of over-feeding, Parra, García et al. (2018) developed a smart sensor system prototype that combines fish presence sensors and a feed detection system in the fish farm's drainage. It is demonstrated that constant monitoring does not only provide information about the feeding process itself. Furthermore, the information can also be used as the basis for automated seafood production.

To meet the requirements of increasingly complex and specialized marine monitoring, highly specialized sensor systems adapted to the respective measuring task are required. The setup of such systems with commercially available sensors often poses a great challenge to the user due to the lack of standards regarding data formats and interfaces, a lack in technical expertise and significant cost implications. Furthermore, marine research increasingly relies on autonomous sensor systems and networks that produce large amounts of data. In order to be able to manage the ever-increasing data volumes in the future, standardization in data processing and an adaptable, tailor-made data management is key (Schulz et al., 2015).
Another limitation is the lack of adaptability of sensor systems for specific applications, because most commercially available products are not open-source systems. Schima et al. (2019) state, that a modular and adaptive sensor concept is the key factor in providing user-specific and service-oriented environmental monitoring systems. Here, it is particularly demonstrated that this can be achieved by open-source based systems. In addition, the ability to access and adjust all parts of the system enables the implementation of sophisticated functions such as autocalibration and adaptive system behaviour.

Applications where prototypes based on the OpenAquaSense platform have been successfully developed in the past include various stationary and mobile environmental monitoring scenarios, as well as observation of fishponds and a sea cucumber farm (Tokaç et al., 2021). The previous studies have been promising and have shown that by using the platform the development effort and time can be significantly reduced. During this paper, the systems applicability for marine measurements is showcased in a tailor-made approach to measure marine turbidity.

Material and Methods

The aim of the open-source sensor prototyping platform OpenAquaSense, that is available online via https://gitlab.com/christoph.strehse/openaquasense, is to simplify the future development of tailor-made sensor systems for marine monitoring applications based on a modular system concept as shown in Figure 1. This concept can be classified into three main parts - one or more sensor probes located underwater, a top side unit located at the surface and the corresponding software. Each partial system feature is represented by one of the modules available in the OpenAquaSense library.

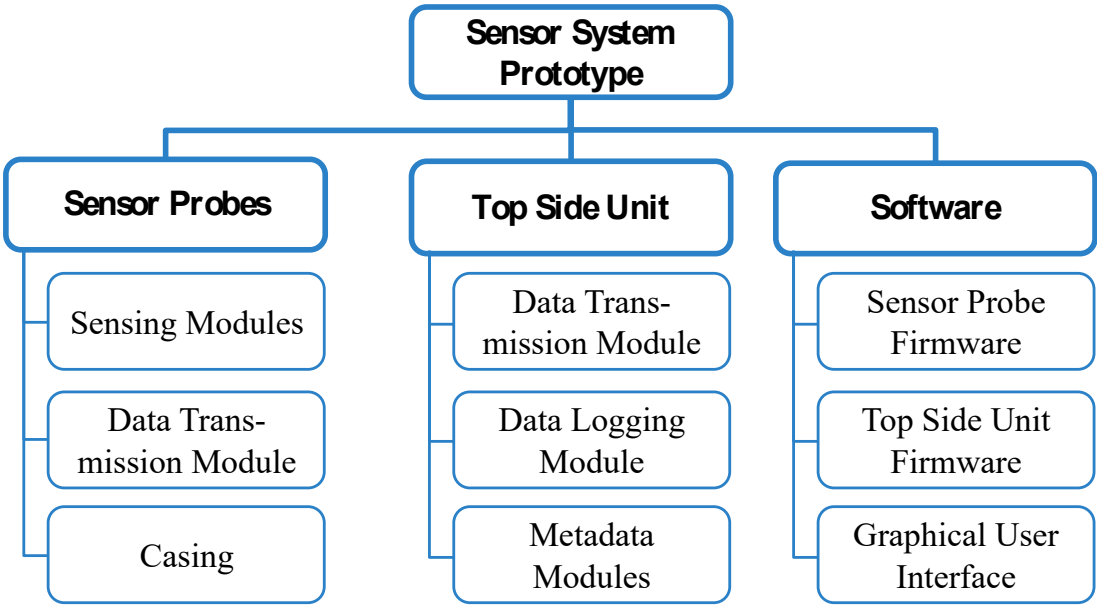

Figure 1
General system concept

The sensor probe includes the sensing modules, consisting of printed circuit boards (PCBs) that contain the required electrical components. Furthermore, a module for transmitting the data to the top side unit is integrated. With the casing being 3D-printed the probe can be shaped and configured individually, according to tasks and site specific requirements.
The top side unit gathers, pre-processes and stores the sensor data using data transmission and logging modules. Optionally, the data can also be forwarded to an end user device like a computer or smartphone. Here, cable and Wi-Fi connections can be realised. In addition, the top side unit can capture metadata such as global positioning system (GPS) coordinates that cannot be accessed underwater.
The software includes the firmware of the sensor probes and top side unit, respectively also providing an automated measurement routine. Optionally, a graphical user interface is available to get instant graphical feedback.

The open-source platform provides a wide range of options. Hence, tailor-made sensor system prototypes can be set up quickly combining the modules required for the respective application. Beyond that the user or other developers can always add individual modules. These are then made publicly available on the platform. Over time, this results in an increasing selection of modules for a wide range of applications.

To ensure that the turbidity measuring system presented in this paper meets the respective requirements, a development cycle, as shown in Figure 2, is applied. To be able to operate the sensor at greater water depth each component is designed to be pressure-tolerant, casted with epoxy resin. This enables the casing to be 3D-printed allowing great freedom with regard to shape. Thus, small, cost-effective and easy-to-handle probes can be realised. After integrating the firmware and additional software modules, the assembly is evaluated and validated. Here, for example, the emitter-detector characteristics, temperature dependencies and pressure tolerance is investigated and the system is calibrated under laboratory conditions before using it in the field for the first time.

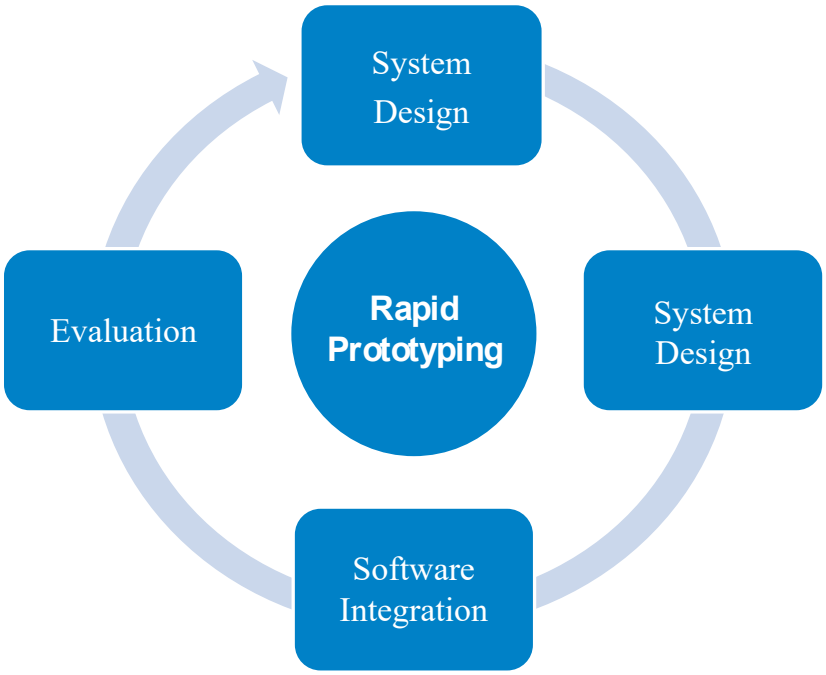

Figure 2
Underlying system development cycle

To demonstrate the possibilities provided by the platform, two sensor systems that have been developed using the OpenAquaSense platform are presented. One is used for mobile turbidity monitoring on a German freshwater lake called “Müritz”. The other one is used for stationary turbidity monitoring in order to investigate sediment settling behaviour.

Mobile Turbidity Monitoring

The system design for the mobile turbidity monitoring application is shown in Figure 3. To enable turbidity measurements, the sensor probe includes two sensing modules, being the infrared (IR) emitter and the detector module. The IR module is based on a SFH 4651 light emitting diode (LED) with a peak wavelength of $\lambda = 860\ nm$, whose brightness can be adjusted by a LP55231 LED driver, as well as a TSL2572 IR photo detector. Both modules communicate via inter-integrated circuit (I^2C) bus.

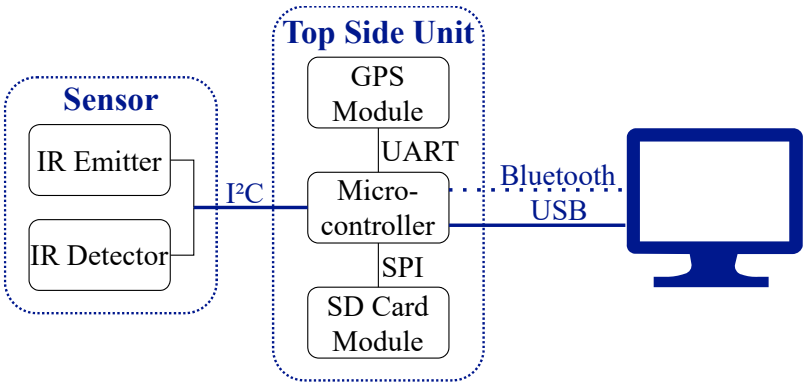

Figure 3
System design for mobile turbidity monitoring system

To reduce the actual size of the sensor components to be integrated, the firmware runs on an Arduino Mega 2560 microcontroller located in the top side unit, connected to the sensor by the I^2C bus. To assign the current position to each turbidity measurement, a NEO-6m GPS module is connected using the universal asynchronous receiver transmitter (UART) interface of the microcontroller. The data is logged to a secure digital (SD) memory card, connected to the microcontroller via the serial peripheral interface (SPI). Additionally, all data can be exported via Bluetooth or universal serial bus (USB). Power is supplied either via USB or an internal battery pack.

To achieve maximum mobility, the sensor modules are integrated into a torpedo-shaped carrier to be towed by a surface vessel, as shown in Figure 4. It consists of three sections and two wings (NACA 4418 profile) to generate the necessary downforce. Bow and stern sections as well as the wings are 3D-printed using polyethylene terephthalate glycol (PETG). Transparent filament is used to implement 3D-printed optical sensor windows. For ease of production, the middle section is built from a polyvinylchloride (PVC) tube.
The sensor modules, including emitter and detector are integrated in the bow. To provide pressure tolerance, the bow section is casted with the epoxy resin CRYSTAL-CLEAR by R&G.

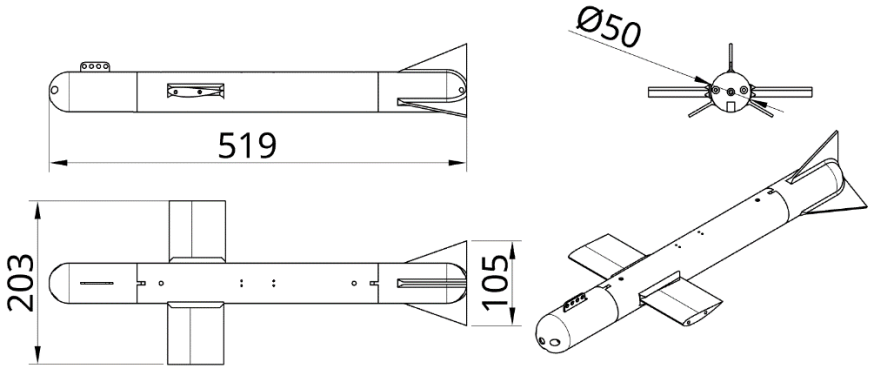

Figure 4
Casing design for a mobile turbidity monitoring system (all values in mm)

To reduce complexity and cost, most of the device is designed to be flooded with water. For reasons of transversal stability and to prevent a total loss of the system in case the tow rope breaks, the stern section includes stabilisers and a foam core is inserted in the upper area of the tube to raise the centre of buoyancy. The top side unit components are mounted in a waterproof polycarbonate (PC) standard casing.

The system firmware runs on the microcontroller located in the top side unit. Besides the control and communication of the sensor probe modules, it provides an automated measurement routine. Before initiating the measurements, this routine starts searching for a GPS signal. If the GPS signal is available, the sensor probe performs an IR measurement using the adjusted settings. The brightness of the LED is adjusted by the LED driver. In this case, it provides a current of $I_{LED} = 4.0\ mA$, while the pulse width modulation (PWM) duty cycle, adjustable between 0 to 255, is set to $PWM = 40$. For the IR detector, an integration time of $T_i = 612\ ms$ is used.
To determine the amount of ambient IR-light, hence the offset, for each measurement an additional measurement is taken with the LED turned off. The measured values are supplemented by general settings, the current position and time before being converted to java script object notation (JSON) and logged to the SD card. This routine then repeats at a sampling rate of $0.05\ Hz$. The values used for all measurement settings are summarized in Table 1.

Table 1
System configuration for mobile turbidity monitoring

Measurement Setting	Value
Sampling Rate	0.05 Hz
PWM	40
I_{LED}	4.0 mA
T_i	612 ms

The field tests are conducted on a north German freshwater lake named “Müritz”. To evaluate the suitability of the system for the designated application, the sensor is towed behind a boat at speeds between $\boldsymbol{4-6\ kn}$.

Stationary Turbidity Monitoring

The system design for the stationary turbidity monitoring system is illustrated in Figure 5. The modules used for IR detector and IR emitter are the same as for the mobile system. However, they are connected to an additional microcontroller within the sensor probe, the ESP32 NodeMCU. This offers over-the-air programming, meaning new firmware or laboratory evaluation routines can be uploaded wirelessly. It also supports a Bluetooth connection to nearby devices. Furthermore, using a microcontroller located in the sensor probe enhances the system for the use of a MCP2515 controller area network (CAN) bus module, connected via the SPI. This bus protocol supports cable lengths of $50\ m$.

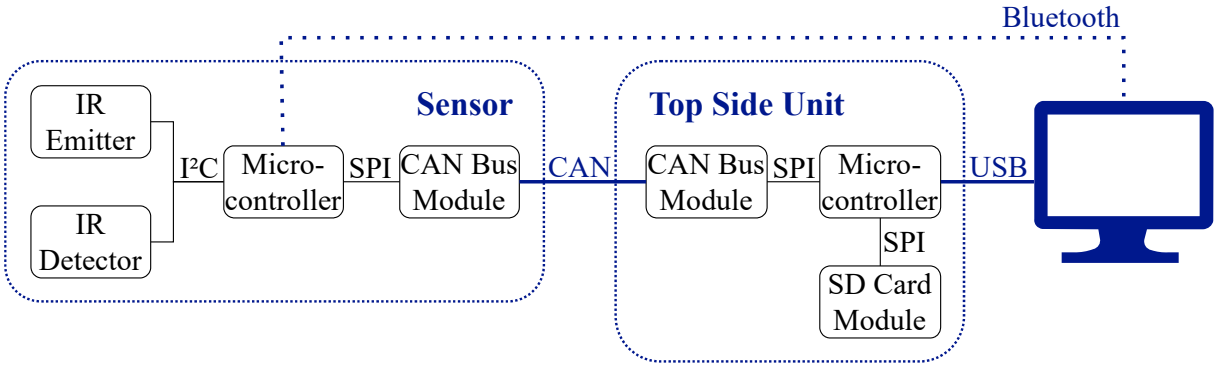

Figure 5
System design for stationary turbidity monitoring system

The sensor casing itself is u-shaped, with detector and emitter modules facing each other. To simplify the assembly and to ensure accurate alignment of the sensing modules, the electrical components are first mounted and wired on a carrier, which is then inserted and fixed into the casing. The assembled system as well as

the dimensions of the casing are shown in Figure 6. Both, casing and carrier are 3D-printed using PETG filament. To achieve maximum signal yield, borosilicate glass is used for the optical sensor windows. As mentioned before, the overall assembly system is casted with CRYSTAL-CLEAR epoxy resin to provide pressure tolerance. The top side unit components are again mounted in a waterproof (PC) standard casing.

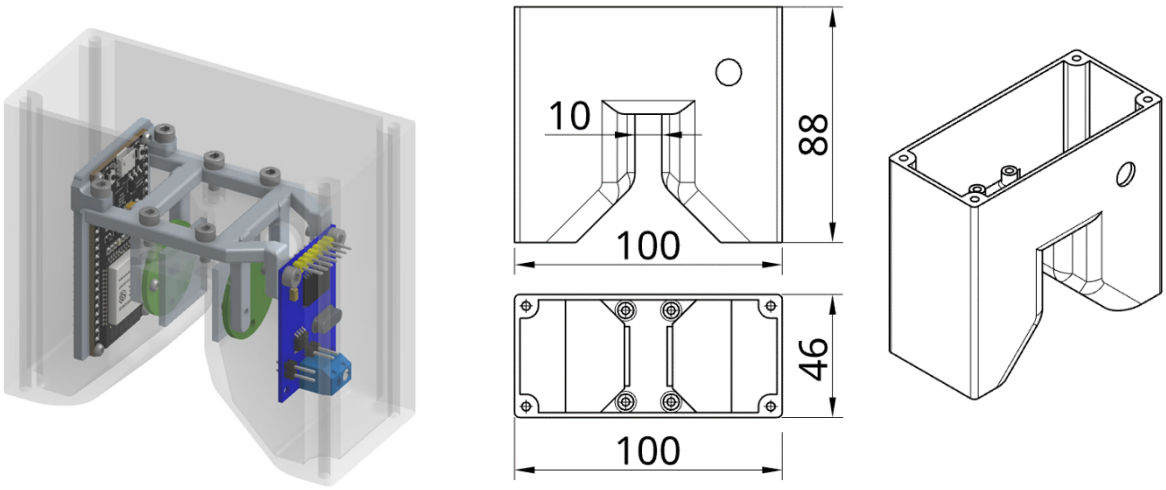

Figure 6
Left: fully assembled sensor for a stationary turbidity monitoring system, middle and right: detailed casing design (all values in mm)

At the end of each measuring cycle (detecting ambient light, measuring IR permeability of the fluid, adding time stamp) the current operating range (OR) is established and adapted to ensure the sensor always operates to its full potential using its maximum resolution. The OR is determined as a combination of PWM, I_{LED} and T_i and is adjusted if the detected IR value exceeds or falls below certain thresholds. In line with the prevailing turbidity gradient, the sampling rate is automatically adjusted to values between 1 and 0.2 Hz. The available measurement settings for all operating points are summarized in Table 2.

Table 2
System configuration for mobile turbidity monitoring

Operating Range	Measurement Setting	Value
OR 1	PWM_1	200
	I_{LED1}	20 mA
	T_{i1}	172 ms

OR 2	PWM_2	255
	I_{LED2}	25.5 mA
	T_{i2}	172 ms
OR 3	PWM_3	255
	I_{LED3}	25.5 mA
	T_{i3}	250 ms
OR 4	PWM_4	255
	I_{LED4}	25.5 mA
	T_{i4}	500 ms
all	Sampling Rate	0.2 Hz, 1 Hz

To evaluate the system's suitability, the sensor probe is lab tested. Here, sediment with a particle size below $63\ \mu m$ was added to fresh water at a mass ratio of 1% and stirred until the water was uniformly turbid. Subsequently, the turbidity was measured until the water optically appeared clear. Since the linear behaviour of the used setup has already been investigated in previous studies (Strehse et al., 2019) a relative signal strength can be calculated according to equation (1), thus making IR values obtained at different operating ranges comparable.

$$IR_{rel} = IR_x \cdot \frac{T_{i4}}{T_{ix}} \cdot \frac{PWM_4}{PWM_x} \cdot \frac{I_{LED4}}{I_{LEDx}} \tag{1}$$

Results

After initial tests have been successfully executed under laboratory conditions, both systems were found to be appropriate to conduct the intended measurement task.

Mobile Turbidity Monitoring

The measurements were conducted on a sunny to partly cloudy day with low wind. Thus, the water surface was relatively calm. The towed carrier could be deployed and retrieved from the boat without any problems. Also, the carrier's path and water depth was stable at all times with the sensor continuously performing measurements.

The sensor integrates how many emitted IR photons reach the detector per time putting these $Counts$ in relation to the overall emitted photons. The more turbid the water is, the fewer photons reach the detector, which means that a high detector signal corresponds to low turbidity and vice versa. Calibrating the sensor using

samples with known turbidity, the detected photon counts can directly be translated into fluid turbidity. During the measurements, the detector has partially reached its saturation of 65535 $Counts$. Since the exact amount of light can no longer be determined in this case these measurements were excluded from the evaluation. Before each IR measurement the amount of ambient IR light was determined and subtracted from the obtained IR value. To reduce the effect of sudden changes to ambient light during an actual measurement the integration time must be as short as possible while increasing the brightness of the LED in order to still obtain a high detector signal.
Figure 7 illustrate the location as well as the corresponding detector count during the mobile campaign. At latitude 53.484, longitude 12.656 (blue dot) a sediment cloud was deliberately stirred up to see if the sensor is working correctly. The values measured indicate that the water in the canal has a higher turbidity (lower photon count) than on the open lake. This corresponds with visual inspections. Overall, the suitability of the system for this application has been successfully proven.

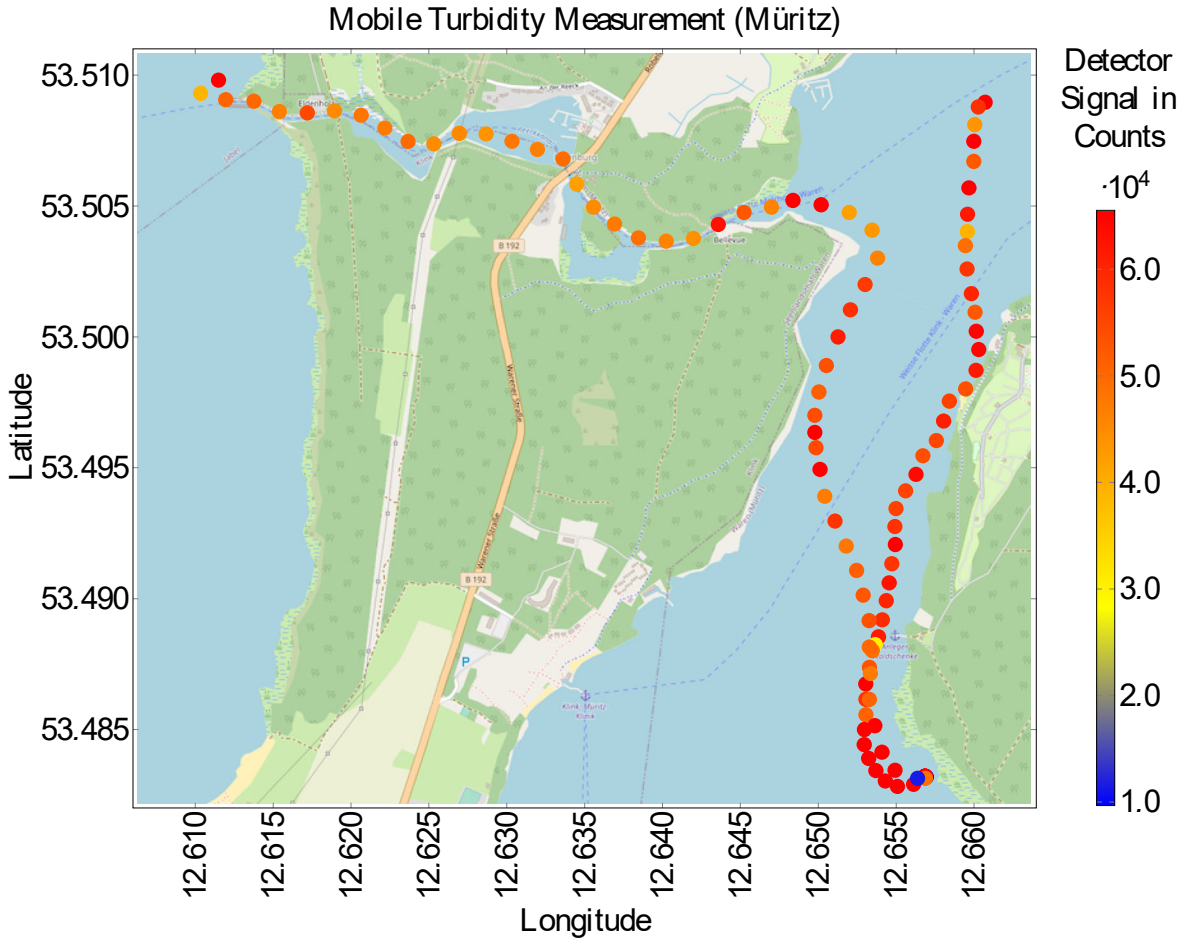

Figure 7
Results for mobile turbidity measurement

Stationary Turbidity Monitoring

After adding the sediment to the water tank, the water apparently became very turbid. To avoid sediment settling on the optical windows, the sensor was placed sideways in the tank. The system has continuously collected data and no error occurred. Due to the adaptive OR adjustment, the detector has not reached saturation at any time. Additionally, the relative measurement range could be increased from $65535\ Counts$ to $310000\ Counts$. Also, the adaptive sampling rate adjustment worked as intended. However, further tests are needed to determine reasonable turbidity gradient thresholds.
The results of this test are presented in Figure 8. It took approximately $670\ s$ for the sediment to settle. The sensor provided plausible data across all ORs. Overall, the suitability of the system for this application has been proven for clear as well as highly turbid water.

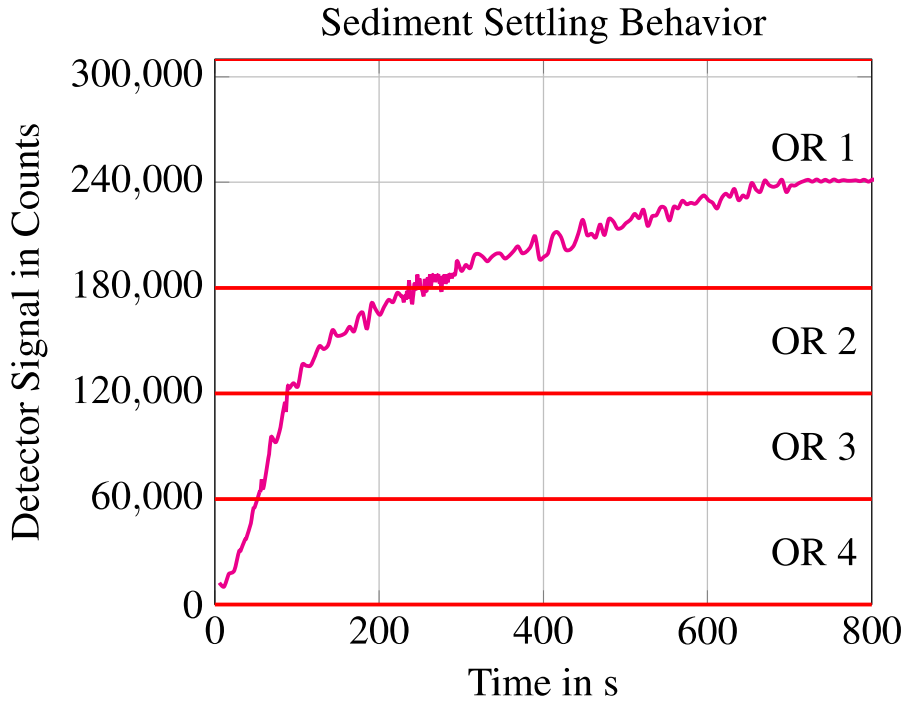

Figure 8
Results for stationary turbidity measurement

Conclusion and Future Work

The aim of this paper was to investigate the suitability of OpenAquaSense as an open-source prototyping platform for tailor-made marine monitoring systems. For this purpose, sensor system prototypes were developed for two measurement scenarios, mobile and stationary monitoring of turbidity. Using the prototyping platform, both systems could be developed cost-effectively while significantly reducing development time and workload.

Particularly the mobile system illustrates the advantages provided by the possibility of integrating the sensor components into an application-specific casing. The developed torpedo-shaped carrier is easy to set up and handle. The sensor system worked reliably over the whole measurement duration. In addition, it has been demonstrated that the customisation of the sensor firmware brings great advantages, as exemplified by filtering ambient light.
The second application demonstrates the potential of a smart sensor, especially for stationary monitoring. By automatically adapting the operating range, the measurement range is considerably extended. Also, an event-based monitoring is executed by an automatic adaption of the sampling rate offering the potential to considerably save power which in turn increases the possible operating time.

Future work will focus on the development of additional system modules, in particular sensing modules, for example for measuring the water temperature, conductivity and many more. In addition, an implementation of a network of smart sensors based on OpenAquaSense is planned. In this network each individual sensor is working adaptively and event-based at its corresponding application site with multiple sensors feeding into one topside combining all measurements into a single data base. Therefore, reasonable thresholds for different applications must first be determined during future tests. Furthermore the pressure tolerance of the sensor probes must be improved to such an extent that they are suitable for use in deep-sea environments of up to $4000\ m$. This will significantly increase the number of possible areas of application.

Acknowledgements

The research documented in this paper was conducted as part of the project “DEEP SEA – Development and evaluation of photonic sensor components for coastal environmental monitoring and assessment of marine resources” that was funded by the ERA-NET Co-fund of the EU, as well as the project “Deep Sea Sampling (DSS) – Entwicklung von Technologien für den vertikalen minimalinvasiven Tiefseebergbau” funded by the German Federal Ministry for Economic Affairs and Climate Action.

References

1. Bilotta, G. S., Brazier, R. E. – Understanding the influence of suspended solids on water quality and aquatic biota – Water Research, 42, 12, June 2008, 2849-2861
2. Kathyayani, S. A., Muralidhar, M., Kumar, T. S., Alavandi, S. V. – Stress quantification in Penaeus vannamei exposed to varying levels of turbidity – Journal of Coastal Research, 86, sp1, November 2019, 177-183

3. Parra, L., García, L., Sendra, S., Lloret, J. – The use of sensors for monitoring the feeding process and adjusting the feed supply velocity in fish farms – Journal of Sensors, October 2018, 1-14
4. Parra, L., Rocher, J., Escrivá, J., Lloret, J. – Design and development of low cost smart turbidity sensor for water quality monitoring in fish farms – Aquacultural Engineering, 81, May 2018, 10-18
5. Schima, R., Krüger, S., Bumberger, J., Paschen, M., Dietrich, P., Goblirsch, T. – Mobile monitoring–Open-source based optical sensor system for service-oriented turbidity and dissolved organic matter monitoring – Frontiers in Earth Science, 7, 184, July 2019
6. Schulz, J., Möller, K. O., Bracher, A., Hieronymi, M., Cisewski, B. et al. – Aquatische optische Technologien in Deutschland – Marine Science Reports, 97, 2015
7. Strehse, C., Paschen, M., Tokaç, A., Mollenhauer, O., Goblirsch, T., Schima, R. – Rapid prototyping development of an in-situ sensor system for open ocean aquaculture – Contributions on the Theory of Fishing Gears and Related Marine Systems, 11, November 2019, 139-151
8. Sutherland, A. B., Meyer J. L. – Effects of increased suspended sediment on growth rate and gill condition of two southern Appalachian minnows – Environmental Biology of Fishes, 80, 4, October 2007, 389-403
9. Tokaç, A., Kostak, E. N., Tolon, M. T., Strehse, C., Kosleck, S. – The photonic sensor application as an in-situ sensor system for sea cucumber tanks – Proceeding Book of the 14th International Symposium on Fisheries and Aquatic Sciences, September 2021, 49-53
10. Zingel, P., Paaver, T. – Effects of turbidity on feeding of the young-of-the-year pikeperch (Sander lucioperca) in fishponds – Aquaculture Research, 41, 2, January 2010, 189-197

A PRELİMİNARY STUDY ON MORPHOMETRİC MEASUREMENTS OF AQUATİC SPECİES USİNG 3D SCANNER IMAGES

Adnan TOKAÇ[1], Mustafa T. TOLON[1], Ozan SOYKAN[1]
[1]Ege University, Faculty of Fisheries, İzmir, 35150, Turkey

Abstract

With this preliminary study, the advantages and disadvantages of morphometric measurements of aquatic species using 3D scanner images instead of classical methods were emphasized. Classical morphometry measurements of aquatic species such as height, width, height, carapace length, which are usually applied by a ruler or caliper, include variations between the measurements of different researchers as well as the variation between the measurements of the same researcher. Furthermore, when required, it is not possible to measure the individual which was previously measured with classical methods. 3D image measurements enable to measure not only metric parameters such as length, width and height, but also area and volume. Since there is no variation in the measurements of the image, there is no need for repetition. On the other hand, during the process of scanning aquatic creatures with a 3D scanner, the long post-processing time required to obtain the final image after scanning was a significant disadvantage previously. However, this process time has been shortened considerably with the recent updates on the 3D scanner software. Thus, it has become easier to conduct morphometric measurements of aquatic species using 3D scanner images. In this paper, species with different body structures from the echinoderm phylum, which can change shape continuously after getting out of the water and therefore bring difficulties during classical measurement methods, sea cucumber (*Holothuria tubulosa*), starfish (*Echinaster sepositus*) and fish with dissimilar body morphology, bogue (*Boops boops*), annular sea bream (*Diplodus annularis*) and axillary sea bream (*Pagellus acerna*) were investigated.

Keywords

Aquatic species, morphometry, 3D, scanner images

Introduction

Classical morphometry measurements of aquatic species such as height, width, height, carapace length, which are usually applied by a ruler or caliper, include variations between the measurements of different researchers as well as the variation between the measurements of the same researcher. Furthermore, when required, it is not possible to measure the individual which was previously measured with classical methods. 3D image measurements enable to measure not only metric parameters such as length, width and height, but also area and volume. Since there is no variation in the measurements of the image, there is no need for repetition. There are morphometric studies on subjects such as morphology, shape changes especially of living things such as starfish and also determination of the movement of skeletal components (Schwertmann et al. 2019). A thorough scrutiny of the literature reveals that several methods are used to evaluate starfish size and these consist of measuring with vernier calipers using different kinds of methods (Barker & Nichols 1983; Penney & Griffiths 1984; Minchin 1987; Scheibling & Lauzon-Guay 2007; Campbell *et al.* 2001; Bernstein *et al.* 1981) On the other hand, during the process of scanning aquatic creatures with a 3D scanner, the long post-processing time required to obtain the final image after scanning was a significant disadvantage previously. However, this process time has been shortened considerably with the recent updates on the 3D scanner software. Thus, it has become easier to conduct morphometric measurements of aquatic species using 3D scanner images. In this paper, species with different body structures from the echinoderm phylum, which can change shape continuously after getting out of the water and therefore bring difficulties during classical measurement methods, sea cucumber (*Holothuria tubulosa*), starfish (*Echinaster sepositus*) and fish with dissimilar body morphology, bogue (*Boops boops*), annular sea bream (*Diplodus annularis*) and axillary sea bream (*Pagellus acerna*) were investigated.

Material and Methods

In this study, three different fish species bogue, annular sea bream, and axillary sea bream, as well as starfish and sea cucumber, a total of five different aquatic species were studied. The methodology followed in the study has been in the form of comparing the classical morphometric measurements applied until now with the measurements made on 3D scanner images for each investigated species. To obtain the correct morphometric measures we used each individual as fresh as possible when measurements were taken. Because, it is very important that the shape of the species measured is not affected by dehydration, depressurization, rigor mortis, or any other factor that could alter the original shape. Artec Space Spider which is a high-resolution 3D scanner based on blue light technology was used in this study.

Results

Measuring bogue (Boops boops) morphology

Bogue has a body slender, with 3 - 5 weak, golden longitudinal stripes and a black spot at the pectoral fin base. The measurement results made with the use of classic and 3D images on the bogue are summarized in Table 1.

Table 1
The measurement results made with the use of classic and 3D images on the bogue

	Total length (cm)	Weight (g)	Volume (ml)
Classical measurement method	21.6	107.9	111
	Total length	Surface area (mm^2)	Volume (mm^3)
Measurement made on the 3D scanner image	21.679	16611.57	108920.05

As it can be seen from the results in Table 1, the total height and volume measurements made by both methods were found to be very close to each other. A graduated cylinder was used to measure the volume of the fish using the classical method. Figure 1 shows the total length, volume, and surface area measurement results on the 3D scanner image. Especially when scanning the shape of the fish in 3D, some deformities may occur due to the hanging of the fish. In order to prevent measurement errors caused by these deformities and to measure on an equal plane, a plate surface can be added to the required place on the 3D scanner image. The pink-colored part seen in the tail of the fish in Figure 1 shows this application.

Apart from this, fish cross sections, which are one of the most important parameters that determine the escape of fish from the codend meshes of the trawl nets, can also be able determined via 3D scanner images, which is actually important progress for further selectivity studies (Figure 2)

Measuring annular sea bream (Diplodus annularis) morphology

Annular sea bream individuals shows ranged from 8.2 to 20.9 cm total length in size and from 8.7 to 137.1 g in weight. The mean length showed an increase with increasing water depth. The species was characterized by protandric her-

maphroditism. The measurement results made with the use of classic and 3D images on the same annular sea bream individual are given in Table 2.

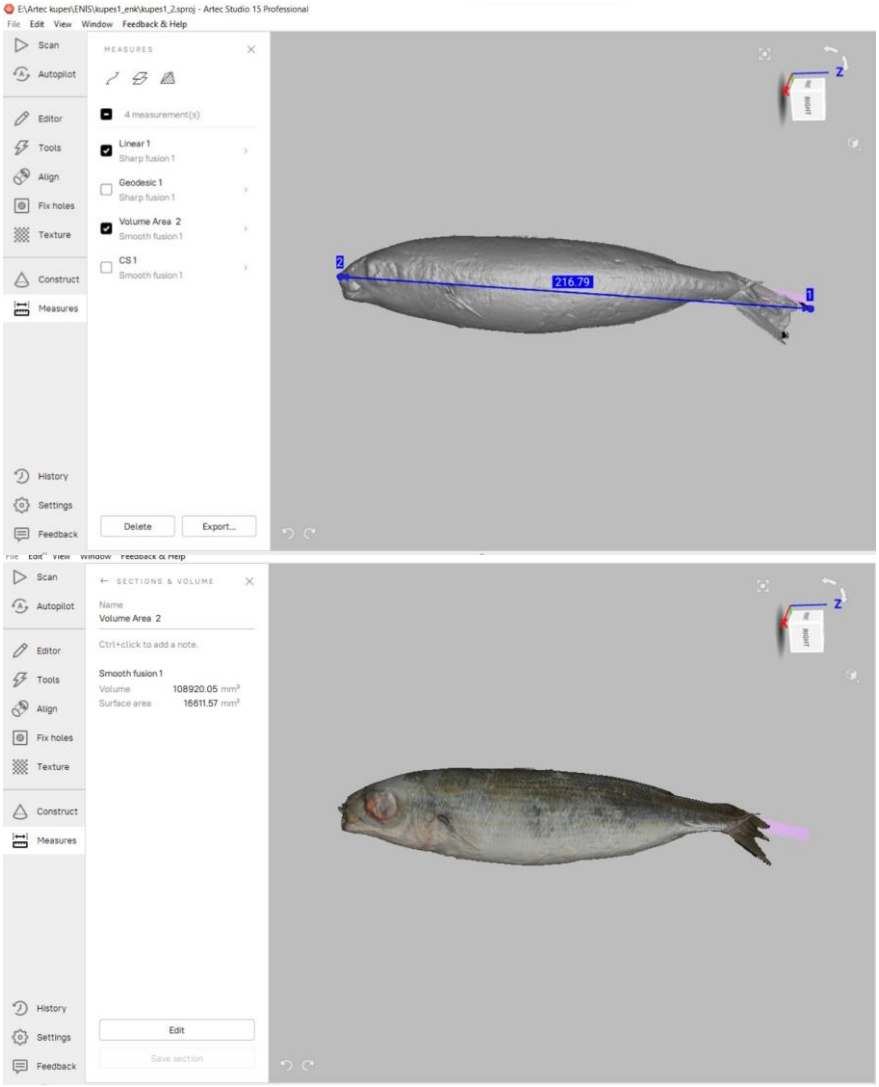

Figure 1
Total length, volume and surface area measurements for bogue via 3D scanner image

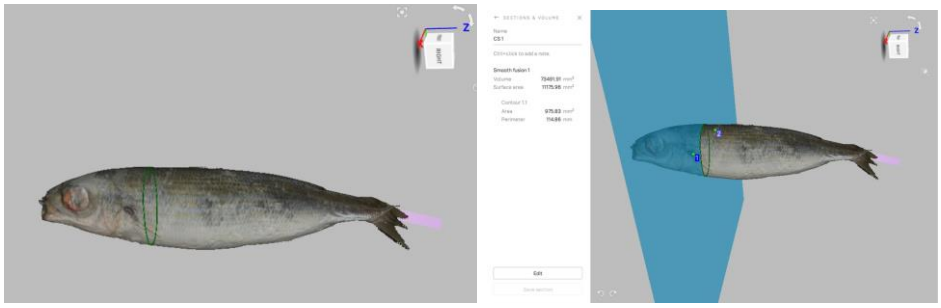

Figure 2
Measuring of fish cros section via 3D scanner images for bogue

Table 2
The measurement results made with the use of classic and 3D images on the annular sea bream

	Total length (cm)	Weight (g)	Volume (ml)
Classical measurement method	14.95	63.7	61
	Total length	Surface area (mm^2)	Volume (mm^3)
Measurement made on the 3D scanner image	14.976	12625.73	62009.77

As can be seen from the results in Table 2, the total height and volume meaurements made by both methods were found to be very close to each other, as in the bogue results.

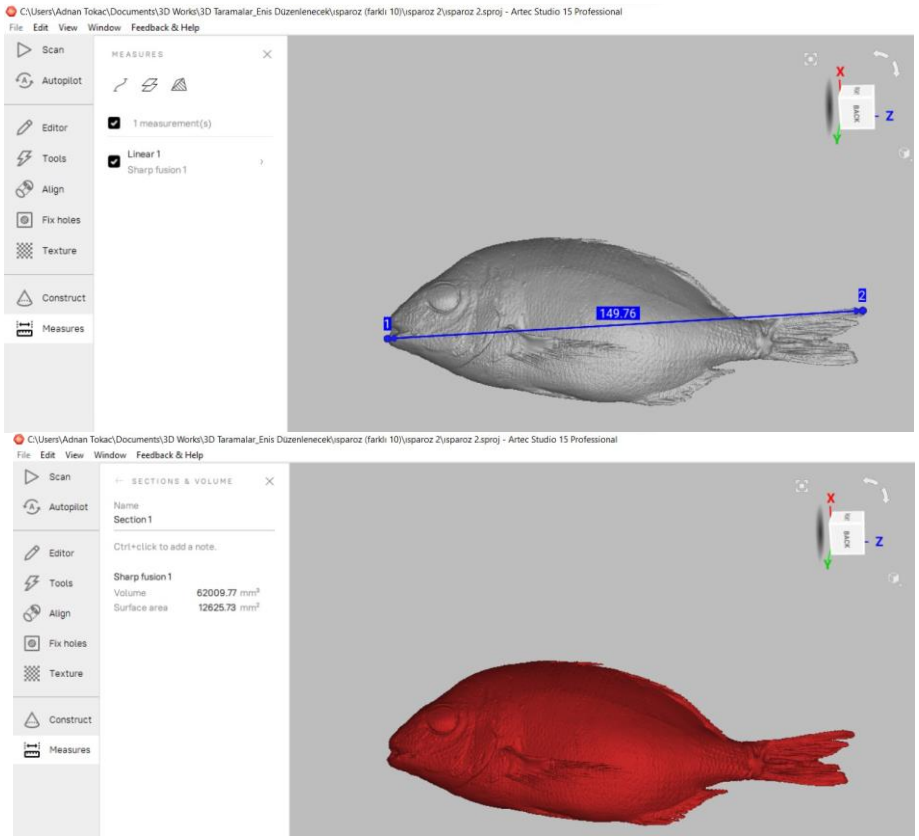

Figure 3
Total length, volume and surface area measurements for annular sea bream via 3D scanner image

It is a very easy species to work with with a 3D scanner, since the body structure of the annular sea bream is tighter and also the body lines are very clear than other fish (Figure 3). In addition to determining the cross sections, the body circumference can be easily measured via 3D scanner images (Figure 4).

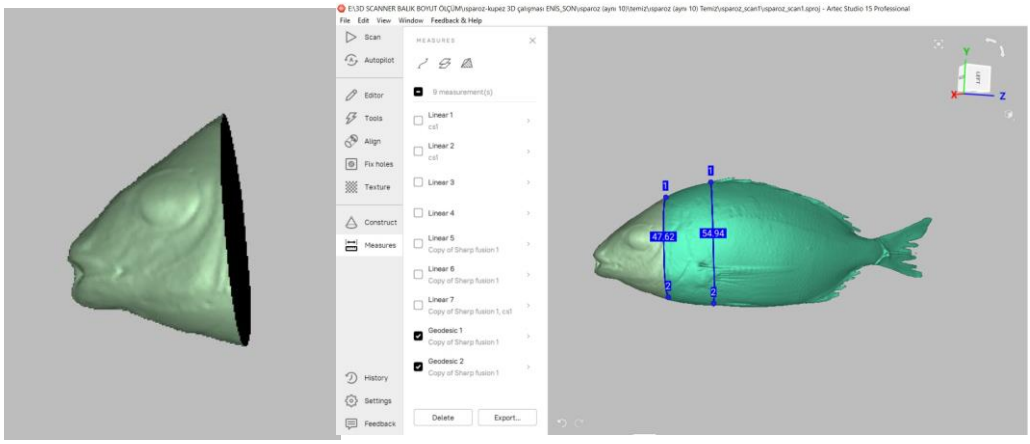

Figure 4
Measuring of fish cros section and body circumference via 3D scanner images for annular sea bream

Measuring axillary sea bream (Pagellus acerna) morphology

Axillary seabream, is a bony fish, which has an economic value in the Mediterranean fisheries. Linear and geodesic distance measurements made on the 3D scanner image of axillary sea bream individual are shown in Figure 5.

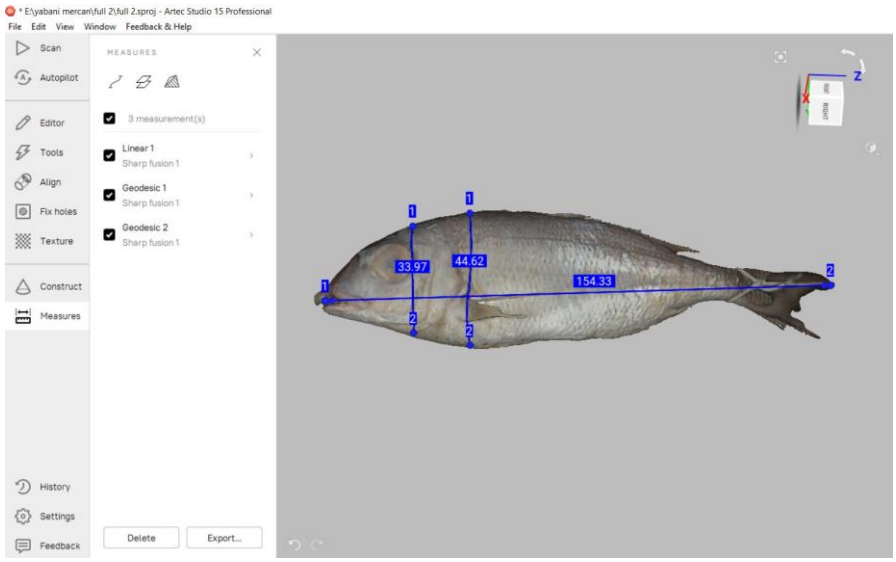

Figure 5
Measuring of fish cros section and body circumference via 3D scanner images for axillary sea bream

Measuring starfish (*Echinaster sepositus*) *morphology*

As a result of the literature search, it is seen that several methods are used to determine starfish size, and most of these consist of measuring, with vernier calipers. However, it is also seen that some of them were not clear about how the measurements were done and how to reproduce them.

Table 3
The measurement results made with the use of classic and 3D images on the starfish

	Arm length (cm)	Arm width (cm)	Mouth radius (cm)
Classical measurement method	9.2	2.5	1.8
	10	2.5	1.8
	10.5	2.5	1.8
	10	2.5	1.8
	9	2.5	1.8
	Arm length (mm)	Arm width (mm)	Mouth radius (mm)
Measurement made on the 3D scanner image	90.22	22.44	18.20
	101.80	20.94	18.18
	105.06	20.34	18.11
	103.27	20.39	18.32
	86.55	21.53	18.84

The measurement values of arm's length, arm width, and mouth radius, respectively, made on the classical measurement method and 3D scanner image of the sea star are given in Table 3. The measurements made on 3D scanner images are shown in Figure 6. When the values are examined, it is seen that the values obtained from both methods agree with each other, similar to the previous results.

Measuring sea cucumber (*Holothuria tubulosa*) *morphology*

Among the examined species, sea cucumber is the most difficult species to make morphological measurements on its. The sea cucumber, which is taken out of the water for measurement, gives out its water during the measurement and constantly changes its shape. For this reason, as can be seen in Table 4, there are differences between the values obtained by both measurement methods compared to the previous species (Table 4). It was observed that the sea cucumber contracted and shortened in length, while it thickened a little, especially during the scanning period with a 3D scanner (Figure 7).

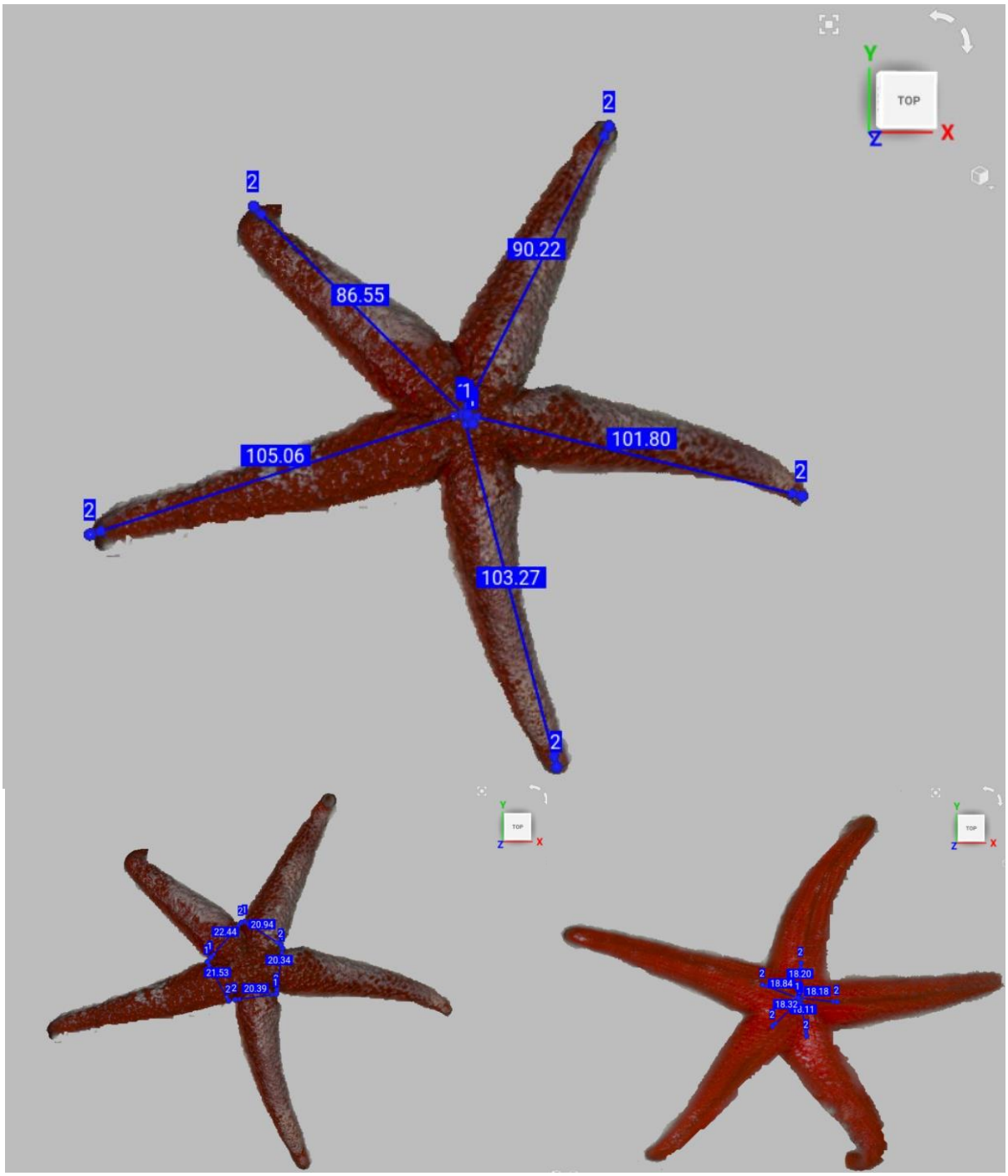

Figure 6
Measuring of starfish section via 3D scanner images

Table 4
The measurement results made with the use of classic and 3D images on the sea cucumber

	Length (cm)	Width (cm)	Weight (g)
Classical measurement method	18.0	4.5	121.8
	12.5	3	51.6
	9.5	3	30.49
	Length (cm)	Width (cm)	Volume (mm)
Measurement made on the 3D scanner image	13.7	5.5	87912.8
	11.3	2.9	30098.8
	7.6	2.5	5214.3

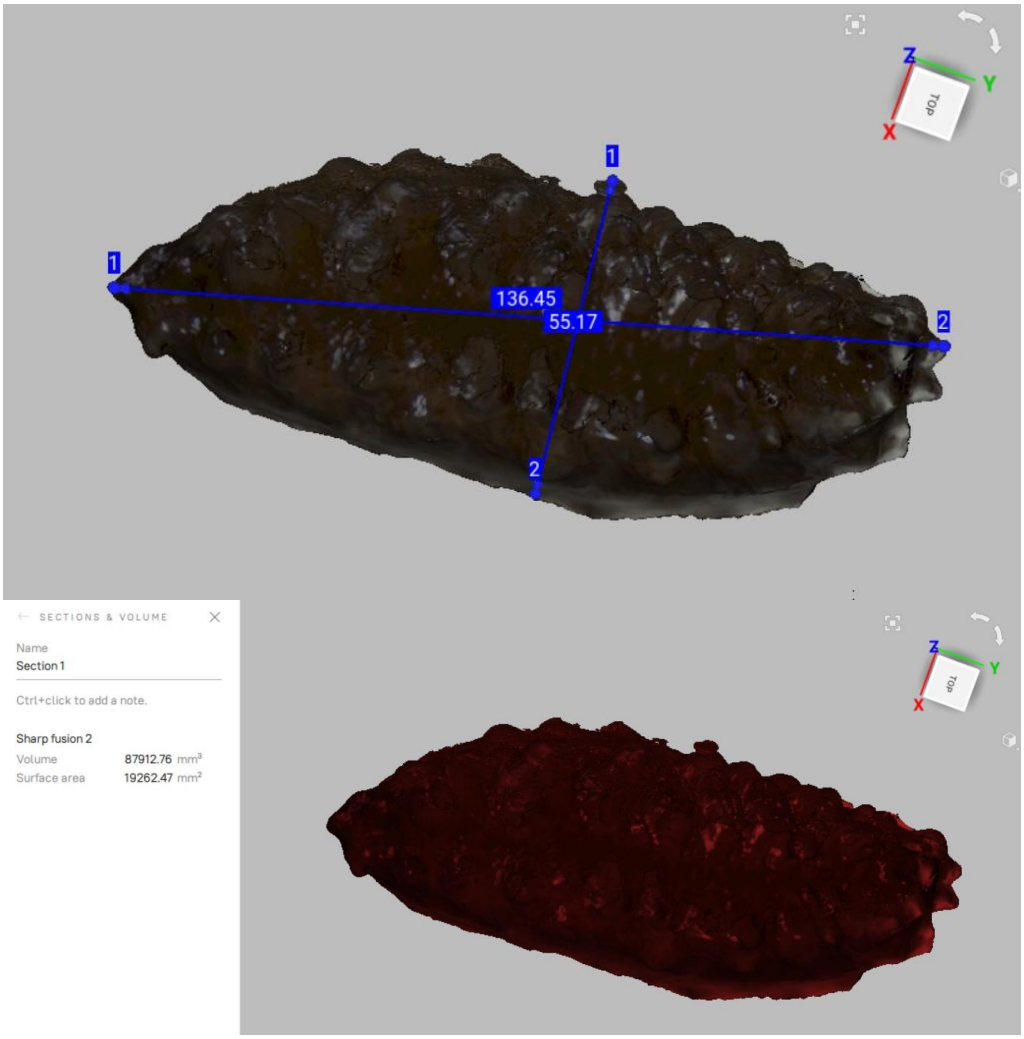

Figure 7
Total length, width and volume measurements for sea cucumber via 3D scanner image

Conclusion and future work

In the scope of this paper, some methods for using 3D scanner images for morphometric measurements are verified. Classical morphometry measurements of aquatic species such as height, width, height, carapace length, which are usually applied by a ruler or caliper, include variations between the measurements of different researchers as well as the variation between the measurements of the same researcher. Furthermore, when required, it is not possible to measure the individual which was previously measured with classical methods. 3D image measurements enable to measure not only metric parameters such as length, width and height, but also area and volume. Among the 5 species examined in the study, the results obtained from both measurement methods were found to be compatible with each other, except for the sea cucumber. For this reason, morphometric measurement methods can be developed quickly over 3D images for other species except sea cucumbers. However, more extensive studies are needed for sea cucumbers.

References

1. Barker MF, Nichols D (1983). Reproduction, recruitment and juvenile ecology of the starfish, *Asterias rubens* and *Marthasterias glacialis*,Journal of the Marine Biological Association of the United Kingdom, 63:745-765.
2. Bernstein BB, Williams BE, Mann KH (1981). The role of behavioral responses to predators in modifying urchins' (Strongylocentrotu droebachiensis) destructive grazing and seasonal foraging patterns, Marine Biology, 63:39-49.
3. Campbell AC, Coppard S, D'Abreo C, Tudor-Thomas R, (2001). Escape and aggregation responses of three echinoderms to conspecificstimuli, Biological Bulletin, 201:175-185.
4. Minchin D (1987). Sea-water temperature and spawning behavior in the seastar Marthasterias glacialis, Marine Biology 95:139-143.
5. Penney AJ, Griffiths CL (1984). Prey selection and the impact of the starfish Marthasterias glacialis (L.) and other predators on the mussel Choromytilus meridionalis (Krauss), Journal of Experimental Marine Biology and Ecology, 75:19-36.
6. Scheibling RE, Lauzon-Guay JS (2007). Feeding aggregations of sea stars (Asterias spp. and Henricia sanguinolenta) associated with seaurchin (Strongylocentrotus droebachiensis) grazing fronts in Nova Scotia, Marine Biology, 151:1175-1183.
7. Schwertmann, L., Focke, O., and Dirks, J-H. - Morphology, shape variation and movement of skeletal elements in starfish (Asterias rubens) - J. Anat. (2019) 234, pp656—667- doi: 10.1111/joa.12964

MODELLING FISHING NETS AS POROUS SURFACES FOR UNDERSTANDING DEMERSAL TRAWLING SEABED IMPACT

Sarath-Krishnan KARUMATHIL[1], Finbarr G. O'NEILL[2], Manuel Jesús GONZÁLEZ CASTRO [1]
[1] Universidade da Coruña, Campus Industrial de Ferrol, Laboratory of Mechanical Engineering, Ferrol, 15403, A Coruña, Spain
[2] DTU Aqua, Technical University of Denmark, 9850 Hirtshals, Denmark

Abstract
Bottom trawling is a globally practised fishing technique where the fishing gears are trawled close to the seabed. It is often associated with large amounts of by-catch, poor fuel efficiency and the alteration of the seabed. This study computationally simulates the flow through fishing nets by modelling them as surfaces for applying porous media models to understand the effect of different parameters associated with bottom trawling.
The netting surface of a demersal fishing gear is complex in shape. However, usually, there are several types of netting panels joined in a single gear making it easy to simulate if modelled as triangulated surfaces. In this study, simulations were carried out of a rigid net panel being trawled close to the seabed. The resulting wall shear stress on the bottom boundary was investigated to provide a better understanding of sediment entrainment in the panels wake.
Results show that the faster and closer we tow the netting to the seabed, the higher the wall shear stress peak experienced on the seabed, the magnitude of which is large enough to mobilise fine sand sediments.

Keywords
Computational simulation, Netting, Porous surface, Demersal trawling, Seabed impact

Nomenclature
u – fluid velocity
p – Kinematic pressure
ν_{eff} – Effective Kinematic viscosity
u_{inf} – Freestream velocity
S_i – Source term for porous resistance
C_d – Drag coefficient
C_l – Lift coefficient
τ_w – Wall shear stress (N/m^2)

ρ – Density of the fluid
A – Area of the netting panel
C_{ij} – Inertial porous resistance coefficient material matrix
D_{ij} – Viscous porous resistance coefficient material matrix
F_{drag} – Drag force
F_{lift} – Lift force

Introduction

Demersal trawling is a fishing technique that is commonly employed around the world to collect marine animals that live near the seafloor. It is a prominent fishing technique that contributes a significant amount of marine food and is well-known for its large bycatch, low fuel efficiency, and ecological impact due to the destruction of the benthic habitat on the seafloor. In this type of fishing, fishing gear is towed close to the seabed to catch target species such as fish and shrimp that live near the seafloor. Understanding the hydrodynamics of demersal fishing gear in fluid flow is essential for enhancing them in all these areas.
There have been many research on the individual impact of fishing gear components such as trawl doors, lines, and so on, but the impact of fishing nets on sediment mobilization has received little attention.

Computational simulation is a fast-growing toolkit which can be used to predict the hydrodynamics for the flow through and around the fishing nets. In this study 3D computational simulations were used to understand the hydrodynamics of fishing nets towed close to the seabed. Fishing nets are flexible structures and their behaviour in water is a fluid structure interaction problem. To simulate the behaviour of nets in the water, considering them as twines and knots (or cylinders and spheres) applying usual non-slip boundary conditions are very computationally expensive. In recent years there were more developments in this area to make simulations more efficient and considering net as a porous medium emerged and has been proven to be a viable choice for simulating fishing nets ([1],[3],[4]). In this study, netting material is modelled as a porous surface. Numerical simulations are carried out to understand the effect of different parameters such as trawling velocity, distance the netting panel make from the seabed. The results are contextualised in relation the wall shear stresses required for sediment mobilisation. The net is considered as rigid and so only the fluid part of the problem is solved during in this study.

Numerical model

The numerical approach used in this study solves the Reynolds Averaged Navier Stokes equations (RANS) with an additional source term to account for the porous resistance offered by the fishing net. A steady state solution for a netting panel in an incompressible, uniform flow is found for the following equations written in vectorial form:
The continuity equation:

$$\nabla \cdot u \; = \; 0 \tag{1}$$

and the momentum equation,

$$\nabla \cdot (u \otimes u) - \nabla \cdot R = -\nabla p + S_i \tag{2}$$

Where R is the Reynolds stress tensor given by:

$$R \; = \; \nu_{eff} \nabla \cdot u \tag{3}$$

The effective Kinematic viscosity needs to be calculated or modelled using turbulence models. In this work, the turbulence is modelled using a two equation shear stress transport turbulence model, $k - \omega \, SST$.
The source term S_i is the resistance offered by the net in the fluid flow calculated using the Darcy-Forchheimer porous media model:

$$S_i \; = \; - D_{ij} \mu u \; - \; \frac{1}{2} C_{ij} \rho |u| u \tag{4}$$

Where D_{ij} is the material matrix for viscous porous resistance coefficients and C_{ij} is the material matrix for inertial porous resistance coefficients. These coefficients vary for different types of net and should be calculated for each type of net individually using fitting approaches with experimental results and analytical models or CFD models. The hydrodynamic force coefficients are found using the following equations:

$$C_d \; = \; \frac{2 \, F_{drag}}{\rho A u_{inf}^2} \tag{5}$$

$$C_l \; = \; \frac{2 \, F_{lift}}{\rho A u_{inf}^2} \tag{6}$$

where F_{drag} is the drag force and F_{lift} is the lift force of the netting panel, A is the total area of the netting panel and u_{inf} is the freestream velocity.

Surface based modelling of fishing nets

The porous media approach generally models netting as a thin solid with the width of the porous media and cells inside this volume were applied the porous resistance forces. This technique tend to have difficulties while simulating fishing nets with complex structures and big deformation. [2] devised a porous media technique that considers nets as a surface to cope with the various forms of trawl gears and to permit easy connection with structural solvers. This method is used here to gain a better understanding of the flow through and around netting panels towed near to the seafloor.

CFD simulation

CFD simulations were carried out using the open source CFD toolkit, OpenFOAM. PorousSimpleFoam, an incompressible steady state solver for turbulent flows with implicit or explicit porous media implementation was used for solving the RANS equations. The solver uses a SIMPLE (Semi-Implicit Method for Pressure Linked Equations) algorithm. The governing equations were solved using a finite volume discretization method.
Triangulated surfaces are used to depict the netting, which has been proved to accurately replicate the three-dimensional complexity of real fishing gears. The net used in this study is a knotless nylon net, having a twine diameter of 2.8 mm, and a mesh bar length of 29 mm, yielding a solidity ratio of 0.184. porous coefficients for this net were given by [3].

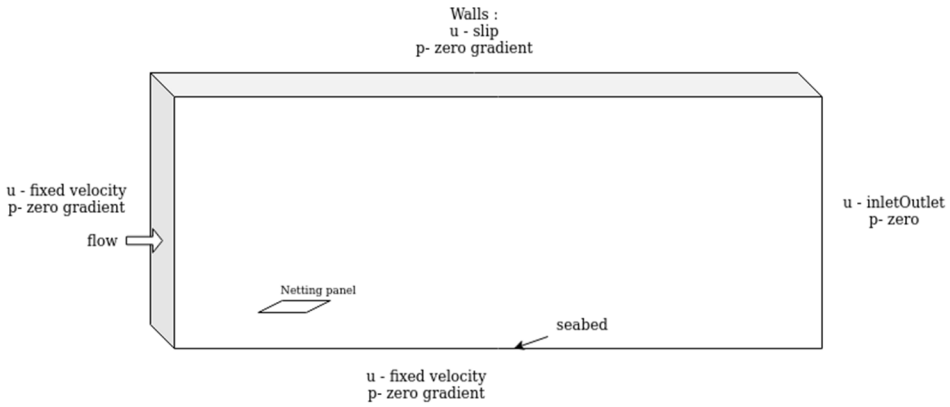

Figure 1
Domain used for simulating the netting panel close to the seabed

Figure 1 shows the domain used to simulate the netting panel towed close to the seabed. The domain is 18 m long, 8 m wide and 5 m deep with the leading edge

of the netting panel 2.5 m from the inlet. The wall shear stress (τ_w) demonstrated in the results were plotted along the center line of the bottom wall which has fixed fluid velocity boundary condition applied on it. A velocity defined flow was achieved using fixed inlet velocity and zero pressure at outlet.

Results and Discussions

Parameters which were varied to understand their importance in demersal trawling and sediment transport were the distance of the netting panel from the seabed and the fluid flow velocity. These parameters were varied over a significant range and their effect on hydrodynamic forces made by the netting panel and the wall shear stress acted on the bottom wall are presented in this section. The critical wall shear stresses were calculated from Shields curve for different particle size sediments, 0.07 N/m^2 for suspending fine silt (8-32 µm), 0.2 N/m^2 for moving fine sands of particle size 63-500 µm and 0.5 N/m^2 for moving coarse sands of particle size 500-2000 µm.

Distance between seabed and netting panel

In bottom trawl fisheries, netting panels usually are at lower angles of attack and towed at different heights from the seabed. A 1 m x 1 m netting panel making 10° with the seabed was simulated for a flow speed of 2m/s with its leading edge making a distance from the seabed from 0.1 m to 1.0 m.

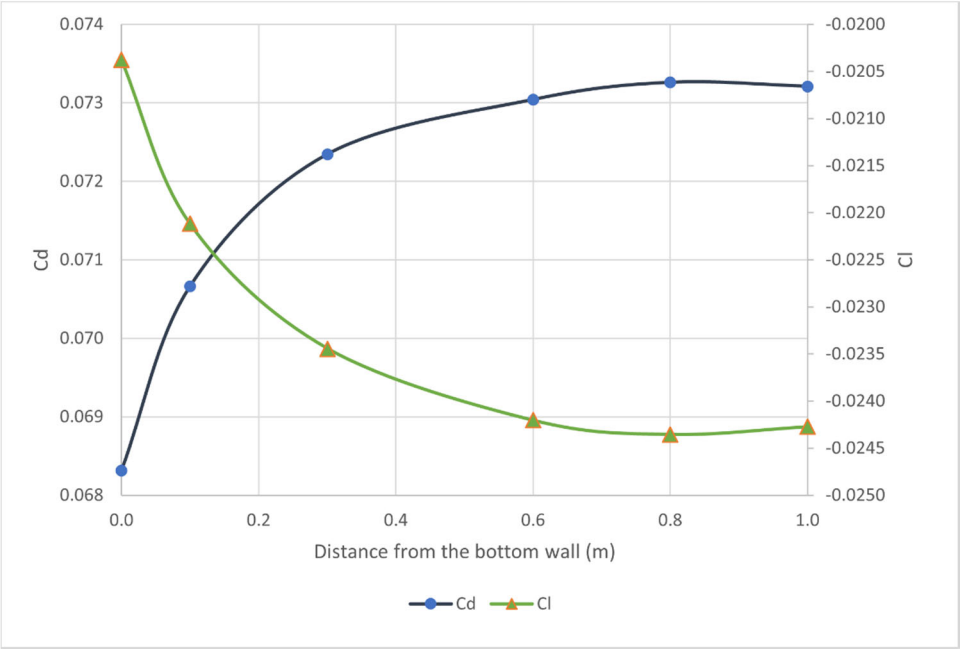

Figure 2

Drag and lift coefficients for towed netting panel making 10° with seabed at 2 m/s

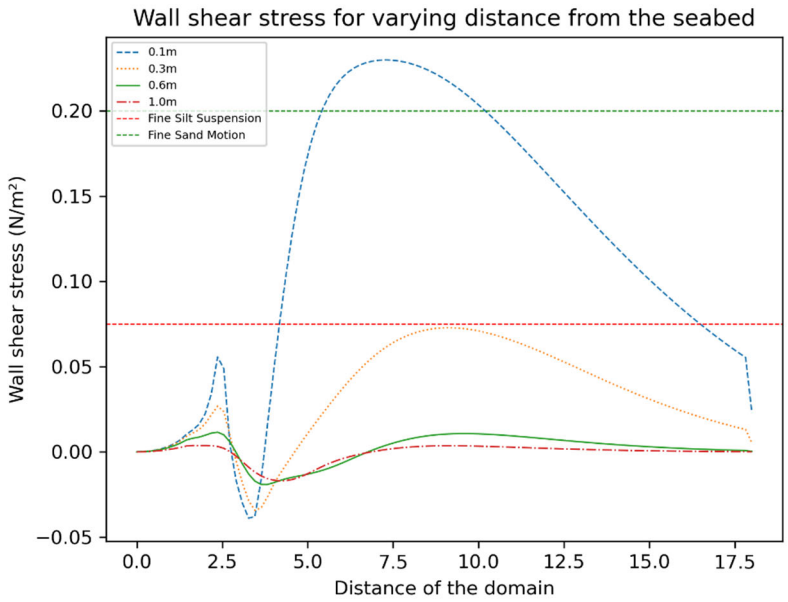

Figure 3
Wall shear stress plotted along the center line of the bottom wall for towed netting panel making 10° angle from seabed at different distances for a towing speed of 2 m/s.

Flow speed

Fisheries around the world operate at different speeds and they vary depending on the size and power of the vessels to the target species. It is important to understand the effect of flow speed on the impact of fishing nets for sediment entrainment. Simulations were carried out for different flow velocities ranging from 0.25 m/s to 3.5 m/s for a netting panel making a distance between the leading edge and bottom wall of 0.1 m and an angle of 10°. Results show a constant coefficient of lift and drag making a parabolic curve for lift and drag forces increasing in magnitude with increasing towing speed.

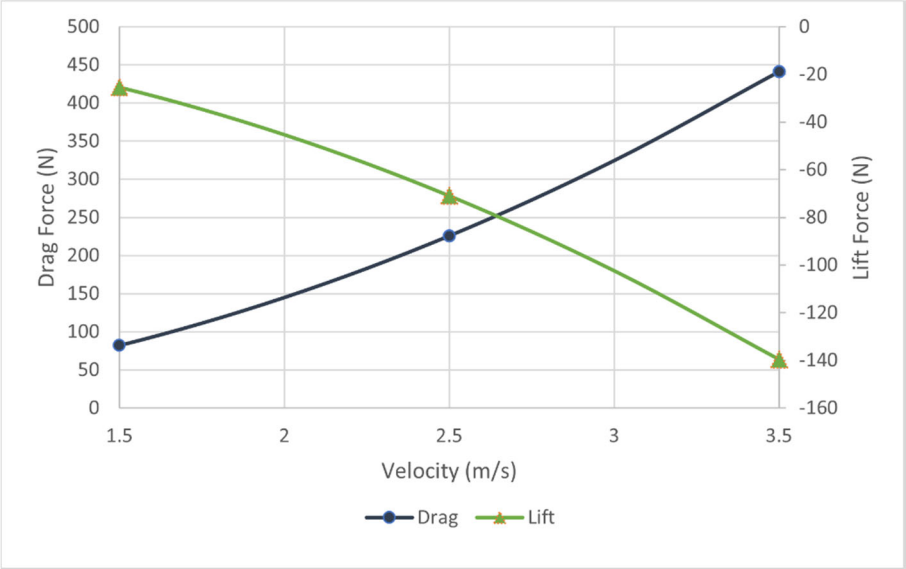

Figure 6
Hydrodynamic forces for netting panel making 0.1m leading edge distance and 10° to the seabed towed at different speeds.

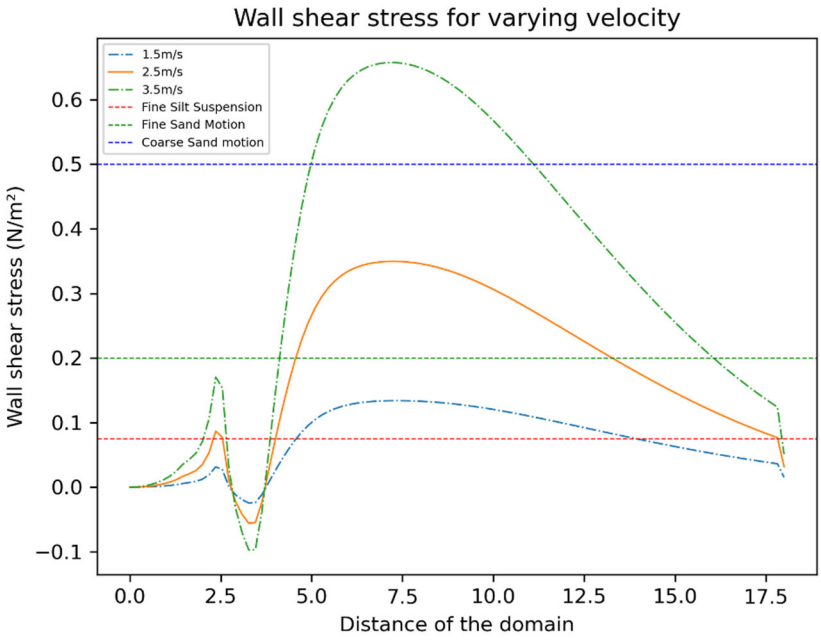

Figure 7
Wall shear stress plotted along the centre line of the bottom wall for netting panel making 0.1 m leading edge distance and 10° to the seabed towed at different speeds.

The figure 7 shows how the speed of the trawling could make a coarse sand move with towing a 1 m x 1 m netting panel at around 3.5 N/m^2. Net used in the trawl fisheries fishing gears are very much longer having more area of netting moving

close to the netting. This study of numerical simulations using porous media model shows it can be used as an effective tool for understanding the impacts of fishing nets in sediment transport while bottom trawling.

Acknowledgements

This research was supported by spanish ministry: Grant PID2019-107345RB-I00 funded by MCIN/AEI/10.13039/501100011033; Grant BES-2017-082013 funded by MCIN/AEI/10.13039/501100011033. The European Maritime and Fisheries Fund (EMFF) and the Ministry of Environment and Food of Denmark in the project 'Using hydrodynamics to develop more selective fishing gears. (HydroSel)' (Grant Agreement No 33113-I-19-130).

References

1. Chen, H., Christensen, E., 2017. Development of a numerical model for fluid structure interaction analysis of flow through and around an aquaculture net cage. Ocean Engineering 142, 597–615.
2. Karumathil, S.K., Gonzalez, M., 2019. Simulation of fluid flow across net structures with a porous media approach, in: Contributions on the Theory of Fishing Gears and Related Marine Systems.
3. Patursson, Ø., Swift, M.R., Tsukrov, I., Simonsen, K., Fredriksson,D.W., and Celikkol, B. 2010.– Development of a porous media model with application to flow through and around a net panel – Ocean Engineering 37, 314–324.
4. Zhao, Y.P., Bi, C.W., Dong, G.H., Gui, F.K., Cui, Y., Guan, C.T., Xu, T.J., 2013. Numerical simulation of the flow around fishing plane nets using the porous media model. Ocean Engineering 62, 25–37.

MODELLING THE STRUCTURAL BEHAVIOUR OF NETTING WITH BEAM FINITE ELEMENTS

Francisco BOTTERO, Manuel Jesús GONZÁLEZ CASTRO
Universidade da Coruña, Campus Industrial de Ferrol, Laboratorio de Ingeniería Mecánica, Ferrol, 15403, A Coruña, Spain

Abstract

Industrial fishing is mostly carried out by trawls or similar gears that produce a high proportion of discards. One of the methods to increase the selectivity of trawls is to modify the shape, size, orientation and stiffness of their meshes. To assess the performance of new designs, fishing trials are required. Since the late 1990s, computational simulation methods have been proposed to predict the structural behaviour of fishing gears and hence reduce the need of fishing trials in the preliminary stages of the design process.
Several numerical models for netting have been proposed. Many of them discretize the twines using spring or bar elements. While these models can accurately predict the planar deformation of netting, preliminary experiments show that they cannot predict the interaction between in-plane and out-of-plane bending that happens in areas of high curvature like cod-ends.
This paper aims to develop numerical models to accurately predict the deformation of netting with mesh resistance to opening. The proposed approach consists of discretizing the twines with 3D beam finite elements. The complexity of these elements is notably higher than springs and bars in terms of element formulation and degrees of freedom of the model. Different beam element formulations have been evaluated, and the most promising results correspond to Euler and Isogeometric Analysis (IGA) beams. The first ones are the simplest and highly efficient for moderate deflections, where shear effects are not important. In contrast, IGA beams have a more sophisticated formulation, where no assumptions about the rotations are made, and show better performance, with better accuracy and lower number of iterations than Euler beams. Even though, it has been observed that the increased complexity of beam models makes them difficult to converge to the equilibrium position from a far initial position.

Keywords

Netting, fishing gear, resistance to opening, simulation, beam element.

Introduction

The selectivity of trawls can be increased by modifying the shape, size, orientation and stiffness of their meshes [5]. Over the last few years, authors have proposed

numerical models to predict the shape and deformation of net panels using springs, bars or triangular elements [3, 6, 7, 8]. The effect of mesh resistance to opening, which is quite important in trawls and has a high impact on the selectivity, can be modelled by introducing rotational springs [4]. These, compared to the model presented here, use simpler formulations, which allow reducing the number of degrees of freedom, and therefore facilitates the convergence of the simulation. However, they do not consider the interaction between in-plane and out-of-plane bending that happens in areas of high curvature (e.g. codends) in netting with high resistance to opening of the meshes.
To avoid this limitation of current models, we propose to discretize the netting using 3D beam finite elements. This article presents an introduction to this approach, which is quite complex due to the number of factors that interfere:

- The formulation used to discretize the beam elements.
- Type of analysis to be carried out, that is, whether it is a dynamic or static analysis, in the latter case for large displacements due to the nature of the problem.
- The time-stepper selected to iterate until reaching the convergence of the system, what means to reach the final equilibrium position.
- Complexity of the problem. By this we mean the number of degrees of freedom of the problem and the shape of the netting. Simulating a small and flat net panel is far easier than simulation a complete trawl codend. Also, the type of constrains and loads that act on the model has an impact on the complexity

To give greater clarity to how a simulation can be affected by these, various models are proposed to be analyzed, gradually increasing their complexity, which allows, by varying these factors and their parameters, to detect which ones favor, or not, the convergence of the simulation.

Methods

Numerical model

The numerical models that we will present and compare in this work have the same netting discretization scheeme, the differentiating element is the type of 3D beam finite element used to discretize the twines and knots of the meshes.
First of all, the mechanical and geometric properties of the netting are defined. In Figure 1, a single netting mesh can be observed, its geometry is completely defined establishing the diameter of the twines, the mesh length L_{mesh} and resting angle φ_0 given by the position of the twine with respect to the horizontal, the knot width a and height b.

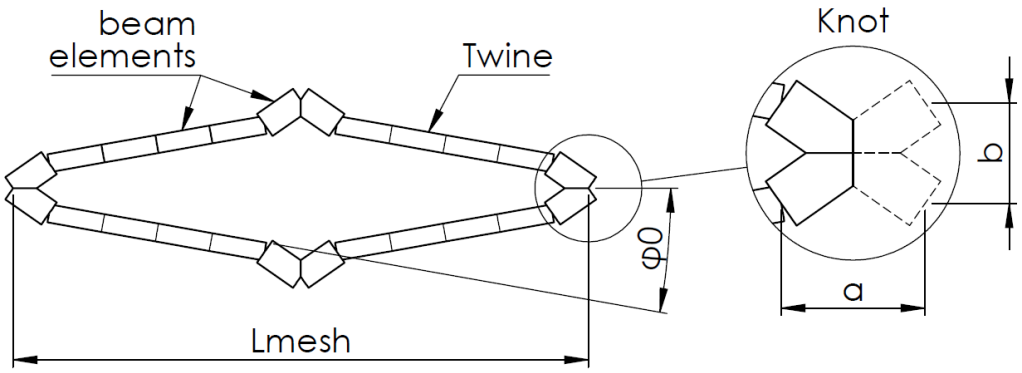

Figure 1
Geometrical properties and discretization in beam elements of a single netting mesh used in the simulations.

Then we proceed to characterize the material and therefore the mechanical properties of the netting. To do this, the axial stiffness EA, the bending stiffness EI and the torsion stiffness GJ of the twines are defined, as well as their density per unit length ρ_l. Once here, the netting is entirely defined and any other parameter required by the program can be calculated from them.
The next step consists in settle the number of meshes of the netting panel under study, in Figure 2 it schematically represented a 2x2 panel, which is generated based on the order of creation of the meshes (numbering in balloons), that goes from left to right (x increasing) and from top to bottom (y decreasing), this made the origin of the coordinates system coincide with the upper left corner of the panel. Likewise, as can be observed the order of creation of the nodes goes clockwise.

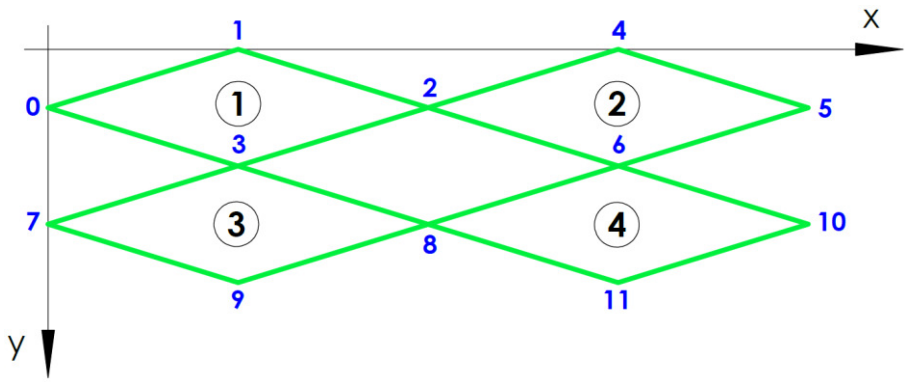

Figure 2
Creation of a netting panel of 2x2 meshes.

Having the mechanical properties, geometry and the logic followed to create the panels, the next step is to discretize the mesh into beam finite elements for the netting twines and knots, as shown in Figure 1. The knots are modeled as a rigid cross of a single beam element per side, whose center starts from the node

generated during the creation of the panel, with the goal of represent the effects induced by the stiffness of the knots on the twines. On the other hand, the twines are discretized using at least a default minimum of four beam elements. As a result, a completely discretized mesh panel is obtained.
We have tested three 3D beam element formulations: Euler, Isogeometric Analysis (IGA) and Absolute Nodal Coordinate Formulation (ANFC). However, the last one was quickly discarded because it proved to be much more inefficient than the others, even for simple problems. In the present work, the results of the two most promising methods, those that use Euler or IGA beams, will be analyzed in detail.
After discretizing the netting into beam finite elements, it only remains to define the constraints of the model, as well as the loads acting on it, which vary depending on the problem configuration. In this work we used simple test cases with small netting panels made up of five meshes in both transverse and normal directions. Different loads were applied to adopt various forms and thus evaluate the convergence capacity of the models. In addition, a more complex example representing a trawl codend is analyzed.

Test cases

Plane deformation of a small netting panel

The first test case consists in holding the netting panel from its upper knots, allowing free displacement of the nodes in the direction of the "x" axis and free rotation with respect to any of its axes. In other words, just to two degrees of freedom are restricted, the translation in "y" and in "z". This is represented in Figure 3.1 by a series of movable hooks. The forces are applied in the direction of the "y" axis, therefore, it is a model in which the network does not leave the "xy" plane in which it was created.

Flexion of a small netting panel

In this case, the net is rigidly hold at the top, allowing only the free translation of the nodes in the direction of the "x" axis. As can be seen in Figure 3.2, no external forces are applied to the net, however, the action of gravity, acting normal to the plane that contains the net, causes the panel flexion due to its own weight. This allows the study to be replicated easily, in a simple test where a netting panel parallel to the surface of the floor and fixed at one end, is let it flex due to its weight.
The twines used to manufacture the nets have an axial stiffness that is considerably higher than the bending or torsion stiffness, so this type of stress will have a much greater effect over the net than a force acting in the plane "xy".

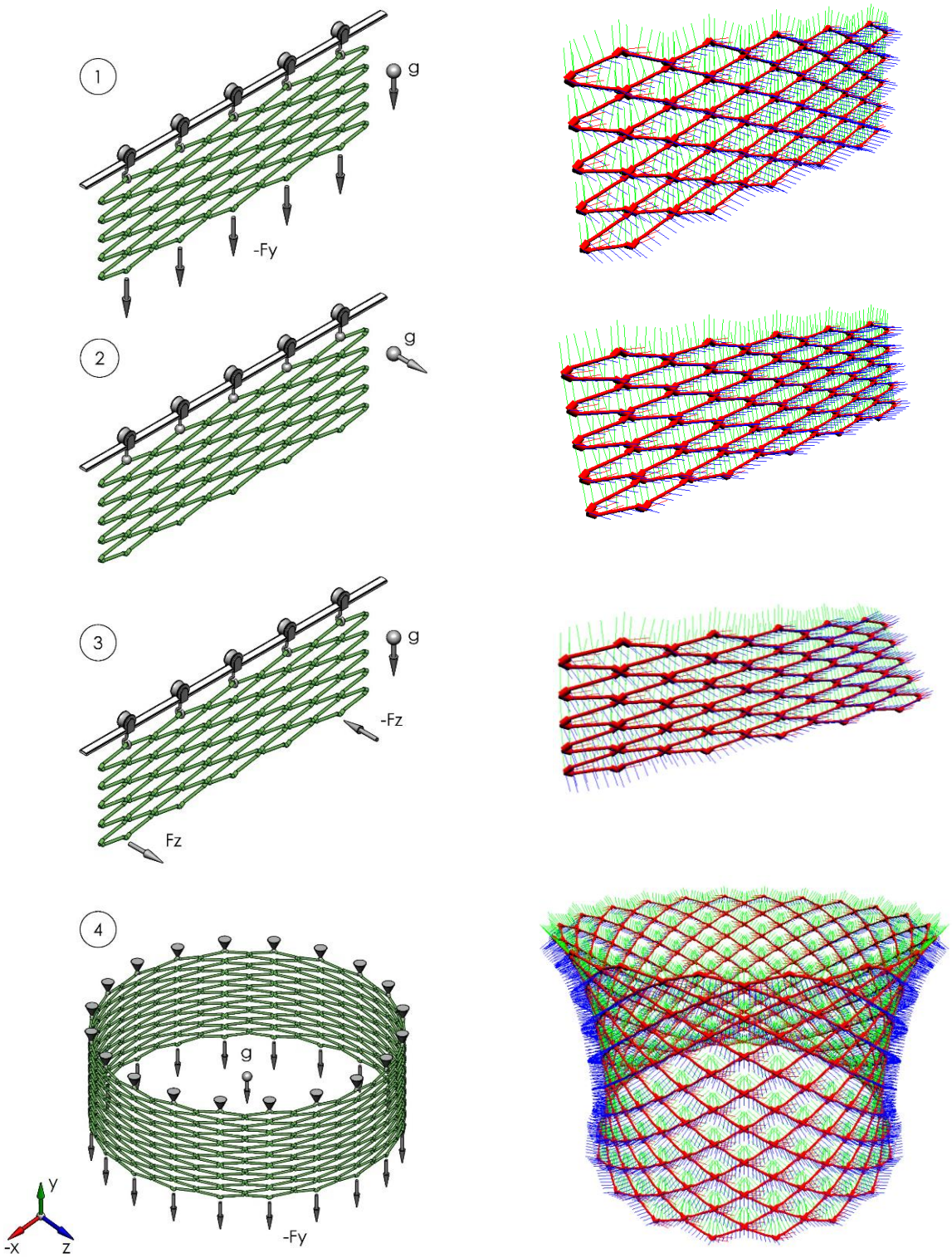

Figure 3
On the left, the setup of the models: 2D panel plane deformation (1), flexion (2) and rotation (3) and trawl codend stretching (4) with the representation of the forces and constrains over the netting. On the right, the equilibrium position of the panel after the simulation, represented with the axis of the beam nodes.

Torsion of a small netting panel

In this last configuration of a simple panel, the restrictions are identical to those indicated for the plane deformation. It can be considered the most complex model of those mentioned so far, that is because as can be seen in Figure 3.3, in addition to the net own weight, a couple of forces that generate its torsion show up. As mentioned for bending, the introduction of normal loads with respect to "xy" plane has important repercussions on the deformation of the netting panel, therefore, the magnitude of the forces compared with the expansion case, will be considerably lower, at less one order of magnitude inferior.

Stretching of a trawling net codend

Once we have the simple panel analyzed, we proceed to study what happens in a trawl codend. Two models were made, the first one, indicated on the right of Figure 3.4 is a scale model, three times smaller than a real fishing codend showed in Figure 5, which allows to do an analysis the netting behavior employing a smaller number of elements and hence, less degrees of freedom. The panel is made up of 20 meshes around the perimeter of the cylinder (whose diameter is also three times smaller than the real one) by 8 meshes in a vertical direction.
The background work required to obtain a cylindrical mesh is much more complex than for simple panels. Despite this, the stages indicated for them are repeated here until a completely discretized net is obtained.

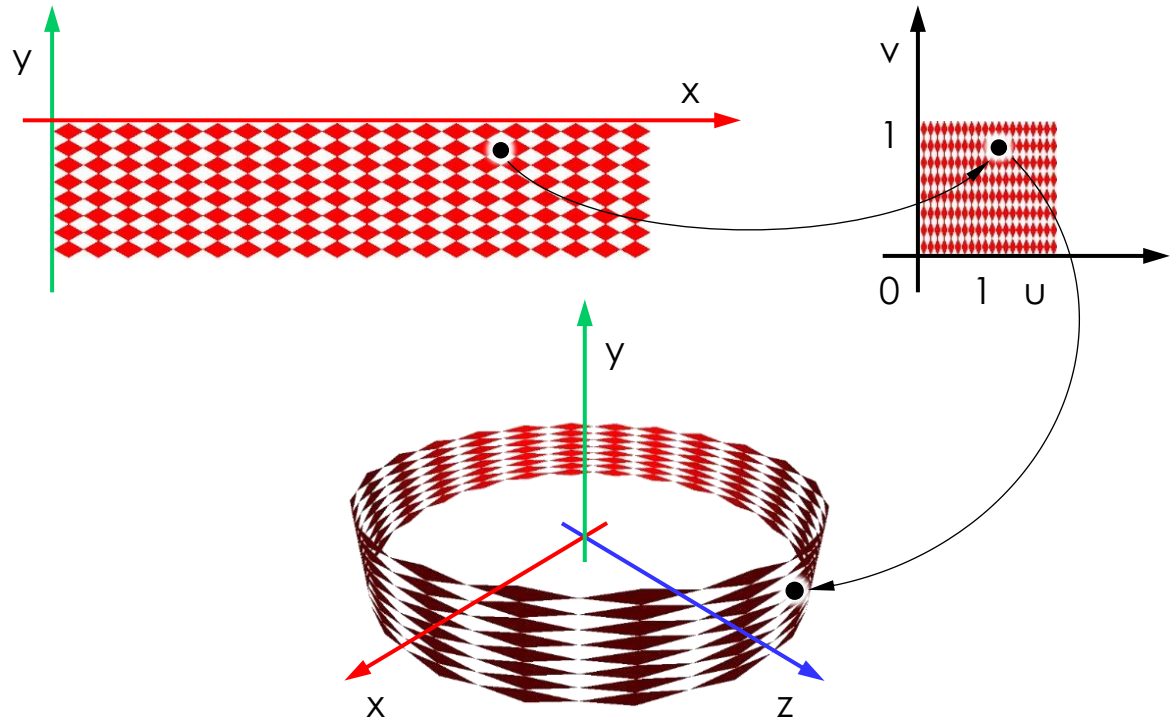

Figure 4
Mapping of a panel contained in the "xy" plane to a cylindrical NURB surface.

Afterward, a bilinear interpolation of the netting panel is performed in such a way that $(x, y) = f(u, v)$ where (x, y) describe the coordinates of the vertices of the quadrilateral with the smallest area that contains the panel in the physical coordinate system, while (u, v) define logical and unitary coordinate system, which contain the panel after the transformation. Then, depending on the coordinates (u, v) of each node, we obtain its position associated with the surface described by a NURB in coordinates (x, y, z) as can be seen in Figure 4, as well as its orientation in space, given by the tangent and normal vectors to the surface at that point. As a result, the cylindrical panel of Figure 3.4 is obtained.
Constraints are introduced at both top and bottom nodes. All of them must remain on their respective circles described by the cylindrical netting panel on the "xz" planes. In this way, the nodes have entire freedom of rotation and translation on the perimeter of the circumference, and they only differ in that the bottom nodes are allowed to move simultaneously along the "y" axis, while the upper ones cannot. Rendering to the loads experimented by the network, we have its own weight, plus a set of forces acting on each bottom nodes in the negative direction of the "y" axis.

Solver

Both static and dynamic simulations were carried out, where the first ones, due to the large displacements experimented by the net, must be analyzed as a non-linear problem. Regarding to the second ones, a cut-off criterion was defined to limit the number of iterations to be carried out, this consists of pre-established a maximum admissible acceleration, below which, the average acceleration of the model nodes must be found to consider the system converged.
Several time-steppers for dynamic simulation were tested: Euler Implicit Linearized, Hilber Hughes Taylor (HHT) and a dynamic relaxation scheeme.
Dynamic relaxation forces dynamic systems to converge to a static equilibrium by adding fictitious damping. In this study, it is proposed to use a method that uses continuous kinetic damping (CKDR) [2], in the implemented method this is done by setting the position, velocity and acceleration of each node to zero after completing a time step.
The convergence rate of the CKDR method increases as the steps and natural frequency of the system increase [1]. During each time step, the frequency is recalculated, and based on it, the next step to be taken is determined. It must be considered that the natural frequency of the models can change very quickly during the simulation, which causes a sudden variation in the step size, and this can lead to a failure of the solver used. To avoid this, it is necessary to maintain the steps fluctuations inside some boundaries previously defined by increase and decrease factors.

Results and discussion

This section begins by clarifying that most part of the studies are focused on the use of the time stepper with dynamic relaxation implemented in this current work, because, comparing its efficiency with respect to the other integrators, its convergence ratio is remarkably higher. Where, by speed of convergence we understand the capacity of the models to reach a final equilibrium position.
Therefore, it remains to be analyzed what happens when we must choose between different beams formulations, type of study and the configuration of the model itself, as well as the loads applied to it.
Talking about the first model, which consist in a small netting panel subjected to stretching, as we do not have lateral forces or deformations, no appreciable differences are denoted in terms of the facility of convergence. Hence, the dynamic relaxation converges in three steps, regardless of the beam formulation used, while the nonlinear static simulations do it in only two.
Similar results can be obtained with the configuration of the panel subjected to bending, where only the effect of gravity is considered, with the unique difference that during the dynamic relaxation of Euler beams, a greater difficulty is observed to reach the final equilibrium position, requiring more numbers of steps, two orders of magnitude higher, than other beam formulations
However, as we introduce new types of loads to the study, the netting panel could reach more complex equilibrium positions, such as the case of torsion or increased bending due to the action of external forces. That causes a considerable variation of the convergence ability depending on the model under study and their simulation parameters.

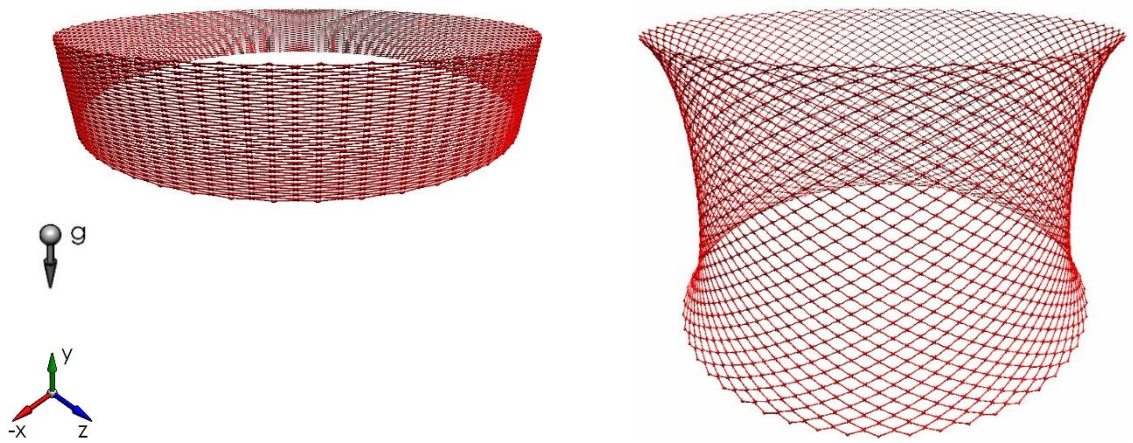

Figure 5
Simulation of a trawling net codend, fixed on the upper knots with a force applied on the bottom knots in -*y* direction. On the left, the initial position, and on the right, the final equilibrium position.

Until here, the statics simulations seem to be much more efficient than dynamics, and they manage to converge in just two iterations regardless of the type of beam used.
Yet, in simulations where there is a greater number of meshes, which increases the number of elements and degrees of freedom, it is impossible for static studies to come up with a solution to the problem. A clear example of that, is what happens when we try to simulate the codend of a traw, either the escalated (Figure 3.4) or the real size one (Figure 5).
On the other hand, regardless of the type of study, the formulation with Euler beams does not achieve good results, requiring a large number of steps, of the order of 1e5 to reach the convergence in the scale model. While, in contrast, a dynamic simulation using IGA beams demonstrates a fast and efficient progression towards the final equilibrium position. The resolution of the full-scale trawl codend model is a clear example of what can be achieved with this combination (Figure 5). However, in this case the number of intervening variables is much higher than in the scale model, which is proportional to the increase in the number of steps and processing time required. Therefore, there is still room for optimization, adjusting the integrator parameters more efficiently for each case.

References

1. Jung, S., Kim T., Yoo W., 2018. Adaptive Step-size Control for Dynamic Relaxation Using Continuous Kinetic Damping.
2. Jung, S., Kim T., Yoo W., 2018. Dynamic Relaxation Using Continuous Kinetic Damping.
3. Lee, C.-W., J.-H. Lee, B.-J. Cha, H.-Y. Kim, and J.-H. Lee. 2005. Physical Modeling for Underwater Flexible Systems Dynamic Simulation. Ocean Engineering 32 (3–4): 331–47.
4. Morvan, B., Priour, D. et al, 2016. Finite element model for the assessment of the mesh resistance to opening of fishing nets. Ocean Engineering Vol 123 pp. 303-313.
5. O'Neill, F.G. and Mutch, K., 2017. Selectivity in Trawl Fishing Gears. Scottish Marine and Freshwater Science Vol 8 No 01.
6. Priour, D. 2013. A Finite Element Method for Netting. New York: Springer.
7. Takagi, T., T. Shimizu, K. Suzuki, T. Hiraishi, and K. Yamamoto. 2004. Validity and Layout of 'NaLA': A Net Configuration and Loading Analysis System. Fisheries Research 66 (2–3): 235–43.
8. Tsukrov, I., O. Eroshkin, D. Fredriksson, M.R. Swift, and B. Celikkol. 2003. Finite Element Modeling of Net Panels Using a Consistent Net Element. Ocean Engineering 30 (2): 251–70.

FEMNET – OPENFOAM COUPLING. A FSI APPROACH TO SIMULATE FISHING GEAR

Karsten BREDDERMANN[1], Uwe LICHTENSTEIN[2], Daniel PRIOUR[3]
[1]University of Rostock, Ocean Engineering, Department of Mechanical Engineering and Marine Technology, Justus-von-Liebig-Weg 2, Rostock, 18059, Germany
[2]Thünen Institut of Baltic Sea Fisheries, Alter Hafen Süd 2, Rostock, 18069, Germany
[3]Ifremer, LCSM, BP70, Plouzane, 29280, France

Abstract
The efficient development of bycatch reduction devices, such as sorting grids in trawls, and flow field manipulators to facilitate the escape of non-target species from the trawl, as well as measures to optimise trawl drag, require the analysis of the interaction between net/trawl structure and flow field. Netting simulation tools generally use a Morison approach to assess the hydrodynamic forces. This approach is based on the hypothesis that the flow field is undisturbed. However, this hypothesis fails in particular when parts of the netting or trawl are in the wake of other components. To overcome this drawback, the objective of the ongoing research project “SimuNet” is to create a link between structural mechanical simulation of net structures and viscous computational fluid dynamics (CFD) simulations in order to achieve a more realistic fluid-structure interaction. Therefore, the structural dynamics solver FEMNET is coupled to the open source toolbox OpenFOAM. The current status of the coupling scheme and first results of a two panel test case will be discussed here.

Keywords
FEMNET, OpenFOAM, numerical modelling, FSI, fluid-structure interaction, partitioned approach

Introduction
The increase in fuel prices as well as the need to employ bycatch reduction devices (BRD) poses new challenges on the development of fishing gear. The shape of a flexible netting structure develops according to the fluid field and the fluid field changes according to the shape of the netting structure. Not taking the interaction into account may lead to erroneous assumption of the gear performance. E. g. wrong or not optimal orientation of BRDs like sorting grids result at worst in a malfunction. Larsen et al. [7] reported from clogging issues of sorting grids for haddock. Veiga-Malta et al. [25] investigated the optimal angle of brown shrimp sorting grids to keep the sorting capabilities on a high level. Simi-

lar, flow field manipulators made from netting to facilitate the escape of non-target species [2, 27] by creating wake regions have to be carefully designed to take the expected shape. Also, measures to optimize trawl drag can only be precisely judged when the interaction between netting and flow is taken into account. Thus, there is a need for superior simulation tools for netting structures which are capable of calculating the shape of the netting as well as the flow field around the netting structure.

Tools to predict the shape of flexible structures are available [18, 26, 8, 12]. However, simulation tools capable of taking the alteration of the fluid field into account are rare. Work from Kristiansen and Faltinsen [5] implemented a wake field approach from Løland [9]. Mjåtveit et al. [11] applied Code_Aster cable elements to represent aquaculture cages in conjunction with a screen force model to represent the fluid loads. The wake field is described by an empirical approach based on preceding RANS simulations.
The coupling of viscous flow solver with structural solver to answer questions in the marine food production is subject to recent research.
Chen and Christensen [3] coupled OpenFOAM with a lumped-mass-model solver to investigate net panels and aquaculture cages. To resolve the netting geometry a local refinement algorithm is applied. Cheng et al. [4] successfully coupled Code_Aster and OpenFOAM. The netting material is represented by an additional source term in the momentum equations. Besides the example of a simple net panel, aquaculture cages under various conditions are investigated.
REEF3D (Martin et al. [10]) is a simulation framework intended to predict wave-structure interactions, sediment transport as well as coastal hydrodynamics. It was extended by a screen force model to simulate net panels and aquaculture cages. The viscous fluid flow is calculated in a discretized fluid domain, whereas the netting is represented by Lagrangian markers to take into account the scale difference of the fluid domain discretization and geometry representation.
Bi et al. [1] as well as Tang et al. [24] coupled ANSYS Fluent to structural solvers to investigate aquaculture cages. Nsangue et al. [13] also investigated a highly simplified bottom trawl model in this way.
A major drawback of all introduced tools is that besides REEF3D, the tools or additions to the solvers mentioned are not open-source and therefore not accessible to the research community. Furthermore, the applications are focused on aquaculture cages, which are comparatively simple structures (i.e. one mesh size, cubic or cylindrical main shape). To model a sophisticated trawl poses a huge challenge in the set-up, as can be seen in [13]

Therefore, the objective is to develop an open source simulation tool which is based on a structural solver written for the simulation of trawls and a viscous flow solver to take the wake field into account.

Coupling Scheme

The major part of the components used for trawls and aquaculture cages are flexible and show large deformation when exposed to a fluid flow. Vice versa the change in geometry alters the fluid field, which requires - as mentioned above – a coupled fluid-structure-interaction approach. Here, a partitioned approach is followed, where the deformation of the net structure and the corresponding flow field are solved separately.
The simulation tool chosen to model the net structure is FEMNET, which was written by D. Priour [18, 19, 20, 21]. FEMNET is based on a finite element method capable to describe flexible line and netting structures including trawls with their rigging up to the fishing vessel. It takes into account twines elasticity, twine flexion, hydrodynamic loads, mesh opening stiffness, fish catch pressure, buoyancy and weight. The netting is represented by triangular elements. Cables, warps and bridles are represented by line elements. Static equilibrium as well as dynamic calculations can be done. The source code is available on https://gitlab.ifremer.fr/dp00644/femnet.

For the fluid flow field simulation the OpenFOAM environment [14, 15, 16] was chosen. It is an environment for the solution of continuum mechanics problems and includes numerous solvers. A focus lies on the simulation of fluid flows and all major methods to simulate these are implemented (potential flow, direct numerical simulation – DNS, large eddy simulation – LES, Reynold-averaged- Navier-Stokes – RANS). A fluid flow simulation includes six basic steps. Creation of a digital model of the object to be investigated, creation of an enclosing fluid domain, discretization of the fluid domain into a numerical grid, boundary condition set up, solving and post-processing of the results. For the discretization of the fluid domain the meshing tool SnappyHexMesh (SHM) is used, which is associated to OpenFOAM.
In Figure 1 the general directory structure is given. It consists of a FEMNET and OpenFOAM case working directory. The “OFcase” directory contains a typical OpenFOAM case set up whereas the “hexa” directory contains the FEMNET related data.

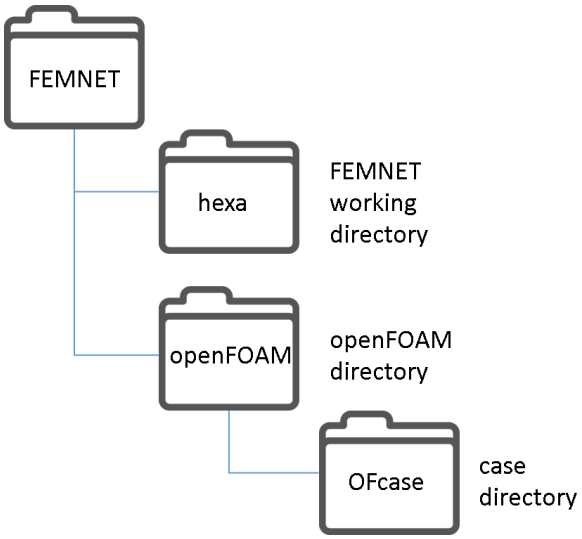

Figure 1
General directory structure.

The FEMNET software was extended to output all files necessary to start the OpenFOAM simulation and writes into the appropriate "OFcase" subdirectories (as required these are blockMeshDict, snappyHexMeshDict, topoSetDict, createBaffleDict, fvOption). The netting geometry is passed over as ".stl" file.
To feed the fluid data back it was decided to realize two options. First, the velocity information is passed back and FEMNET uses an updated velocity field to calculate the loads on the netting according to Landweber [6] and Richtmeyer [22]. Second, the pressure across the netting is passed back and this information is used to calculate the hydrodynamic loads by a screen force model. The pressure loss option is not yet functional.
To have a joint FEMNET-OpenFOAM post-processing option the FEMNET output was extended to write ".vtk" files readable by the open source data analysis and visualization software ParaView [17].
In Figure 2 the flow chart of the coupling is given. A simulation run starts with the read in of the convergence criteria and an initial shape prediction of the net structure. At this point, a variation of the flow field is not taken into account; the hydrodynamic loads are calculated according to [6, 22]. The initial net geometry and the parameters describing the enclosing fluid volume are passed over to the OpenFOAM directory and are discretized according to the dictionary files created by FEMNET for OpenFOAM. Furthermore, the boundary conditions and the parameter for the porous medium, which represents the netting, are set. Two options are available to create the porous medium. Either as a number of cells grouped together (volume) or as a so called porous baffle (surface). The hydrodynamic properties of the netting are described by linear and quadratic loss coefficients [2]. These may be a function of the solidity, angle of attack, fluid veloci-

ty and type of netting and a functional description has to be established. The solidity of the netting is a result of the shape calculation whereas the angle of attack and the fluid velocity are given in the iterations of the fluid field simulation.

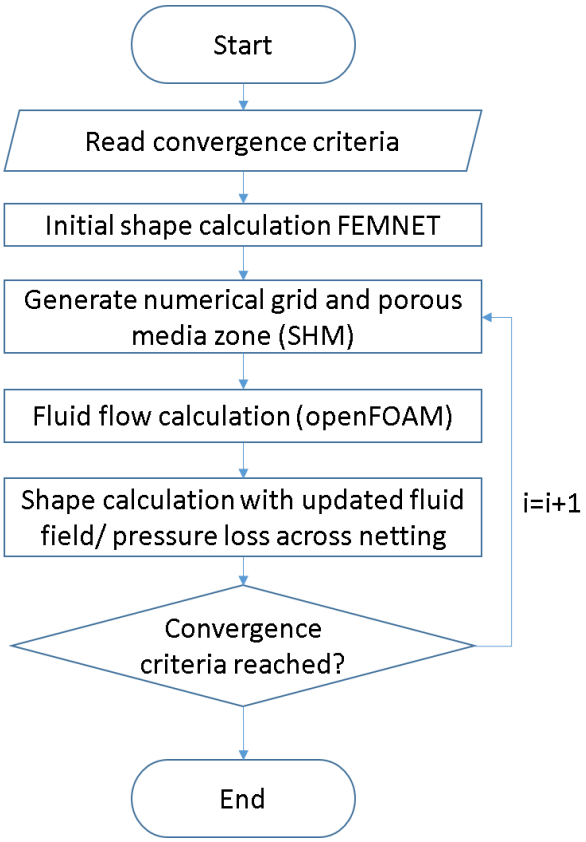

Figure 2
Flow chart of the program steps.

However, the porous medium approach is not yet fully functional. From FEMNET the solidity of the netting is given for every triangular element representing the netting surface. This information is not yet used since the standard porous models in OpenFOAM do not support variable solidities. At this point, only an averaged solidity is passed over.
With these preparations done, the solving process is started. The discretization of the netting in FEMNET and OpenFOAM differ. Thus, it requires to map the resulting velocity field (or pressure field) to the netting discretization used in FEMNET. A new shape with the updated velocity (or pressure) field is calculated. It has to be noted here that the algorithms of FEMNET to find a static equilibrium of the net structure are used. Thus the application is limited to quasi-static problems.

Finally, the convergence criteria are checked to verify whether a state of equilibrium has been reached. If so, the run finishes, if not the latest net geometry calculated is used for a further fluid field simulation.

Test case

A two panels test case was created to evaluate the functionality of the coupled software parts. In Figure 3 the set up is given. Two net panels with a half mesh size of 50 mm a hanging ratio of 0.6 and a twine diameter of 5.7 mm are suspended with a distance of 2000 mm to each other. Sinker lines with a diameter of 16 mm, a length of 1980 mm and a density of 4800 kg/m³ are attached to the bottom. To calculate the porous loss coefficients the formula from Løland is used [9].

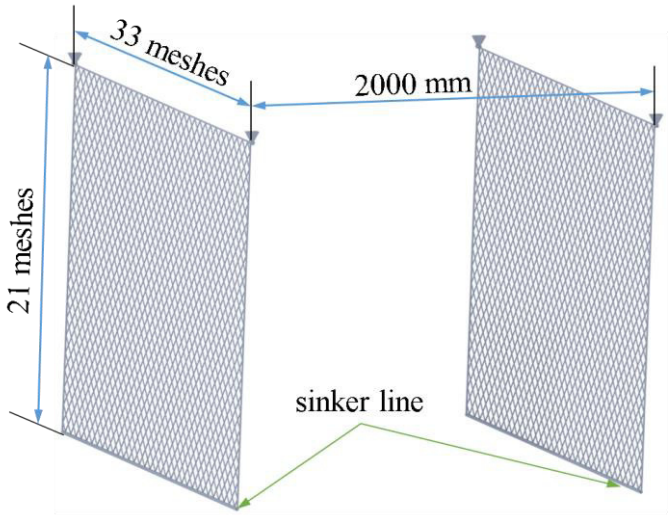

Figure 3
Test case set up made of two panels, one in front of the other.

Given in Figure 4 is the evolution of the net panels shape. The flow direction is aligned with the x-axis. Depicted in grey are the panels deformed by their weight and weight of the sinker lines. In green the shape is given for a flow velocity of 0.514 m/s. The loads are calculated according to [6, 22], the flow is not disturbed by the panels. Both shapes are the same. The first flow field simulation (Figure 5) taken into account results in the shape depicted in purple. Clearly visible is the interaction between the panels and the different deformation. A further iteration (blue) shows minor changes in this case.

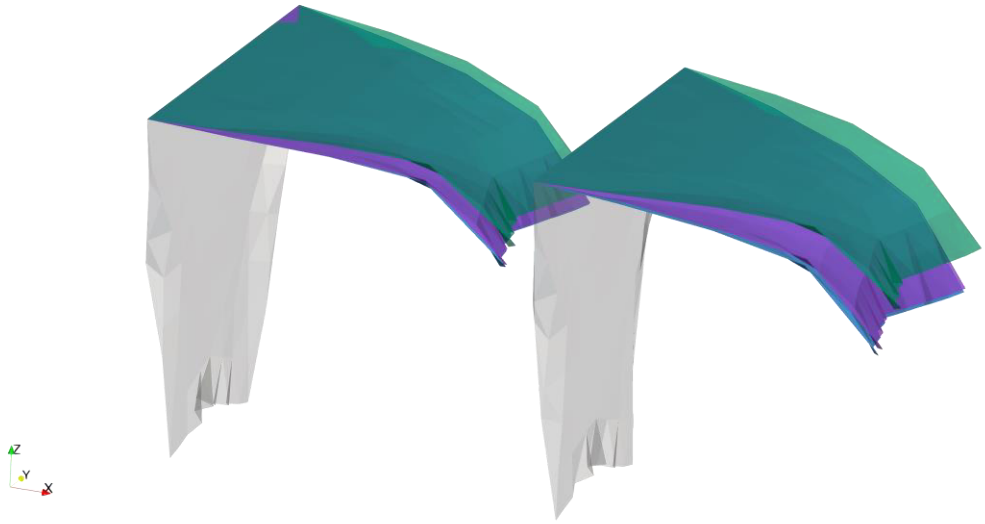

Figure 4
Evolution of the net panels shape. The flow direction is aligned with the x-axis. Grey: no flow. Green: initial shape prediction, both panels are of the same shape. Purple: 1st iteration with flow field data taken into account. Blue: 2nd iteration.

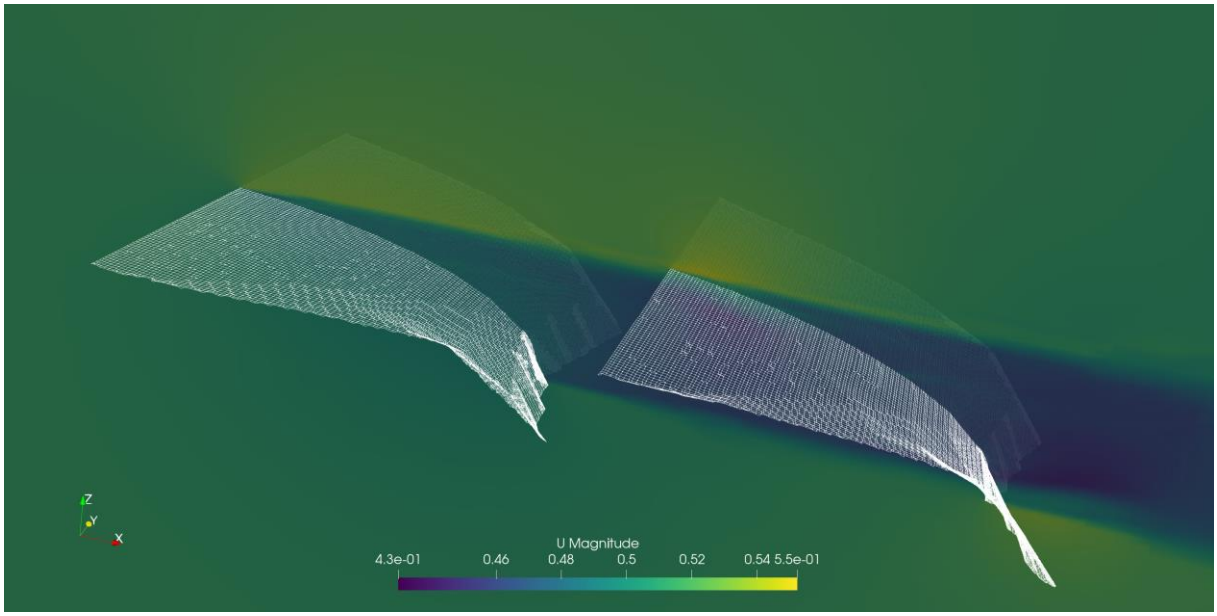

Figure 5
Flow field simulation of the initial shape prediction. The velocity contour is depicted in the centre plane.

Conclusion

A first test case was presented to provide a functional proof of the coupling of the structural dynamics solver FEMNET to the computational fluid dynamics simulation options of OpenFOAM. The coupling scheme is explained in general. As mentioned above, the porous model does not yet take into account local changes in solidity. Thus, in the ongoing research project the focus is on the further development of the porous model. Flume tank experiments are also planned to record datasets for validation purposes.
In future work, mesh deformation and overset mesh algorithms have to be explored to reduce processing time in the discretization phase.

Acknowledgements

The research described in this paper was funded by the European Maritime and Fisheries Fund and the Federal state of Mecklenburg – Western Pomerania, Germany, under ID no. MV-I.16-LM-002, SimuNet - Ein Werkzeug zur Fanggeräteoptimierung.

References

1. Bi, C. W., Zhao, Y. P., Dong, G. H., Xu, T. J., & Gui, F. K. – Numerical simulation of the interaction between flow and flexible nets – Journal of Fluids and Structures 45, 2014, 180-201
2. Breddermann, K., Stone, M., and Yochum, N. – Flow analysis of a funnel-style salmon excluder – Proceedings DEMaT 2019, ISBN 978-3-8440-6995-2, p. 29ff
3. Chen, H., & Christensen, E. D. – Development of a numerical model for fluid-structure interaction analysis of flow through and around an aquaculture net cage – Ocean Engineering 142, 2017, 597-615
4. Cheng, H., Ong, M. C., Li, L., & Chen, H. – Development of a coupling algorithm for fluid-structure interaction analysis of submerged aquaculture nets – Ocean Engineering 243, 2022, 110208.
5. Kristiansen, T. and Faltinsen O. M. – Experimental and numerical study of an aquaculture net cage with floater in waves and current – Journal of Fluids and Structures 54, 2015, 1-26
6. Landweber, L., and Protter, M. H. – The shape and tension of a light flexible cable in a uniform current – J. Appl. Mech., 1947, 14(2): A121-A126
7. Larsen, R. B., Herrmann, B., Sistiaga, M., Grimaldo, E., Tatone, I., & Brinkhof, J. – Size selection of cod (Gadus morhua) and haddock (Melanogrammus aeglefinus) in the Northeast Atlantic bottom trawl fishery with a newly developed double steel grid system – Fisheries Research 201, 2018, 120-130

8. Lee, C.-W., Lee. J.-H., Cha, B.-J, Kim, H.-Y., Won, S.-J. – Calculation model to describe the fishing gear behavior – Proceedings DEMaT 2001, ISBN 3-935319-88-6, 2001, p.15ff
9. Løland, G. – Current force on and flow through fish farms – Dr. Eng. Dissertation. Division of Marine Hydrodynamics, Norwegian Institute of Technology, 1991, ISBN 82-7119-269-8
10. Martin, T., Tsarau, A. & Bihs, H. – A numerical framework for modelling the dynamics of open ocean aquaculture structures in viscous fluids – Applied Ocean Research 106, 2021, 102410
11. Mjåtveit, M. A., Cheng, H., Ong, M. C., & Lee, J. – Comparative study of circular and square gravity-based fish cages with different dimensions under pure current conditions – Aquacultural Engineering 96, 2022, 102223.
12. Niedzwiedz, G. – Model specification and further applications of the calculation of rope systems – Proceedings DEMaT 2001, ISBN 3-935319-88-6, 2001, p. 83ff
13. Nsangue, B. T. N., Tang, H., Xu, L., Hu, F., Dong, S., Achille, N. P., & Zou, B. – Comparison between physical model testing and numerical simulation using two-way fluid-structure interaction approach of new trawl design for coastal bottom trawl net – Ocean Engineering 233, 2021, 109112.
14. OpenFOAM®, Aug . 2022, retrieved from https://www.openfoam.com/
15. OpenFOAM-The OpenFOAM Foundation, Aug. 2022, retrieved from https://openfoam.org/
16. OpenFOAM-extend, Aug. 2022, retrieved from https://sourceforge.net/p/foam-extend/foam-extend-4.1/ci/master/tree/ReleaseNotes
17. ParaView, Aug. 2022, retrieved from https://www.paraview.org/
18. Priour, D. – Calculation of net shapes by the finite element method with triangular elements – Communications in Numerical Methods in Engineering 15(10), 1999, 755-763
19. Priour, D. – Introduction of mesh resistance to opening in a triangular element for calculation of nets by the finite element method – Communications in numerical methods in engineering 17(4), 2001, 229-237
20. Priour, D. – Analysis of nets with hexagonal mesh using triangular elements – International journal for numerical methods in engineering 56(12), 2003, 1721-1733
21. Priour, D. – A Finite element method for netting: Application to fish cages and fishing gear. Springer Science & Business Media, 2013, ISBN: 978-94-007-6843-7
22. Richtmeyer, R. D. – Design and operation of mark IV magnetic mine sweeping gear – Bureau of ships scientific group report No12, 1941

23. Takagi,T., Suzuki, K., Hiraishi, T. – Calculation and visualization Method of Dynamic Fishing Net Shape – Proceedings DEMaT 2001, ISBN 3-935319-88-6, 2001, p.159ff

24. Tang, H., Thierry, N. N. B., Pandong, A. N., Sun, Q., Xu, L., Hu, F., & Zou, B. – Hydrodynamic and turbulence flow characteristics of fishing nettings made of three twine materials at small attack angles and low Reynolds numbers – Ocean Engineering 249, 2022, 110964

25. Veiga-Malta, T., Breddermann, K., Feekings, J.P, Krag, L.A., Paschen, M. – Understanding the hydrodynamics of a size sorting grid in a crustacean fishery – Journal of Ocean Engineering, ISSN 0029-8018, Volume 198, 2020, 106961, https://doi.org/10.1016/j.oceaneng.2020.106961

26. Vincent, B. – A new generation of tools for trawls dynamic numerical simulation – Proceedings DEMaT 1999, ISBN 3-929544-95-4, 1999, p. 99ff

27. Yochum, N., Stone, M., Breddermann, K., Berejikian, B. A., Gauvin, J. R., David J. Irvine, D. J. – Evaluating the role of bycatch reduction device design and fish behavior on Pacific salmon (Oncorhynchus spp.) escapement rates from a pelagic trawl – Fisheries Research, ISSN 0165-7836, Volume 236, 2021, 105830, https://doi.org/10.1016/j.fishres.2020.105830

ISBN 978-3-946694-06-9

www.MENZEL-Verlag.de